SECTION A

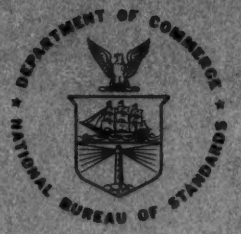

JOURNAL OF RESEARCH

of the NATIONAL BUREAU OF STANDARDS

JNBAAR 79A(5) 609–670, Sept.–Oct. 1975

U.S. DEPARTMENT OF COMMERCE / National Bureau of Standards

Physics and Chemistry

Journal of Research

of the

National Bureau of Standards

A. Physics and Chemistry

Sept.–Oct. • 1975

VOLUME • 79A

NUMBER • 5

Editor: C. W. Beckett

Associate Editor: D. D. Wagman

Publication dates:
Feb. 1, Apr. 1, June 1, Aug. 1, Oct. 1, Dec. 1, 1975

J. Res. Nat. Bur. Stand. (U.S.), A

JOURNAL OF RESEARCH

The National Bureau of Standards Journal of Research reports research and development in the fields of activity shown at right. Also included from time to time are survey articles on topics closely related to the Bureau's scientific and technical program.

The Journal is published in two separate sections as follows:

A. Physics and Chemistry

Contains papers of interest primarily to scientists working in these fields. Issued six times a year. Annual subscription: domestic, $17.00; foreign $21.25. Single copy, varies.

B. Mathematical Sciences

Presents studies and compilations designed mainly for the mathematician and the theoretical physicist. Issued quarterly. Annual subscription: domestic, $9.00; foreign, $11.25. Single copy, $2.25.

The National Bureau of Standards[1] was established by an act of Congress March 3, 1901. The Bureau's overall goal is to strengthen and advance the Nation's science and technology and facilitate their effective application for public benefit. To this end, the Bureau conducts research and provides: (1) a basis for the Nation's physical measurement system, (2) scientific and technological services for industry and government, (3) a technical basis for equity in trade, and (4) technical services to promote public safety. The Bureau consists of the Institute for Basic Standards, the Institute for Materials Research, the Institute for Applied Technology, the Institute for Computer Sciences and Technology, and the Office for Information Programs.

THE INSTITUTE FOR BASIC STANDARDS provides the central basis within the United States of a complete and consistent system of physical measurement; coordinates that system with measurement systems of other nations; and furnishes essential services leading to accurate and uniform physical measurements throughout the Nation's scientific community, industry, and commerce. The Institute consists of a Center for Radiation Research, an Office of Measurement Services and the following divisions:

Applied Mathematics — Electricity — Mechanics — Heat — Optical Physics — Nuclear Sciences[2] — Applied Radiation[2] — Quantum Electronics[3] — Electromagnetics[3] — Time and Frequency[3] — Laboratory Astrophysics[3] — Cryogenics[3].

THE INSTITUTE FOR MATERIALS RESEARCH conducts materials research leading to improved methods of measurement, standards, and data on the properties of well-characterized materials needed by industry, commerce, educational institutions, and Government; provides advisory and research services to other Government agencies; and develops, produces, and distributes standard reference materials. The Institute consists of the Office of Standard Reference Materials and the following divisions:

Analytical Chemistry — Polymers — Metallurgy — Inorganic Materials — Reactor Radiation — Physical Chemistry.

THE INSTITUTE FOR APPLIED TECHNOLOGY provides technical services to promote the use of available technology and to facilitate technological innovation in industry and Government; cooperates with public and private organizations leading to the development of technological standards (including mandatory safety standards), codes and methods of test; and provides technical advice and services to Government agencies upon request. The Institute consists of a Center for Building Technology and the following divisions and offices:

Engineering and Product Standards — Weights and Measures — Invention and Innovation — Product Evaluation Technology — Electronic Technology — Technical Analysis — Measurement Engineering — Structures, Materials, and Life Safety[4] — Building Environment[4] — Technical Evaluation and Application[4] — Fire Technology.

THE INSTITUTE FOR COMPUTER SCIENCES AND TECHNOLOGY conducts research and provides technical services designed to aid Government agencies in improving cost effectiveness in the conduct of their programs through the selection, acquisition, and effective utilization of automatic data processing equipment; and serves as the principal focus within the executive branch for the development of Federal standards for automatic data processing equipment, techniques, and computer languages. The Institute consists of the following divisions:

Computer Services — Systems and Software — Computer Systems Engineering — Information Technology.

THE OFFICE FOR INFORMATION PROGRAMS promotes optimum dissemination and accessibility of scientific information generated within NBS and other agencies of the Federal Government; promotes the development of the National Standard Reference Data System and a system of information analysis centers dealing with the broader aspects of the National Measurement System; provides appropriate services to ensure that the NBS staff has optimum accessibility to the scientific information of the world. The Office consists of the following organizational units:

Office of Standard Reference Data — Office of Information Activities — Office of Technical Publications — Library — Office of International Relations.

[1] Headquarters and Laboratories at Gaithersburg, Maryland, unless otherwise noted; mailing address Washington, D.C. 20234.
[2] Part of the Center for Radiation Research.
[3] Located at Boulder, Colorado 80302.
[4] Part of the Center for Building Technology.

U.S. DEPARTMENT OF COMMERCE
Rogers C. B. Morton, Secretary
NATIONAL BUREAU OF STANDARDS
Ernest Ambler, Acting Director

Order all publications from the Superintendent of Documents
U.S. Government Printing Office, Washington, D.C. 20402

The Secretary of Commerce has determined that the publication of this periodical is necessary in the transaction of the public business required by law of this Department. Use of funds for printing this periodical has been approved by the Director of the Office of Management and Budget through June 30, 1976.

JOURNAL OF RESEARCH of the National Bureau of Standards—A. Physics and Chemistry
Vol. 79A, No. 5, September–October 1975

Surface Films on Poly(oxymethylene) Single Crystals*

Janice Breedon Jones and P. H. Geil**

(June 30, 1975)

The deformation of single crystals of poly(oxymethylene) grown from 0.01 percent bromobenzene solution has been studied by deposition on a deformable substrate. Slight decoration of the crystal surfaces with gold prior to mechanical deformation of the composite reveals breaks in the gold which are displaced with respect to cracks in the underlying polymer crystals. These observations are interpreted to imply the existence of a very thin discrete film on the surface of the polymer crystals which can slip during deformation. Such a film might arise from polymer molecules adsorbed on the crystal surface.

Key words: Adsorbed polymer, deformation, fold surface, gold decoration, polymer crystals, poly(oxymethylene), surface layer.

In the course of some investigations [1][1] on the formation of microcracks in single crystals of poly(oxymethylene) (POM), some intriguing observations have been made which appear to shed some light on the nature of the fold surfaces of solution-grown crystals.

*An invited paper

**Present address: Case Western Reserve University, Department of Macromolecular Science, Cleveland, Ohio 44106

[1]Figures in brackets indicate the literature references at the end of this paper.

The crystals were of Delrin 500 grown by ambient cooling from 0.01 percent solution in bromobenzene. They were deposited on Mylar film to be stretched using the method first developed by Geil [2], and were lightly decorated with gold in a diffusion pump vacuum before being drawn. The crystals were stretched in air at room temperature or at 96 °C.

Figure 1 is an electron micrograph of some crystals which were gold decorated, drawn at room temperature,

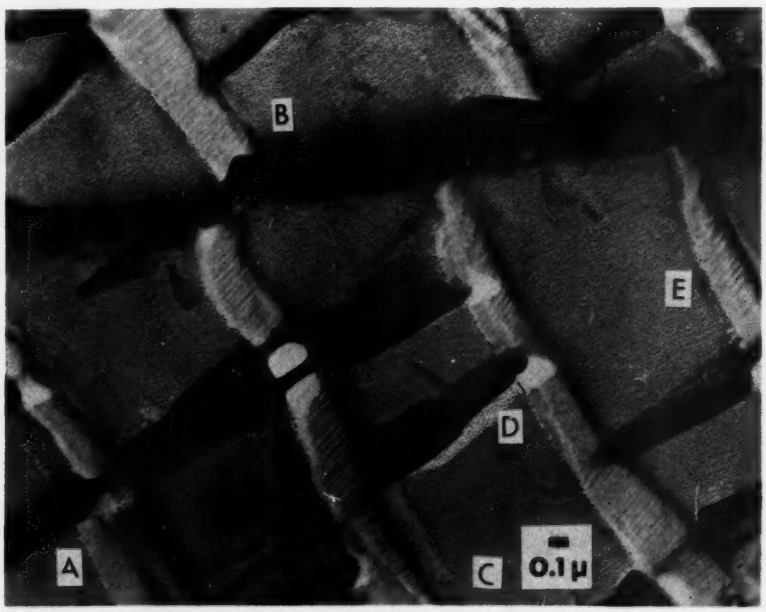

FIGURE 1. *POM single crystal gold decorated before draw and shadowed obliquely with* Pt/C *parallel to the draw direction after it was drawn.*

The draw direction is perpendicular to the cracks and parallel to the wrinkles in both figures.

and then shadowed obliquely with platinum/carbon to reveal the topography of the drawn crystal. In spite of the existence of well-separated gold particles on the surface, the gold has deformed as a separate layer. Only a few of the gold particles have been pulled out onto the fibrils bridging the cracks. The gold "layer" seems to have broken in a brittle manner at the microcracks, but the break in the gold is often displaced with respect to the actual crack. This is particularly conspicuous at the points marked with the letters. At point A, the gold layer is completely displaced from the crack, possibly even sagging into it. At point B, the gold appears to be hanging over the edge on one side of the crack, while not reaching the edge on the other side. At point C, a narrow strip of the gold layer has been bent off the main mass as the two edges separated. Estimation of the thickness of the layer supporting the gold was not possible. Where a shadow could be seen, it appeared to be cast mostly by the gold particles and was certainly several times shorter than that cast by single lamellae of spiral growths seen in other micrographs of the same preparation. Therefore, it is highly unlikely that the layer is simply an upper crystal lamella that is being displaced across the lower crystals.

Figure 2 is an electron micrograph of some crystals that were gold decorated and then stretched at 96 °C. Again the breaks in the gold are displaced with respect to the cracks, and the displacements are not all in the same direction. The breaks in the gold corresponding to cracks A and B are shifted toward each other. Also, cracks B and C, whose tips meet at a pleat, show opposite displacement of the gold. Also visible in the cracks (and to a lesser extent in those in fig. 1) is a diffuse darkening of the edges and fibrils which appears to be decoration by residual poly(acrylic acid) used in the preparation of the samples [1].

While not all cracks in all crystals showed this displacement of the gold particles, it was seen often enough to be a phenomenon that appears to be typical of these crystals. The evidence points to the existence of a discrete film on the fold surface which apparently can slip across it during deformation. The film may even be somewhat elastic, as suggested by the region in figure 2 where the film seems either to have shrunk or not to have stretched enough between two neighboring cracks. In other micrographs, regions could be seen in which some of the gold at both ends of a given fibril had been pulled noticeably toward, but never onto, the fibril. These observations all suggest that the film is flexible and coherent with a small amount of ductility.

The most likely explanation for this surface film is that it consists of adsorbed polymer molecules. This would account for the observed flexibility, coherence, and possible elasticity. That it might be cilia extending from the crystal seems unlikely because of the extent of the displacement and the fact that the displacement is always in the same direction on both sides of a crack. The possibility exists that the layer is some type of contamination introduced before or during the gold evaporation step. However, contamination such as pump oil from the vacuum system [3] would probably have such low molecular weight that it would either lack the coherence necessary for the effects seen in the micrographs.

Observations of an approximately 200 Å wide region at the edges of similar cracks in Penton and poly (4-

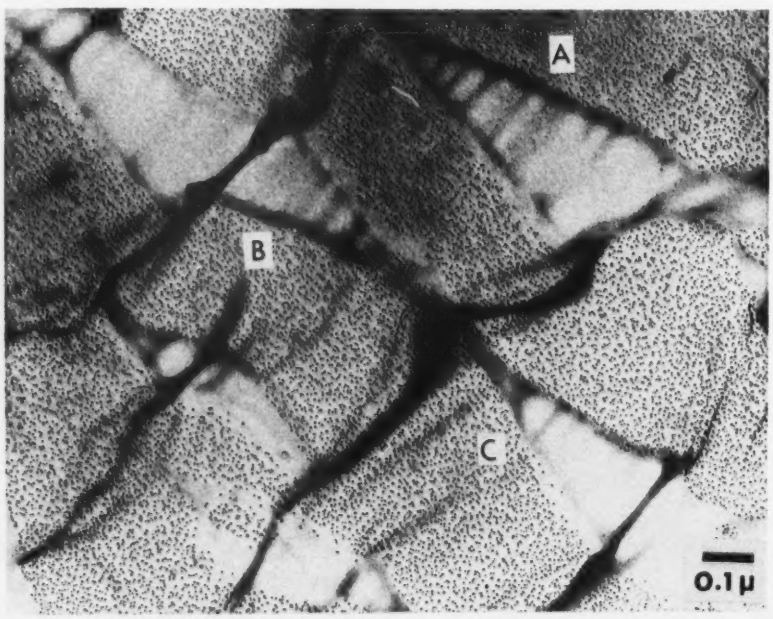

FIGURE 2. *POM single crystal gold decorated before draw at* 96 °C.

methyl pentene-1) crystals, which region has surface properties differing from the rest of the crystal [1], may be due to a surface film similar to that found for POM. In these preparations, the crystal appears to have been drawn out from underneath the film, thus exposing the fold surface.

Such a polymer film has been postulated by Lauritzen and Hoffman [4] and Hoffman, Davis, and Lauritzen [5] as part of some recent work on the theory of polymer crystallization. They suggest that before molecules are added onto the growth face of the crystal, they are first adsorbed onto the lateral and/or fold surfaces of the growing crystal, and then migrate across the surface to the growth sites. A film, possibly in equilibrium with the solution, of adsorbed molecules that never reached the growth face would likely be left on the surface of the crystal. The film could also be chains that for some reason were rejected from the growing crystal, or adsorbed chains that play no part in the crystallization process. Also, the possibility cannot yet be completely ruled out that polymer molecules were deposited onto the fold surface (and Mylar) while the crystal suspension was drying on the Mylar before deformation. An attempt was made to find such a film at cracks in a thin layer of brittle carbon that had been evaporated onto some Mylar before crystals were deposited and drawn. The carbon formed large cracks across which both the crystals and any film between them from the deposition process would be drawn. However, no slippage of the gold layer relative to the cracks was seen in the regions between the crystals, suggesting that the film only exists, or at least only is mobile, on the fold surfaces of the crystals.

While insufficient evidence exists at this time to determine the origin of the film, it does seem to be polymeric in nature. One puzzling aspect of it, however, is its apparent rigidity. The film is not totally rigid, as evidenced by the observations in which there was seen some pulling of the particles toward the fibrils, but it is rigid enough to have shifted always in the same direction on opposite sides of a given crack. This rigidity persists up to at least 96 °C in POM, well above T_g (while there is some question as to the exact T_g for POM, it is well below room temperature [6]).

While further study of this surface film is needed, these preliminary results suggest the presence of an adsorbed polymeric film which could have many ramifications in other areas such as the determination of percent crystallinity or the nature of the molecular folding process. Several of these ramifications are described in the accompanying paper [7]. Further work in these areas may add greatly to our understanding of polymer morphology.

References

[1] Breedon, J. E., Masters Thesis, Case Western Reserve University (1975).

[2] Geil, P. H., Polymer Single Crystals (Wiley Interscience, New York, 1963).

[3] Frederick, P. S., and Hruska, S. J., J. Appl. Phys. **45**, 3215 (1974).

[4] Lauritzen, J. I., Jr. and Hoffman, J. D., J. Appl. Phys. **44**, 4340 (1973).

[5] Hoffman, J. D., Davis, G. T., and Lauritzen, J. I., Jr. in Treatise on Solid State Chemistry, N. B. Hannay ed. (Plenum Press, New York, Vol. **3** Chapter 6, 1976).

[6] Sauer, J. A., Richardson, G. C., and Morrow, D. R., J. Macromol. Sci. Revs. Macromol. Chem. **C9**, 149 (1973).

[7] Hoffman, John D., and Davis, G. Thomas, J. Res. Nat. Bur. Stand. (U.S.), **79A** (Phys. and Chem.), No. **5** (Sept.–Oct. 1975).

(Paper 79A5–861)

JOURNAL OF RESEARCH of the National Bureau of Standards—A. Physics and Chemistry
Vol. 79A, No. 5, September–October 1975

On the Origin of the Amorphous Component in Polymer Single Crystals and the Nature of the Fold Surface

John D. Hoffman and G. Thomas Davis

Institute for Materials Research, National Bureau of Standards, Washington, D.C. 20234

(June 30, 1975)

A model for the surface of folded-chain polymer single crystals is presented in which the "amorphous" phase is composed of polymer molecules physically adsorbed on surface sites of a fairly regularly folded surface. The evidence for the presence of an amorphous phase in polymer single crystals is reviewed briefly as well as the evidence for regular folding and adjacent reentry. The proposed model would allow simultaneous acceptance of the evidence for both an amorphous layer and a surface composed of regularly folded molecules; such evidence was heretofore contradictory. Experimental evidence for such a model is discussed and some predictions are made concerning the properties of such an adsorbed layer.

Key words: Adsorbed layer; amorphous component; fold surface; polymer crystals; regular folds.

The objective of this note is to present a possible resolution to the problem of "regular" folds *versus* an "amorphous" layer as a model for the surface of a chain-folded polymer single crystal. There is a considerable body of experimental evidence (e.g., density and heat of fusion data) that points to the existence of an "amorphous" layer that is in some way associated with the fold surface in single crystals. This has been widely interpreted as leading inexorably to the conclusion that most of the folds are either long and loose, or that nonadjacent reentry with intervening loops occurs on a large scale, or both (fig. 1A). On the other hand, there also exists an equally credible body of experimental evidence, based mainly on crystallographic, spectroscopic, and morphological observations, that suggests that certain polymer single crystals exhibit rather regular folding with mostly adjacent reentry (fig. 1B). From this it is frequently concluded that there is little place for the amorphous layer suggested by the density and heat of fusion data. Thus, acceptance of the aforementioned conclusions leads to a paradox, since "regular" folding and the presence of an "amorphous" component have been hitherto regarded as mutually exclusive or contradictory concepts. In the present work we shall suggest that the amorphous layer can in fact exist in most (but perhaps not all) cases, and that when it occurs that it is to a considerable extent the result of polymer molecules that are *physically adsorbed* on a fairly regularly folded surface (fig. 1C). The adsorbed layer is expected to resemble a two-dimensional random coil (or a highly flattened three-dimensional one) with "loops" or traverses between the points of attachment on the fold surface, and may be detachable under appropriate circumstances. If this suggestion is correct, the paradox is essentially resolved, since then neither the evidence for an amorphous layer nor that for rather regular folding with mostly adjacent reentry need be rejected.

Lauritzen and Hoffman were originally led to the suggestion of an adsorbed layer on polymer crystals by analysis of growth rate and lamellar thickness data [1].[1] Parameters resulting from the best fit of the data could be interpreted in terms of a model where a three-dimensional random coil in the subcooled liquid or solution state was adsorbed on the lateral surface as a quasi two-dimensional coil, the segments of which then migrated across that surface to the site of crystallization. This led to the subsequent prediction that a broadly similar adsorption effect probably took place on the fold surface [2].

Before proceeding with the main discussion, we briefly outline the experimental evidence leading to the apparently contradictory conclusions noted above regarding the fold surface. In the interest of brevity, we concentrate on polyethylene, and even this case is not treated exhaustively.

The density of polyethylene single crystals formed from solution has been studied extensively. Despite some early data showing near-perfect single crystal densities [3], the main body of results [4–6] in the literature leave little doubt on two points. One is that the density is well below that of a "perfect" crystal predicted from unit cell dimensions ($\rho_{25°C} = 1.00$ g/cm^3)

[1] Figures in brackets indicate the literature references at the end of this paper.

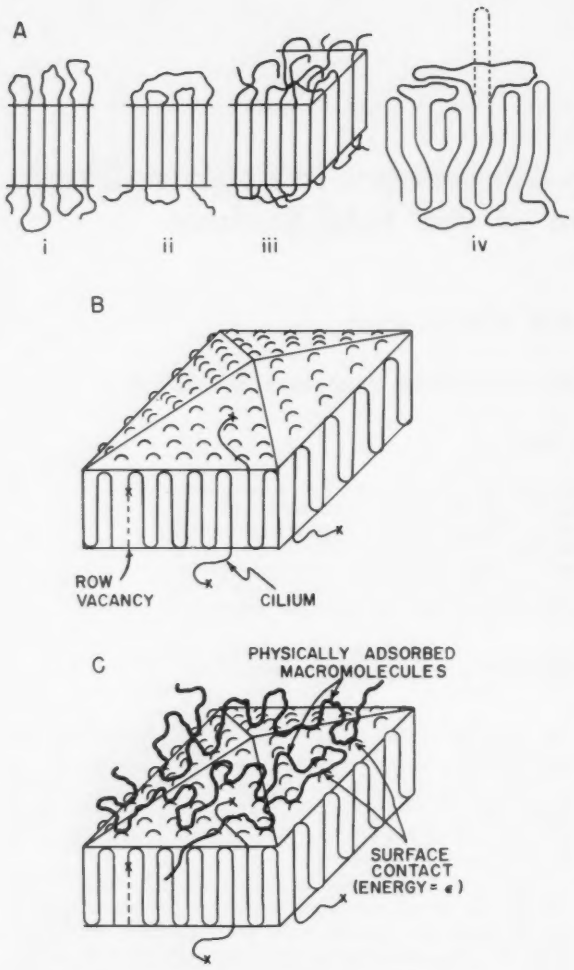

FIGURE 1. *Models for polymer single crystals (schematic).*

A. Models with loose loops where amorphous phase is part of the fold zone: (i) adjacent reentry with loose loops in growth plane (see ref. [11]), (ii) nonadjacent reentry with loops in growth plane (see ref. [13]), (iii) nonadjacent reentry, commonly known as the "switchboard" model (see ref [14]), (iv) mostly adjacent reentry with some loose folds and some "buried" folds (see ref. [12]).

B. Model with regular folds and adjacent reentry forming a smooth or slightly rough fold surface with no amorphous phase.

C. Proposed model with mostly adjacent reentry and smooth or slightly rough fold surface and same crystal defects as in B, but with an amorphous phase that consists mostly of polymer molecules that are physically adsorbed on sites on the fold surface.

and the other is that the density increases as the crystals become thicker [7–10]. Several models for a noncrystalline phase associated in some manner with the fold surface have been proposed to account for this density deficiency. Zachmann [11] has considered loose loops between adjacent crystal sequences whereas Keller et al. [12] have attributed it to a combination of loose loops and "buried" folds. A surface region composed of long cilia and loose loops resulting from nonadjacent reentry within the growth plane was suggested by Frank [13] and a more or less random reentry of molecules into the crystal has been advanced by Flory [14]. (The presence of a density defect, however, does not necessarily prove the existence of extensive nonadjacent reentry or a large number of loose loops.) We note that the density of the single crystals of a given overall thickness has been reported to depend upon the solvent from which the crystal was grown [9], e.g., crystals from *n*-hexadecane were consistently about 0.004 g/cm^3 more dense than those of equal thickness grown from tetralin and decalin. This implies that the nature of the amorphous surface layer is dependent on the solvent. It has also been suggested that the density of the crystals may increase slightly with time when stored in the presence of solvent [4].

Studies of the heat of fusion of polyethylene single crystals have also been made which point to the conclusion that the observed heat of fusion for single crystals is always substantially below the theoretical value for a crystal of infinite thickness ($\Delta h_f \cong 293$ J/g) [15–17]. A small part of the reduced heat of fusion can be explained by the heat stored in the folds [2] (*circa* 15 J/g) but the deficiency is still so large as to clearly suggest the existence of a noncrystalline component that is in some way associated with the fold surface of the crystal. More recently, low angle x-ray intensity measurements on single crystal mats of polyethylene have been interpreted in terms of a two-phase model [18, 19]. Also, the low angle x-ray spacing of single crystal mats has been shown to increase and then decreases reversibly upon the addition and subsequent removal of solvents [20], implying the existence of an amorphous zone capable of being swollen by solvent. A more detailed study [21] has shown that the magnitude of the increase in low-angle spacing depends upon the molecular weight of the polymer and the crystallization conditions, from which it may be inferred that the nature of the amorphous surface layer depends upon these variables. A slightly rough fold surface could account for part of the density deficiency but it cannot account for all of the other observations.

The above is sufficient to establish the necessity of considering the existence of an amorphous layer of some type on single crystals of polyethylene. Studies on other polymers are sufficient in scope to establish the phenomenon as a quite general one. For the sake of brevity, we have omitted evidence based on relaxation measurements (NMR, dielectric, and mechanical).

Consider now the evidence for fairly "regular" folding in polymer single crystals. By "regular" we mean folding with mostly adjacent reentry and without a substantial fraction of long loop-like folds. Certainly some "mistakes" such as occasional nonadjacent reentry in the growth plane must be allowed, as well as some defects such as row vacancies and cilia (figs. 1B and 1C). Also, a slight roughness of the fold surface including a few "buried folds" may be permitted, but nothing to the extent shown in figure 1A is intended under the definition of "fairly regular."

Geil [22] has summarized the crystallographic and morphological evidence of many workers, notably Bassett, Frank, and Keller, and Reneker and Geil, and Niegisch and Swan, for essentially regular folding in polyethylene single crystals of various types. Al-

though many cases are discussed, the evidence is epitomized by his discussion of hollow pyramidal single crystals of polyethylene. The best way to explain the existence of these well-known sectorized single crystals is the staggered regular packing of chain folds by analogy with a terra cotta roof. It would seem practically impossible to explain the details of the crystal structure and morphology of such crystals with any of the models shown in figure 1A. There is nothing inconsistent with the explanations summarized by Geil in case the rather regular fold surface were subject to an adsorbed layer of polymer molecules: all that would be added would be the amorphous layer suggested by other measurements.

Further evidence for rather regular chain folding with predominantly adjacent reentry lies in the nature of the fracture in different sectors of the same crystals [23] and the slight difference in crystallographic spacing in adjacent sectors of the same crystal [24]. Clear evidence for mostly adjacent reentry in polyethylene single crystals has been given by Bank and Krimm [25] based on an analysis of the IR spectra of mixed crystals of deuterated and hydrogen bearing chains. Finally, we mention the work of Holland and Lindenmeyer [26], who found dislocation networks between polyethylene single crystals, and the more extensive work of Sadler and Keller [27] who showed the phenomenon to be specific for molecular weights below 3000. Dislocation networks provide clear evidence for crystallographic contact between layers and hence regularity of the folds—in this case it is clear that no substantial amorphous layer intervenes between the crystals. (Subsequently, we shall suggest possible reasons for the virtual absence of an amorphous layer in material of sufficiently low molecular weight.) In any case, it is clearly not admissible to ignore the sum of the evidence for fairly regular folding in polyethylene crystals formed from dilute solution.

Accordingly, if the experimental evidence for an amorphous layer and for fairly regular folding is simultaneously accepted, one is led to the model shown in figure 1C which depicts a crystal with a fairly regular fold surface and an independent surface layer composed of physically adsorbed polymer. We may now ask if there is any evidence for such a model.

Direct experimental evidence for the existence of a thin mechanically detachable layer on single crystals of several polymers has been found by Jones (nee Breedon) and Geil [28, 29]. (See preceding article in this journal where details are given for the case of poly(oxymethylene).) From this work there is good reason to believe that single crystals of a number of polymers of normal molecular weight possess a mechanically detachable layer on their fold surfaces. Accordingly, it is believed that the model shown in figure 1C is a reasonable representation of the situation. The adsorbed molecules on the fold surface provide the amorphous component suggested by heat of fusion and density measurements among other results, and simultaneously provide the material that strips off the fold surface during fracture. The underlying fold surface itself could be fairly regular (including mostly adjacent reentry) in keeping with the requirements of crystallographic, morphologic, and spectroscopic evidence. The proposed representation is a true "two-phase" model with a quite abrupt phase boundary between the two phases (as suggested by Fischer et al. [18] and as shown experimentally by Strobl and Müller [19]).

We turn now to certain practical and theoretical considerations relating to adsorption of polymer molecules on surfaces. Considerable insight may be obtained by sketching out what is known about polymer adsorption on foreign substrates, since little revision is needed to adapt this information to the case of adsorption of molecules on chain folds consisting of the same monomer units.

Theoretical calculations by various workers [30–33] show that an isolated polymer molecule will form something that roughly resembles a two-dimensional or an appreciably flattened three-dimensional random coil on a foreign substrate. Each single surface contact has an energy taken to be ϵ. Traverses or "loops" intervene between runs of adsorbed segments. Defining θ as the fraction of polymer segments adsorbed for each molecule, statistical mechanical calculations have been made giving θ as a function of ϵ/kT for various chain lengths. In general, the results show an increasing θ with increasing values of ϵ/kT, as shown schematically in figure 2A. Although somewhat dependent on the specifics of the model chosen [33], it is characteristic of such calculations to show a low value of θ for $|\epsilon/kT| << 1$, and a relatively high value of θ for values of $|\epsilon/kT| \geq 1$. In the case of a monomer unit attaching itself at some appropriate point on a chain fold, where this point represents a surface site, values of ϵ that are roughly comparable to kT do not seem unreasonable. Even a low θ, arising from a low value of ϵ/kT, can involve a considerable amount of amorphous polymeric material being associated with the fold surface; in this case most of the mass of the amorphous material will be in loops between occupied surface sites. The total amount of the material on the surface will depend on the molecular weight and the crystallization conditions, including the solvent from which the crystal was formed, so some variation in the average thickness of the adsorbed layer is to be expected. In broad aspect, this probably underlies the differences noted earlier in the amorphous fraction detected in polyethylene single crystals crystallized from different solvents [9] and the dependence of the amount of swelling on molecular weight and temperature of crystallization [20, 21].

Experiments on the rate of adsorption and desorption of polymer molecules on foreign substrates [34, 35] show two important facts that are relevant to the suggested model shown in figure 1C. First, the rate of adsorption is rapid compared to the rate of desorption. In the case of polystyrene on a chromium surface the rate of desorption is extremely slow: in some cases 80 percent of the original adsorbed polymer still remains after 3 weeks. The basic reason for the low rate of desorption is that, even when ϵ is rather small, all the points of contact have to be removed in the period of time required for diffusion away from the

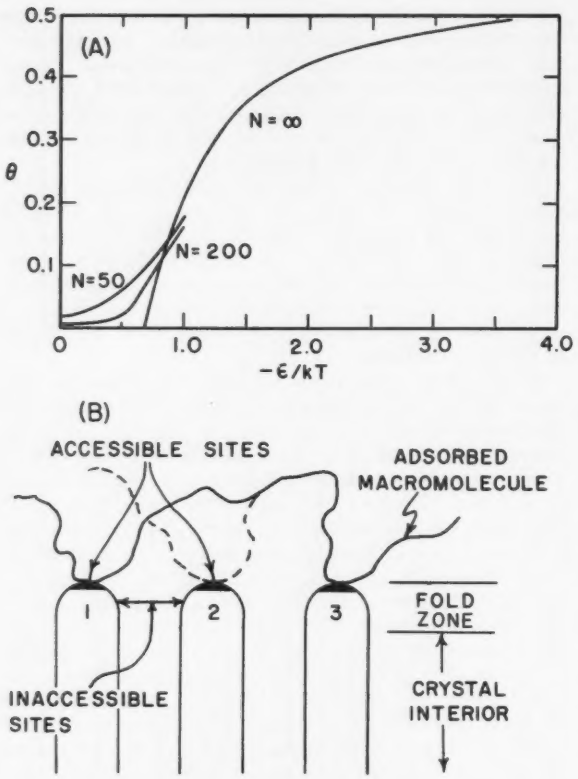

FIGURE 2. *Physical adsorption of macromolecules on surfaces (schematic).*

A. Fraction of chain segments θ adsorbed at the surface as a function of $-\epsilon/kT$. The quantity ϵ is the energy of attachment per chain segment and N is the number of segments in the chain (adapted from ref. [31]).

B. Model showing possible origin of reduced mobility of molecules adsorbed on fold surface.

surface, which is a statistically improbable event [34]. As applied to the present situation, these results imply that the adsorbed layer on the chain fold surface will very likely be highly persistent for material of moderate and high molecular weight. This leads us to the second point, which is that the rates of adsorption and desorption are a function of molecular weight [35]. When expressed as mass per unit area, the lower molecular weight polymer adsorbs more slowly and desorbs more rapidly than does the higher molecular weight. Accordingly the adsorbed surface layer on a fold surface may be tenuous in specimens of low molecular weight. (In such cases cilia are expected to be more numerous, and contribute to the "amorphous" character of the crystal.) In moderate and high molecular weight material, the adsorbed layer will have more segments in contact with the surface and desorb much more slowly. This may explain the fact that dislocation networks, which require intimate contact between two crystals over a considerable area, are found in low molecular weight polyethylene single crystals, but not in ones of moderate to high molecular weight [27].

It has been noted earlier [2] that the adsorbed layers on the *lateral* surface are apparently mobile, and move across that surface to the site of crystallization. We must now raise the question as to why the material postulated to exist on the fold surface does not share the same fate as that adsorbed on the lateral surface, namely, rapid crystallization. We speculate that a reduced surface mobility of the polymer molecules on the fold surface may be explained as follows. Referring to figure 2B, it is seen that it is reasonable to propose that a considerable distance intervenes between "allowed" sites for attachment of the adsorbed polymer molecule; movement which results in the molecule going from site 1 to site 2 requires total desorption because of the intervening "inaccessible" sites resulting from spatial considerations. Because the sites are much closer together on the lateral surface, the barriers to be surmounted for mobility could be considerably smaller on this surface. (The mobility on the lateral surface in bulk polymers varies as exp $[-U^*/R(T-T_\infty)]$ where $U^* \cong 1500$ cal (6275 J) and $T_\infty \cong T_g - 30°$) [2]. We note that our basic concept here would eventually permit migration to a lateral surface and some crystallization of the layer adsorbed on the fold surface. However, it is reasonable to expect this to be very slow (except in low molecular weight material) because of the postulated reduced mobility of the molecules adsorbed on the fold surface, and the large distances over which transport of molecules would have to take place to reach the lateral surface where crystallization would take place. Such a slow migration followed by crystallization may account for the increase of density found in aged preparations of single crystals [4]. It should be mentioned that the presence of long cilia [36] could also account for many of the observations described above but one would not expect such a layer to be easily detached as in the fracture experiments nor removable by prolonged storage in solvent.

Though it is necessarily highly speculative, some comments on how the adsorbed amorphous surface layer might be reduced or even removed are in order. It is already clear from the work of Jones and Geil that portions of the layer can be removed in fracture experiments, but the area deprived of the amorphous layer is small in these cases, and we therefore concentrate on techniques that might reduce or remove the layer on a larger scale. It has already been remarked that certain solvents yield higher density crystals, implying the presence of less amorphous material. Crystallization from extremely dilute solution for long periods of time might also yield crystals with less adsorbed material. Beginning with such crystals, it might be possible by long extraction in proper solvents below the dissolution temperature of the crystal to dissolve the amorphous layer and remove it or eventually crystallize it by prolonged storage. It is conceivable that the presence of appropriate liquids may tend to render the amorphous layer on the fold surface more mobile, and allow it to crystallize. Progress in removing the amorphous layer could be detected by density or heat of fusion measurements, or in extreme cases, by looking for dislocation

networks. Removal of the adsorbed layer by chemical attack is problematical, since one must expect the strained bonds in the folds to also be ruptured at a rather early time. However, the molecular weight of the adsorbed layer might be reduced by brief chemical attack in a manner sufficient to allow its removal by other means.

Consider now the properties to be expected of the adsorbed layer on the fold surface. It need not be of constant amount and density in all preparations but may depend on molecular weight, crystallization temperature, solvent used and time of storage. In the presence of liquids of good solvent power, the layer may be solvated and expanded. In the presence of poorer solvents, it should be less expanded and rather flattened onto the fold surface. In the dried or contracted state, the layer is expected to have a density not far from that of the corresponding subcooled liquid or glassy state. In relaxational studies, the "loops" between the point of contact should exhibit the mobility and chain motions typical of short-range motions at low temperatures in the glassy state (i.e., the γ_a transition) [37], but it is impossible to state at this juncture whether or not a true glass transition (i.e., a β relaxation) with a typical T_g should appear; we would anticipate that any T_g that did appear would be weak and have abnormal characteristics. Few, if any, single crystal preparations show a β relaxation in dynamic mechanical or dielectric measurements.

A slow increase of density and heat of fusion on prolonged storage in the presence of solvent may be found, resulting from a low but finite surface mobility with subsequent crystallization. In general, the hypothesis of an adsorbed surface layer on a fairly regular fold surface offers a vehicle for alternative explanations of a number of phenomena observed for polymer single crystals.

Although this paper deals primarily with the possibility of an adsorbed layer on polymer single crystals, a number of the considerations may apply to polymers crystallized from the melt. This possibility is discussed in a recent review [2], where it is brought out that an adsorbed layer may account for a considerable portion of the amorphous content $\alpha = 1 - \chi$ in highly crystalline specimens ($\chi \cong 0.85$ to $\chi = 0.90$). Amorphous material in concentrations higher than $\alpha \doteq 0.1$ to 0.15 or so may be ascribed at least in part to the presence of interlamellar entanglements that prevent crystallization on a large scale. DiMarzio and Rubin [32] have carried out calculations for the adsorption of molecules between two parallel plates. A long molecule frequently adsorbs on both plates, producing an amorphous link between them. The analogous situation may occur in polymers crystallized from the melt, leading to an increased amorphous content.

References

[1] Lauritzen, J. I., Jr., and Hoffman, J. D., J. Appl. Phys. **44**, 4340 (1973).

[2] Hoffman, J. D., Davis, G. T., and Lauritzen, J. I., Jr., in Treatise on Solid State Chemistry, N. B. Hannay, Ed., (Plenum Press, New York, Vol. 3, Chapter 6, 1976).

[3] Kawai, T., and Keller, A., Philos. Mag. **8**, 1203 (1963).

[4] Martin, G. M., and Passaglia, E., J. Res. Nat. Bur. Stand. (U.S.), **70A** (Phys. and Chem.) No. 3, 221–224 (May-June 1966).

[5] Blackadder, D. A., and Lewell, P. A., Polymer **9**, 249 (1968).

[6] Sharma, R. K., and Mandelkern, L., Macromolecules **2**, 266 (1969).

[7] Fischer, E. W., and Lorenz, R., Kolloid Z. Z. Polym. **189**, 97 (1963).

[8] Kitamaru, R., and Mandelkern, L., J. Polym. Sci. A-2, **B**, 2079 (1970).

[9] Nakajima, A., Hayashi, S., Korenaga, T., and Sumida, T., Kolloid Z. Z. Polym. **222**, 124 (1967).

[10] Davis, G. T., Weeks, J. J., Martin, G. M., and Eby, R. K., J. Appl. Phys. **45**, 4175 (1974).

[11] Zachmann, H. G., Z. Naturforschg. **19A**, 1937 (1964).

[12] Keller, A., Martuscelli, E., Priest, D. J., and Udagawa, Y., J. Polym. Sci., A-2, **9**, 1807 (1971).

[13] Frank, F. C., referred to by A. Keller, Kolloid Z. Z. Polym. **231**, 386 (1969).

[14] Flory, P. J., J. Am. Chem. Soc. **84**, 2857 (1962).

[15] Fischer, E. W., and Hinrichsen, G., Polymer **7**, 195 (1966); Kolloid Z. Z. Polym. **213**, 93 (1966).

[16] Hendus, H., and Illers, K. H., Kunststoffe **57**, 193 (1967).

[17] Mandelkern, L., Allou, A. L., Jr., and Gopalan, M., J. Phys. Chem. **72**, 309 (1968).

[18] Fischer, E. W., Goddar, H., and Schmidt, G. F., J. Polym. Sci. **B5**, 619 (1967).

[19] Strobl, G. R., and Müller, N., J. Polym. Sci. Polym. Phys. Ed., **11**, 1219 (1973).

[20] Udagawa, Y., and Keller, A., J. Polym. Sci. A-2, **9**, 437 (1971).

[21] Ergöz, E., and Mandelkern, L., J. Polym. Sci. **B10**, 631 (1972).

[22] Geil, P. H., Polymer Single Crystals, Interscience, New York, pp. 125–139 (1963).

[23] Lindenmeyer, P. H., J. Polym. Sci. **C1**, 5 (1963).

[24] Bassett, D. C., Philos. Mag. **12**, 907 (1965).

[25] Bank, M. I., and Krimm, S., J. Polym. Sci. A-2, **7**, 1785 (1969).

[26] Holland, V. F., and Lindenmeyer, P. H., J. Appl. Phys. **36**, 3049 (1965).

[27] Sadler, D. M., and Keller, A., Kolloid Z. Z. Polym. **239**, 641 (1970) and **242**, 1081 (1970).

[28] Jones, J. B., and Geil, P. H., J. Res. Nat. Bur. Stand. (U.S.), **79A** (Phys. and Chem.), No. 5, 609–611 (Sept.–Oct. 1975).

[29] Breedon, J. E., Crack Formation in Polymer Single Crystals, Masters Thesis, Case Western Reserve Univ. (1975).

[30] Silberberg, A., J. Chem. Phys. **46**, 1105 (1967).

[31] DiMarzio, E. A., and McCrackin, F. L., J. Chem. Phys. **43**, 539 (1965).

[32] DiMarzio, E. A., and Rubin, R. J., J. Chem. Phys. **55**, 4318 (1971).

[33] Rubin, R. J., J. Chem. Phys. **43**, 2392 (1965).

[34] Stromberg, R. R., Grant, W. H., and Passaglia, E., J. Res. Nat. Bur. Stand. (U.S.), **68A** (Phys. and Chem.), No. 4, 391–399, (July-Aug. 1975).

[35] Grant, W. H., Smith, L. E., and Stromberg, R. R., to be published in Discuss. Faraday Soc. (1975).

[36] Sanchez, I. C., and DiMarzio, E. A., J. Chem. Phys. **55**, 893 (1971).

[37] Hoffman, J. D., Williams, G., and Passaglia, E., J. Polym. Sci. **C14**, 173 (1966).

(Paper 79A5–862)

JOURNAL OF RESEARCH of the National Bureau of Standards—A. Physics and Chemistry
Vol. 79A, No. 5, September–October 1975

Some Thermodynamic Properties of Bromobenzene from 0 to 1500 K*

Joseph F. Masi and Russell B. Scott*****

(June 17, 1975)

Measurements were made of the heat capacity of crystalline and liquid bromobenzene from 11 to 300 K, of the triple point and heat of fusion at the triple point and of the heat of vaporization at one temperature. The adiabatic calorimeter used was precise over most of its range to ±0.1 percent; the purity of the sample was 99.998 mol percent. The triple point of pure bromobenzene is 242.401 K (−30.749 °C) ± 0.010°; the enthalpy and entropy of fusion are, respectively, 10702 ± 5 J mol^{-1} and 44.150 ± 0.022 J K^{-1} mol^{-1}. The heat and entropy of vaporization at 293.00 K are, respectively, 43 963 ± 60 J mol^{-1} and 150.0 ± 0.2 J K^{-1} mol^{-1}. Tables are given for the thermodynamic functions of the condensed phases from 0 to 300 K; the functions for the ideal gas from 100 to 1500 K, calculated from spectroscopic and molecular data using statistical mechanical methods, are also tabulated. The entropy of the ideal gas at 293.00 K and one atmosphere, from statistical mechanics, is 323.63 J K^{-1} mol^{-1}; the same quantity from the experimental measurements (third law) is 323.73 J K^{-1} mol^{-1}. No anomalies or additional transitions were observed.

Key words: Bromobenzene; calorimetry; enthalpy; entropy; Gibbs energy; heat capacity; heat of fusion; heat of vaporization; thermodynamic properties, triple point.

1. Introduction

The experimental work reported in this paper was carried out at the National Bureau of Standards in 1945, as part of a program supported by the Office of Rubber Reserve. The calculations of results were not completed, and the work was never reported, both because of the pressure of more urgent research, and because the desired inclusion of ideal-gas properties was not possible with the incomplete and controversial molecular data available at that time.

Although the literature on the physical and molecular properties of bromobenzene is voluminous, there has been reported only one set of heat capacity measurements [1][1] over a wide range of temperature. Since these extended no lower than 90 K, and were performed by a method which is inherently less accurate than the adiabatic calorimeter, it was thought desirable to make a complete set of measurements of thermal properties of the condensed phases of bromobenzene from room room temperature down to near 11 K, these limits being imposed by the precise adiabatic calorimetry apparatus then available.

Measurements were made of the heat capacity of solid and liquid bromobenzene, the triple point, the heat of fusion at the triple point, and the latent heat of vaporization at one temperature (293 K). Recently these measurements have been smoothed, adjusted to more modern units and scales, and combined with a new calculation of ideal-gas properties to create the consistent set of thermodynamic properties presented here.

*An invited paper.
**Present address: Air Force Office of Scientific Research, Bolling Air Force Base, Washington, DC 20332.
***Deceased.
[1] Figures in brackets indicate literature references at the end of this paper.

2. Experimental Detail

2.1. Calorimetric Apparatus

The identical calorimetric apparatus described in great detail by Scott, Meyers, Rands, Brickwedde, and Bekkedahl [2] was used for all the measurements on bromobenzene. Only a brief resumé need be given here. The copper sample container (the calorimeter proper), with its heater and calibrated platinum resistance thermometer, was suspended by a long, vertical, rigid Monel tube from a valve exposed to ambient conditions. Thus the calorimeter could be evacuated and samples could be introduced and removed by vaporization without disturbing the assembly. The copper radiation shield surrounding the calorimeter had three separate control heaters on its surface, and two more were used for the tube above the calorimeter and for the bundle of electrical leads. A brass can, connected to a high-vacuum system, enclosed the calorimeter and shield. This can was in turn immersed in a Dewar which contained appropriate coolants or baths for the various temperature regions investigated. For the lowest temperature region, a multiple Dewar system was used. The inner Dewar was filled with liquid hydrogen, and the pressure above it was reduced by a high-capacity pump to less

than that of the triple point of hydrogen. An outer Dewar contained liquid air at ambient pressure.

The whole apparatus was designed for rapid temperature equilibration within the calorimeter, rapid response in the manual adiabatic control system, nearly complete thermal isolation of the calorimeter from its surroundings, and precision and accuracy in the measurement of temperature and electrical energy. The temperatures were determined to a precision of one millidegree over most of the range; time intervals were recorded with an accuracy of one hundredth of a second; and the voltage and current of the steady DC power supply were measured to one-tenth millivolt and one microampere, respectively. The various electrical instruments had been recently calibrated by the Electricity Division of the National Bureau of Standards. Details may be obtained by consulting reference [2].

2.2. Sample

A quantity of distilled bromobenzene was furnished through the kindness of Dr. D. R. Stull of the Dow Chemical Company. About one liter of this material was redistilled at atmospheric pressure using a column 75 cm long packed with stainless steel helices and fitted at the head with a platinum resistance thermometer. The change of temperature during the distillation followed closely the change in barometric pressure, giving no indication of fractionation; nevertheless, only the middle third of the distillate was used for further purification. The latter was accomplished by four successive freezings and meltings in vacuum; the portions of material (20–30 ml) which remained unfrozen or were the first to melt, each time, were discarded without breaking the vacuum. The remaining 75 ml (approximately) of purified material were transferred to a clean, evacuated weighing container and subsequently vaporized into the evacuated calorimeter vessel. The mass of the sample was 104.4904 g.

The purity of the sample is discussed below (sec. 2.4) in connection with the triple-point measurements. It was so high that chemical analyses could have added no useful information, and none were made.

2.3. Heat Capacity

Measurements of the heat capacity of the calorimeter plus sample were carried out in the usual manner by obtaining ratios of measured increments of added electrical energy to the resulting temperature increments. The temperature increments used were of the order of ten degrees over most of the range and as low as two degrees in the region below 30 K.

A total of 89 observations of $\Delta Q/\Delta T$, in eleven "runs," were made. These were corrected to dQ/dT by the method of Osborne, Stimson, Sligh, and Cragoe [3] wherever necessary; the maximum correction was 0.3 percent for two measurements at very low temperature, with most corrections amounting to less than a few hundredths percent. All of the energy values have been converted from the "international" units, in which the measuring instruments were calibrated, to the presently used (absolute) joule (1 international joule = 1.000165 (absolute) joules); likewise, mean temperatures were changed slightly to correspond with the International Practical Temperature Scale of 1948 [4] above 90 K, and to the NBS-1955 provisional scale (numerically 0.01° lower than the NBS-1939 scale [5]) below 90 K. Other possible corrections, such as for impurities or for pre-melting of the solid, were calculated to be negligible.

The differences between the observed values of $C = dQ/dT$ and values calculated from empirical functions of temperature (two for solid bromobenzene, overlapping in the region of 35 K, and one for the liquid) were plotted on large scale and smooth curves drawn through them. From these functions and the corresponding difference curves, tables of C at closely spaced equal temperature intervals were constructed, then smoothed by a 9-point smoothing formula [6]. The deviations of the observed values from the smoothed table are plotted against the mean temperatures of the observations in figure 1. In the figure, lines are used to connect the observations within a run. It is seen that, with the exception of three inexplicably low values, the measurements are precise to about 0.1 percent or better.

A normal procedure would have been to make measurements also of the heat capacity of the calorimeter containing a very small quantity of bromobenzene, over the entire temperature range, so that the two sets of measurements could be subtracted with little or no correction for vapor. This procedure was not followed because time could be saved by using an already smooth and accurate table of heat capacities of the completely empty calorimeter from 90 to 300 K [7], and because it was estimated that the vapor correction would be extremely small and amenable to precise calculation. Therefore, after all sample had been removed, heat capacity measurements were made on the calorimeter itself from 14 to 95 K. After corrections were made for curvature and for a few torr pressure of helium added to promote rapid thermal equilibrium, the observed values were used to form a smooth table at closely spaced equal temperature intervals. This table was found to connect smoothly with that above 90 K. Deviations of observed heat capacity of the empty calorimeter from the smooth table were smaller than in the case of the calorimeter plus sample, there being none greater than 0.1 percent of net heat capacity down to 50 K, and none as large as one percent, even at the lowest temperature of measurement.

This table was converted from international to absolute joules and shifted by 0.01 K because of the newer temperature scales mentioned above. Values obtained from this table by 4-point Lagrangian interpolation were then subtracted from the observed values of C (calorimeter plus sample); the differences were converted to molar units, using a molecular weight calculated from the most recent atomic weights [8], and are listed as C_{net} in table 1. These results are plotted in figure 2, to indicate the shapes of the solid and liquid heat capacity curves. It will be noted that run 4 is missing; only fusion data were obtained from it.

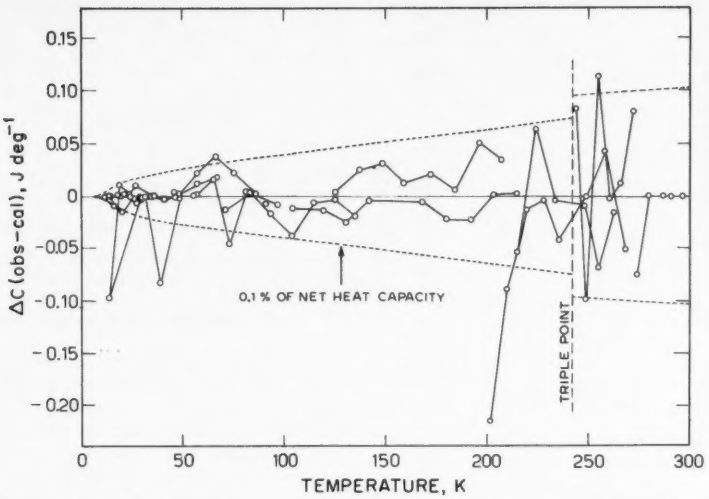

FIGURE 1. *Deviations of the heat-capacity measurements on sample plus calorimeter.*

TABLE 1. *Observed heat capacity of bromobenzene* (C_6H_5Br)

Gram molecular weight = 157.0095 g, T deg K = t deg C + 273.15

T	C_{net}	T	C_{net}	T	C_{net}	T	C_{net}
K	J K^{-1} mol^{-1}	K	J K^{-1} mol^{-1}	K	J K^{-1} mol^{-1}	K	J K^{-1} mol^{-1}
Run 1		Run 5		Run 8		Run 10	
243.310	144.489	11.279	6.318	14.141	11.167	125.358	68.957
248.692	145.007	13.502	10.251	20.305	19.159	137.083	72.778
254.565	146.293	16.675	14.590	27.342	26.563	148.248	76.466
260.388	147.061	20.430	19.307	34.177	32.109	158.975	80.001
266.166	148.081	26.643	25.932	40.340	36.140	172.173	84.543
271.897	149.201	35.557	33.097	48.172	40.410	184.101	88.747
Run 2		45.467	39.016	56.920	44.562	195.667	93.104
104.036	61.993	55.318	43.801	65.071	48.100	206.905	97.548
118.713	66.799	Run 6		73.107	50.902	Run 11	
130.361	70.516	30.831	29.554	81.245	54.086	202.003	95.179
141.447	74.153	38.904	35.157	90.387	57.601	209.909	98.587
168.039	83.055	47.748	40.193	45.650	39.111	219.557	102.842
180.209	87.292	56.904	44.570	56.616	44.407	228.024	106.519
191.994	91.584	66.019	48.493	66.428	48.616	235.376	109.583
203.438	96.082	75.094	51.710	Run 9		249.334	145.251
214.567	100.704	85.732	55.923	71.110	50.249	257.790	146.693
Run 3		96.726	59.567	82.858	54.753	267.696	148.246
215.147	100.869	Run 7		93.353	58.502	Run 12	
224.101	104.942	12.548	8.707	103.503	61.791	273.951	149.301
233.548	108.861	15.682	13.266	114.578	65.493	279.454	150.413
247.755	145.001	19.933	18.690	125.042	68.846	286.737	151.824
255.219	146.104	24.284	23.540	134.546	71.882	290.496	152.614
262.629	147.428	28.981	28.019			296.358	153.891
Note: Run 4 consisted of fusion measurements		13.418	9.914				
		18.458	16.906				
		23.978	23.237				
		28.007	27.179				

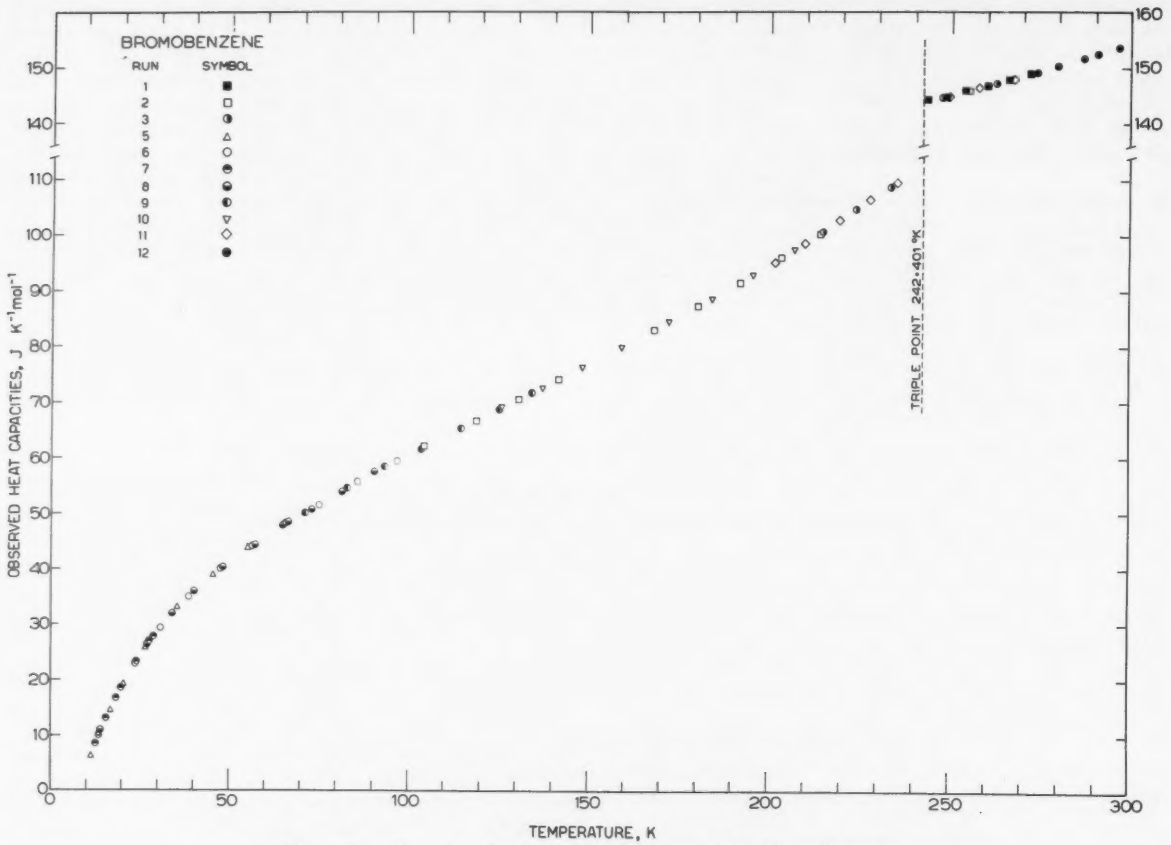

FIGURE 2. *Observed values of the molal heat capacity of bromobenzene.*

2.4. Triple Point and Heat of Fusion

The heat of fusion and triple point of bromobenzene, as well as the purity of the sample used, were studied experimentally in runs 3, 4, and 11. In run 11, the calorimeter and sample were heated continuously from a temperature several degrees below the triple point to a second temperature slightly above the triple point. In runs 3 and 4, heating was discontinued at several points during the melting and the equilibrium temperatures were measured. In all three cases, the heat of fusion was obtained by subtracting from the measured energy input the necessary integrals of the heat capacities of the solid and liquid (plus calorimeter), below and above the triple point. The values obtained from runs 3, 4, and 11 were respectively 10 705, 10 704, and 10 696 J mol^{-1}. Since there seems to be no bias in the results, the mean value, 10 702 ± 5 J mol^{-1}, is taken as ΔH_{fusion} for bromobenzene. Correspondingly, $\Delta S_{fusion} = 44.150 \pm 0.021$ J K^{-1} mol^{-1}. The indicated imprecision is twice the standard deviation of the mean.

The temperatures measured in runs 3 and 4 are plotted in figure 3 with the reciprocal of the fraction melted as abscissa. A line drawn through these points has for its temperature intercept the triple point of pure bromobenzene (242.401 K = 30.749 °C) and has a slope proportional to the mole fraction of impurity in the sample used. The proportionality constant is $-\Delta H_{fusion}/RT^2$ fusion and the calculation indicates less than 20 moles per million of soluble impurity. Such impurities would presumably include most hydrocarbon and all halo-hydrocarbon species. Other possible impurities, such as air, water, and carbon dioxide, if present in sufficient amount to affect the thermal measurements, would have been detected by transition heats during the heat capacity measurements. It seems likely that the sample used can be regarded as essentially 99.998 percent bromobenzene.

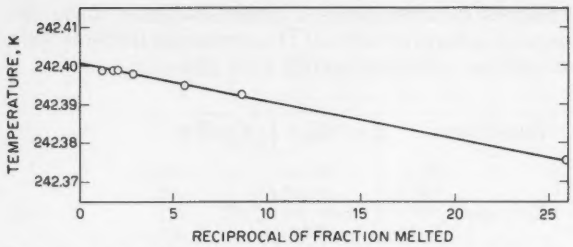

FIGURE 3. *Graphical determination of triple point of bromobenzene and purity of sample.*

2.5. Latent Heat of Vaporization

Since it was not feasible to modify the apparatus to operate at temperatures above ambient, and since the vapor pressures of bromobenzene up to room temperature are very low, it was decided to measure the latent heat of vaporization at only one temperature, just below that of the room. Four determinations were made, by withdrawing vapor into a cold weighing container after steady-state conditions of temperature, flow, and power input had been established. During the withdrawal of each weighed sample, constant temperature was maintained by slight adjustments of the power at measured times. It would have been desirable to make measurements at different flow rates, in order to determine the effect of any unmeasured self-cooling of the vapor. However, the low vapor pressure made it necessary to keep the calorimeter valve nearly wide open in each experiment. The data for the four determinations are given in table 2.

The discrepancies among the four values of Q/W become systematic when the values are plotted against the square of the run time, as in figure 4. The straight line which results indicates a heat loss, δQ, which is proportional to the cube of the time, since the mass of sample, W, is roughly proportional to time. The most reasonable explanation for such a heat loss is that part of the measured energy went into the formation, by conduction, of an undetected "hot spot" on a calorimeter or tube surface. This "spot" or region, δT degrees warmer than the controlled temperature of the calorimeter and the shield, then lost heat by radiation; thus, $\delta Q \propto (\delta T)^3 \propto t^3$. This explanation has been tentatively accepted as the best available for the results obtained, but it should be pointed out that no such effect was observed in a previous determination of latent heats of vaporization with the same calorimeter [2].

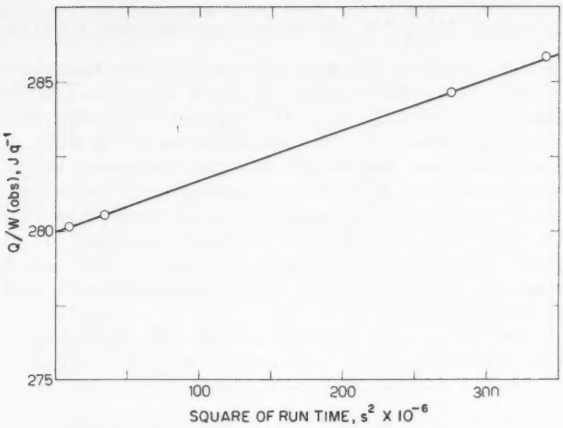

FIGURE 4. *Extrapolation to zero time of the observed ratios of energy to vaporized mass, at 293 K.*

The value of Q/W obtained by extrapolation to zero run time, and the resulting values of ΔH_{vap} and ΔS_{vap} at 293 K, where

$$\Delta H_{vap} = M \frac{Q}{W}\left(1 - \frac{v}{V}\right), \tag{1}$$

are given in table 2. In equation (1), v and V are the specific volumes of the saturated liquid and vapor, respectively. The expression in parentheses has the value 0.999726 in this instance, and accounts for the fact that a small amount of the vapor formed does not leave the calorimeter but replaces the vaporized liquid.

3. Thermodynamic Functions of the Solid and Liquid

The smoothed tables of heat capacity of the full and empty calorimeter at equal temperature intervals (see sec. 2.3) were substracted; the resulting tables of heat capacity of solid and liquid bromobenzene were converted to molar units and again smoothed slightly where necessary. The table for the solid was extended to 0 K by the function

$$C = aD\left(\frac{\theta}{T}\right) \tag{2}$$

TABLE 2. *Measurement of the latent heat of vaporization of bromobenzene*

Run	T, K	Q, J	W, g	time, s	rate, g h^{-1}	Q/W (293 K), J g^{-1}
1	291.983	160.367	0.5724	3029.82	0.6801	280.17
2	293.076	228.344	.8139	5828.30	.5027	280.56
3	293.188	924.325	3.2335	18457.8	.6307	285.86
4	292.891	838.549	2.9456	16576.4	.6397	284.68
				Extrapolated Q/W		280.0
				ΔH_{vap} (293 K), J mol^{-1}		43 963 ± 60
				ΔS_{vap} (293 K), J K^{-1} mol^{-1}		150.04 ± 0.2

in which $D\left(\frac{\theta}{T}\right)$ is the Debye specific heat function as tabulated by Beattie [9] and the constants $a=37.971$ J K^{-1} mol^{-1} and $\theta=81.184$ K were fitted to the lower and (12 to 20 K) of the experimental table. The resulting values for the observed heat capacity of bromobenzene, which are along the saturation curve, were converted to C_p at one atmosphere. The adjustment was found to be negligible at all temperatures for the solid. The four highest values in the table of net heat capacity for the liquid required a very small negative adjustment [10] which amounted to one part in 4000 at 300 K.

The values thus obtained for C_p of bromobenzene, plus the values at the triple point and at 0 *C* and 25 *C* obtained by extrapolation or interpolation, form the second column of table 3. The remaining columns were calculated straightforwardly from this one, i.e.:

$$\text{Enthalpy:} \quad H_T - H_0^c = \int_0^T C_p dT$$

$$\text{Entropy:} \quad S_T = \int_0^T \frac{C_p}{T} dT \tag{3}$$

Gibbs free energy:

$$-(G_T - H_0^c) = \int_0^T S_T^{dT}.$$

TABLE 3. *Thermodynamic functions for bromobenzene, solid and liquid*

Gram molecular wt = 157.0095 g; T K = t °C + 273.15

T	C_p	$H_T - H_0^c$	$(H_T - H_0^c)/T$	S_T	$-(G_T - H_0^c)$	$-(G_T - H_0^c)/T$
K	*J K^{-1} mol^{-1}*	*J mol^{-1}*	*J K^{-1} mol^{-1}*	*J K^{-1} mol^{-1}*	*J mol^{-1}*	*J K^{-1} mol^{-1}*
0	0	0	0	0	0	—
5	0.691	0.864	0.173	0.231	0.288	0.058
10	5.058	13.336	1.334	1.790	4.559	.456
15	12.253	56.312	3.755	5.183	21.415	1.428
20	18.782	134.43	6.721	9.624	58.059	2.903
25	24.295	242.51	9.700	14.425	118.11	4.725
30	28.911	375.87	12.529	19.275	202.39	6.746
35	32.735	530.28	15.151	24.029	310.73	8.878
40	35.938	702.18	17.555	28.615	442.39	11.060
45	38.753	889.03	19.757	33.013	596.54	13.256
50	41.300	1089.3	21.786	37.231	772.22	15.445
55	43.646	1301.7	23.667	41.277	968.99	17.610
60	45.936	1525.7	25.428	45.174	1184.7	19.746
65	48.045	1760.8	27.087	48.935	1420.1	21.848
70	49.876	2005.6	28.652	52.564	1673.8	23.912
75	51.630	2259.4	30.126	56.066	1945.5	25.940
80	53.555	2522.2	31.528	59.457	2234.4	27.929
85	55.629	2795.2	32.885	62.766	2539.9	29.881
90	57.485	3078.1	34.201	66.000	2861.9	31.799
95	59.027	3369.5	35.468	69.150	3199.8	33.682
100	60.659	3668.6	36.686	72.219	3553.3	35.533
105	62.351	3976.1	37.869	75.220	3921.9	37.351
110	64.010	4292.1	39.019	78.158	4305.3	39.139
115	65.639	4616.2	40.141	81.040	4703.4	40.899
120	67.244	4948.4	41.237	83.868	5115.6	42.631
125	68.841	5288.6	42.310	86.645	5541.9	44.335
130	70.442	5636.9	43.360	89.375	5982.0	46.015
135	72.060	5993.1	44.393	92.064	6435.6	47.671
140	73.696	6357.5	45.411	94.715	6902.6	49.304
145	75.346	6730.1	46.415	97.330	7382.7	50.915
150	76.998	7110.9	47.406	99.912	7875.8	52.506
155	78.651	7500.1	48.387	102.463	8381.8	54.076
160	80.323	7893.5	49.360	104.987	8900.4	55.627
165	82.025	8303.3	50.324	107.485	9431.6	57.161
170	83.751	8717.7	51.281	109.959	9975.3	58.678
175	85.497	9140.9	52.234	112.412	10532.	60.178
180	87.266	9572.8	53.182	114.845	11099.	61.663
185	89.057	10013.	54.127	117.260	11679.	63.133
190	90.888	10464.	55.070	119.659	12272.	64.589
195	92.769	10922.	56.012	122.044	12877.	66.032

TABLE 3. *Thermodynamic functions for bromobenzene, solid and liquid*—Continued

Gram molecular wt = 157.0095 g; T K = t °C + 273.15

T	C_p	$H_T - H_0^c$	$(H_T - H_0^c)/T$	S_T	$-(G_T - H_0^c)$	$-(G_T - H_0^c)/T$
K	*J K⁻¹ mol⁻¹*	*J mol⁻¹*	*J K⁻¹ mol⁻¹*	*J K⁻¹ mol⁻¹*	*J mol⁻¹*	*J K⁻¹ mol⁻¹*
200	94.701	11391.	56.956	124.418	13492.	67.462
205	96.696	11869.	57.901	126.781	14120.	68.880
210	98.765	12358.	58.849	129.136	14760.	70.287
215	100.90	12858.	59.802	131.485	15412.	71.683
220	103.08	13368.	60.761	133.829	16075.	73.068
225	105.24	13888.	61.725	136.170	16750.	74.445
230	107.38	14419.	62.694	138.506	17437.	75.812
235	109.51	14962.	63.668	140.838	18135.	77.170
240	111.64	15515.	64.646	143.166	18845.	78.520
242.401 (solid)	112.66	15784.	65.115	144.281	19190.	79.166
242.401 (liquid)	144.24	26486.	109.265	188.431	19190.	79.166
245	144.60	26861.	109.64	189.97	19682.	80.334
250	145.35	27586.	110.34	192.90	20639.	82.556
255	146.15	28314.	111.04	195.79	21610.	84.748
260	146.99	29048.	111.72	198.63	22597.	86.911
265	147.84	29784.	112.39	201.44	23597.	89.045
270	148.71	30526.	113.06	204.21	24611.	91.152
273.15	149.27	30996.	113.47	205.94	25257.	92.466
275	149.59	31272.	113.72	206.95	25639.	93.233
280	150.50	32022.	114.36	209.65	26681.	95.288
285	151.46	32776.	115.00	212.32	27735.	97.318
290	152.47	33537.	115.64	214.96	28804.	99.323
295	153.56	34301.	116.28	217.58	29885.	101.30
298.15	154.29	34786.	116.68	219.22	30573.	102.54
300	154.74	35072.	116.91	220.18	30980.	103.27

These integrals were found by the appropriate Debye and Einstein functions up through 16 K, and at all higher temperatures by a 4-point Simpson's rule formula applied to each temperature interval. For the purpose of integration, the intervals were two degrees up to 50 K, and five degrees from 50 to 300 K. Internal consistency was checked at each point by the identity

$$S_T = \frac{H_T - H_0^c}{T} - \frac{G_T - H_0^c}{T}.$$

In order further to promote the increasing use of the joule as the most fundamental unit of energy, it is retained in table 3 as well as elsewhere in this paper. The tabulated values may be converted to calories by dividing by 4.1840.

4. Thermodynamic Functions of the Ideal Gas

The Raman spectra of bromobenzene have been obtained by a number of investigators [11, 12, 13, 14, 15, 16, 17, 18, 19]. (Many others, not referenced here, have published spectra but have not tabulated the frequency shifts). Infrared bands have been investigated by Plum [20], by Plyler, Allen, and Tidwell [21], and by Josien and LeBas [22, 23], among others. Assignments of the observed frequencies to the 30 fundamental vibrations (always assuming C_{2v} symmetry) have been attempted in several papers [19, 21, 23, 24]. The work by Kohlrausch and Wittek [19] was done before the fundamentsl of benzene itself were well established. The assignments by LeBas [23], and by Plyler et al. [21] cover only the infrared bands. The most complete analysis appears to be that of Whiffen [24]; he also published a short table of thermodynamic functions. A review of frequency assignments for several aromatic compounds, including the monohalogenated benzenes, has been made by Wilcox, Stephenson, and Coburn [25].

By means of the usual rigid-rotator, harmonic-oscillator approximation, the thermodynamic properties of bromobenzene in the ideal-gas state were calculated. The planar C_{2v} model was assumed, in which all bond angles are 120°. The bond distances used—1.4020 Å for C-C, 1.0698 Å for C-H, and 1.8674 Å for C-Br—were those given by Rosenthal and Dailey [26] from microwave measurements. Previously reported values of the C-Br distance by Schoppe [27] and by Yuzawa and Yamaka [28] are in agreement but less precise. The product of the moments of inertia thus became 1.2533×10^{-112} g^3 cm^6. The frequency assignment of Whiffen [24] was accepted unchanged. Although there are several discrepancies between this assignment and others, such as that of Plyler et al. [21],

588-458 O - 75 - 2

the differences do not significantly affect the thermodynamic functions. The results of the calculations from 100 to 1500 K are given in table 4. Previously reported calculations, with which this table is in essential agreement, are those of Whiffen [24] and of Butler and Lielmezs [29]. Again, the tabular values may be divided by 4.1840 to obtain energy in calories.

5. Discussion of Results

When the entropy of vaporization at 293 K (table 2) is added to that of the liquid at the same temperature, from table 3, and the pressure and non-ideality corrections are applied to the sum, there is obtained the value 323.73 J K^{-1} mol^{-1} for the entropy of the ideal gas at one atmosphere and 293 K. (In calculating the change of entropy with pressure, a vapor pressure of 4.4 torr at 293 K was used, as obtained from Young [30]. More recent measurements, such as those of Thomas, Smith and Meatyard [31], require a lengthy extrapolation to obtain a value at this temperature). This may be compared with the value calculated directly from statistical mechanics as it would appear in table 4, 323.63 J K^{-1} mol^{-1}. The agreement, while to some extent fortuitous, gives added confidence in the entire set of results, and in particular lends support to the extrapolation (fig. 4) of the heat of vaporization measurements.

The heat capacities of table 3 are compared in table 5 with those reported by Stull [1]. The deviation of the earlier values from those of this research show a quite regular trend with increasing temperature, particularly in the solid region. Andrews and Haworth [32] reported heat capacity measurements on the solid at eight temperatures from 100 to 232 K. Since the method of measurement was in principle the same as that of Stull (rate of heat transfer), it is perhaps not surprising that these measurements show a similar trend with temperature. The deviations from table 3 of the eight measurements of Andrews and Haworth range from −2.6 percent at 101.2 K to 18.4 percent at 231.7 K. Williams and Daniels [33] have measured heat capacities of liquid bromobenzene from 20 to 80 °C; their equation expressing the results gives increasingly negative deviations from the present work in the short range (273.15 to 300 K) of comparison. Other heat capacity measurements in the literature are either values at single temperatures or average values over a range of temperatures.

Stull [1] reported a triple point of 242.42 K and a heat of fusion corresponding to 10627 J mol^{-1}; the latter agrees with the present work well within the stated accuracy of Stull's measurements (3 percent). There appear to be no other direct measurements of these quantities for comparison; values of temperature and heat of melting in the presence of the atmosphere, as found referenced in handbooks, are reasonably close to the triple point and heat of fusion reported here. An experimental heat of vaporization at 298.15 K has been reported by Wadso [34]; his value of 44 540 ± 40 J mol^{-1} is unaccountably higher than that reported here. A number of equations for the latent heats have been derived, usually based on the extensive vapor pressure data of Young [30]. The equation of Jones and Bowden [35] yields a value of $\Delta H_{vap} = 44130$ J mol^{-1} at 293 K. The agreement with the result of the present work (table 2) is quite good for a value based on vapor pressures and extrapolated below 30 °C.

TABLE 4. *Thermodynamic functions for bromobenzene, ideal gas*

Gram molecular wt = 157.0095 g, T deg K = t Deg C + 273.15

T	C_P°	$H^\circ - H_0^\circ$	$(H^\circ - H_0^\circ)/T$	S°	$-(G^\circ - H_0^\circ)$	$-(G^\circ - H_0^\circ)/T$
K	*J K⁻¹ mol⁻¹*	*J mol⁻¹*	*J K⁻¹ mol⁻¹*	*J K⁻¹ mol⁻¹*	*J mol⁻¹*	*J K⁻¹ mol⁻¹*
100	44.559	3644.0	36.440	253.59	21715	217.15
150	56.545	6166.3	41.109	273.88	34914	232.77
200	70.00	9322.8	46.614	291.95	49068	245.34
250	84.834	13190	52.760	309.15	64096	256.39
273.15	91.954	15236	55.780	316.97	71344	261.19
298.15	99.658	17631	59.136	325.36	79373	266.22
300	100.23	17816	59.388	325.97	79975	266.58
350	115.25	23206	66.303	342.56	96690	276.26
400	129.29	29324	73.311	358.88	114227	285.57
450	142.06	36114	80.253	374.86	132572	294.61
500	153.51	43508	87.017	390.43	151706	303.41
550	163.72	51444	93.535	405.55	171607	312.01
600	172.82	59862	99.770	420.19	192253	320.42
700	188.26	77944	111.35	448.03	235680	336.68
800	200.80	97417	121.77	474.02	281798	352.25
900	211.17	118032	131.15	498.29	330427	367.14
1000	219.84	139598	139.60	521.00	381403	381.40
1100	227.17	161964	147.24	542.31	434579	395.07
1200	233.39	184990	154.16	562.34	489822	408.18
1300	283.72	208600	160.46	581.24	547010	420.78
1400	243.29	232710	166.22	599.10	606036	432.88
1500	247.24	257240	171.49	616.02	666800	444.53

TABLE 5. *Deviation of* Cp *values of Stull* [1]

T	Cp(this work)	Cp(Stull)	Percent deviation [a]
K	J K^{-1}·mol^{-1}	J K^{-1}·mol^{-1}	
		Solid	
90	57.485	54.89	−4.5
100	60.659	58.49	−3.6
110	64.010	61.92	−3.3
120	67.244	65.65	−2.4
130	70.442	69.54	−1.3
140	73.696	73.64	−0.1
150	76.998	77.95	1.2
160	80.323	82.01	2.1
170	83.751	86.27	3.0
180	87.266	90.71	3.9
190	90.888	95.31	4.9
200	94.701	99.75	5.3
210	98.765	104.81	6.1
220	103.08	109.96	6.7
230	107.38	115.48	7.5
240	111.64	121.17	8.5
		Liquid	
250	145.35	146.36	0.7
260	146.99	150.33	2.3
270	148.71	152.97	2.9
280	150.50	154.31	2.5
290	152.47	154.89	1.6
300	154.74	155.52	0.5

[a] $\left(\frac{Cp(\text{Stull}) - Cp(\text{this work})}{Cp(\text{this work})}\right) \times 100.$

In consideration of the precision of the experiments and the possible sources of systematic error, the accuracy of table 3 is estimated to be within ±0.2 percent at temperatures above 50 K; the uncertainty increases at lower temperatures and may be as high as ±2.0 percent at 15 K. A more complete picture of the thermodynamic properties of bromobenzene would be obtained if precise measurements of the heat capacity and heat of vaporization of the liquid could be continued up to at least the boiling point. Especially desirable for confirmation of the ideal-gas properties would be precise measurements of the vapor heat capacity, since the calculated heat capacity is much more sensitive than is the entropy to frequency values and anharmonicities.

Tables 3 and 4 can be extended to include the thermodynamic functions for formation of bromobenzene from the elements, by application of the heat of formation determined by Smith and Bjellerup [36].

The completion of the work and the preparation of this paper have been made possible by the fact that one of us (JFM) was assigned by the Air Force Office of Scientific Research (Office of Aerospace Research) to the University of Rome, Italy, for an academic year. Many thanks are therefore due to the Air Force, to Professor G. Sartori for his invitation to the Istituto di Chimica Generale e Inorganica, Universita di Roma, and to the many members of the staff of that institute who have helped out with such important items as computer programming, preparation of figures, and typing.

Grateful acknowledgement is made to the many people who assisted, at various times, with the experimental measurements and calculations in the Heat Division, National Bureau of Standards. Among these may be mentioned Ruth K. Cheney, W. J. Cross, W. J. Ferguson, R. E. McCoskey, Jane W. Mellors, B. Petkof, and P. F. Wacker.

6. References

[1] Stull, D. R., J. Am. Chem. Soc. **59** 2726–33 (1937).
[2] Scott, R. B., Meyers, C. H., Rands, Jr., R. D., Brickwedde, F. G. and Bekkedahl, N., J. Res. Nat. Bur. Stand. (U.S.) **35,** 39–85 (1945) RP1661.
[3] Osborne, N. S., Stimson, H. F., Sligh, T. S. and Cragoe, C. S., BS Sci. Pap. **20,** 65–110 (1925) *S* 501.
[4] Stimson, H. F., J. Res. Nat. Bur. Stand. (U.S.) **65A** (Phys. and Chem.) 139–145 (1961).
[5] Hoge, H. J. and Brickwedde, F. G., J. Res. Nat. Bur. Stand. (U.S.) **22,** 351–373 (1939) RP1188.
[6] Whittaker, E. T. and Robinson, G., The Calculus of Observations. A Treatise on Numerical Mathematics, pp. 285–316, 4th ed. (Blackie and Sons, London, 1944).
[7] Scott, R. B. and Brickwedde, F. G., J. Res. Nat. Bur. Stand. (U.S.) **35,** 501–512 (1946) RP1684.
[8] IUPAC Division of Inorganic Chemistry, Commission on Atomic Weights, Pure and Appl. Chem. **30,** 637–649 (1971).
[9] Beattie, J. A., J. Math. Phys. **6,** 1–32 (1926).
[10] Hoge, H. J., J. Res. Nat. Bur. Stand. (U.S.) **36,** 111–117 (1946) RP1693.
[11] Fujioka, Y.,Sci. Papers Inst. Phys. Chem. Research, Tokyo, **11,** 208–222 (1929).
[12] Dadieu, A. and Kohlrausch, K. W. F., Phys. Z. **30,** 384–391 (1929).
[13] Petrikaln, A. and Hochberg, J., Z. Phys. Chem. **B3,** 217–228 (1929).
[14] Bhagavantam, S. and Venkateswaran, S., Proc. Roy. Soc., **A127,** 360–73 (1930).
[15] Cleetin, C. E. and Dufford, R. T.,Phys. Rev. **37,** 362–72 (1931).
[16] Murray, J. W. and Andrews, D. H., J. Chem. Phys. **1,** 406–13 (1933).
[17] Kohlrausch, K. W. F. and Pongratz, A., Monatsh. **63,** 427–44 (1933).
[18] Kahovec, L. and Reitz, A. W., ibid. **69,** 363–76 (1936).
[19] Kohlrausch, K. W. F. and Wittek, H., ibid. **74,** 1–24 (1941).
[20] Plum, W. B., J. Chem. Phys. **5,** 172–8 (1937).
[21] Plyler, E. K., Allen, Jr., H. C. and Tidwell, E. D., J. Res. Nat. Bur. Stand. (U.S.) **58,** 255–63 (1957) RP2758.
[22] Josien, Marie-Louise and LeBas, Jeanne-Marie, Bull. Soc. Chim. France (Memoirs) **1956,** 53–64.
[23] LeBas, Jeanne-Marie, J. Chim. Phys. **59,** 1072–81 (1962).
[24] Whiffen, D. H., J. Chem. Soc. **1956,** 1350–6.
[25] Wilcox, W. S., Stephenson, C. V. and Coburn, Jr., W. C. (Southern Research Institute), WADD Tech. Rept. 60–333, Sept., 1960; also Spectrochim. Acta **17,** 933–46 (1961).
[26] Rosenthal, E. and Dailey, B. P., J. Chem. Phys. **43,** 2093–2110 (1965).
[27] Schoppe, R., Z. Phys. Chem. **B34,** 461–470 (1936).
[28] Yuzawa, T. and Yamaka, M., Bull. Chem. Soc. Japan, **26,** 414–416 (1953).
[29] Butler, J. B. and Lielmezs, J., J. Chem. Eng. Data, **14,** 335–341 (1969).
[30] Young, S., J. Chem. Soc., **55,** 486–521 (1889).

[31] Thomas, L. H., Smith, H. and Meatyard, R., J. Sci. Instruments [2], **1**, 1119–1121 (1968).
[32] Andrews, D. H. and Haworth, E., J. Am. Chem. Soc. **50**, 2998–3002 (1928).
[33] Williams, J. W. and Daniels, F., ibid. **47**, 1490–1502 (1925).
[34] Wadso, I., Acta Chem. Scand. **22**, 2438–2444 (1968).
[35] Jones, W. J. and Bowden, S. T., Phil. Mag. **37**, 480–489 (1946).
[36] Smith, A. and Bjellerup, L., Acta Chem. Scand. **1**, 566–570 (1947).

(Paper 79A5–863)

JOURNAL OF RESEARCH of the National Bureau of Standards—A. Physics and Chemistry
Vol. 79A, No. 5, September–October 1975

Relativistic Effects on Line Strengths for Transitions in the Hydrogenic Isoelectronic Sequence*

S. M. Younger and A. W. Weiss**

Institute for Basic Standards, National Bureau of Standards, Washington, D.C. 20234

(July 3, 1975)

Relativistic line strengths have been computed for a large number of transitions using Dirac wave functions for the one-electron, hydrogen-like ions. As expected, the results indicate that relativistic effects are quite small for low stages of ionization. However, in general, they also remain small throughout a large portion of the isoelectronic sequence, becoming typically of the order of 10 percent in the vicinity of $Z=50$, after which they grow quite rapidly. This suggests that for multielectron ions a basically nonrelativistic theory might well be adequate for light atom isoelectronic ions through as much as 30 or 40 stages of ionization.

Key words: Dirac theory; hydrogen; line strength; oscillator strength; relativistic corrections; spectroscopy.

1. Introduction

The regular behavior of atomic oscillator strengths along isoelectronic sequences has proved to be a useful tool for analyzing a large body of f-value data [1].[1] The graphical analysis of such data has also made possible the prediction, by interpolation, of much previously unknown data for ionized species [2].

The theoretical underpinning of such analyses is the charge expansion theory [3] which predicts that the large Z limit for a multiplet strength is essentially given by the hydrogenic case. If there is no large Z degeneracy, e.g., the $2s$-$2p$ degeneracy, then the limiting value is the hydrogenic strength multiplied by a many-electron angular factor appropriate to the particular LS-states involved. If there is an asymptotic degeneracy, then one must coherently mix the square roots of the line strengths by a simple first order energy diagonalization; the radial integrals, however, are still hydrogenic.

This scheme is based on a perturbation expansion of the nonrelativistic, many-electron Schrödinger equation in inverse powers of the nuclear charge. The theory thus encompasses an entire isoelectronic sequence at a time. For large nuclear charge, however, it is natural to expect that relativistic corrections will become important, so that eventually these isoelectronic sequence analyses must break down. If one is interested in predictions for highly ionized species, then it is important to determine at what stage of ionization and in what way relativistic effects begin to make themselves felt.

The most obvious effect, and probably the first in importance, is the traditional intermediate coupling [4]. In this scheme multielectron states of different L and S are coupled together by the off-diagonal spin-orbit interaction, as obtained from a Pauli-approximation reduction of the Dirac Hamiltonian. The wave function is still a linear combination of nonrelativistic functions, and the line strengths are affected by a coherent mixing of the nonrelativistic transition moments.

In addition to this, however, relativistic effects also modify the orbitals themselves, thus more directly affecting the line strengths. To get some idea of the magnitude of this orbital effect for highly ionized systems, we have therefore computed the hydrogen-like line strengths according to Dirac theory for a large number of transitions, following them along the entire isoelectronic sequence through $Z=100$, and comparing with the non-relativistic predictions.

While a number of authors have discussed the Dirac line strengths for large Z ions, they seem to have concentrated on the $1s$-np resonance lines, primarily in order to approximate the K-shell x-ray intensities [5–8]. Our orientation here is somewhat different.

* Supported by Energy Research and Development Administration.
** Permanent address: University of Maryland, College Park, Md. 20740.
[1] Figures in brackets indicate the literature references.

We would like to look on these calculations as a kind of prototype of the relativistic orbital effects one might find in highly ionized multielectron species. Thus, e.g., the $2s$-$2p$ line strengths are calculated with an eye to the resonance lines of the lithium isoelectronic sequence. While we are primarily interested in the qualitative questions of the manner and rate of growth of relativistic effects along the sequence, our results may prove useful as approximate correction factors for some nonhydrogenic ions.

2. Formulas and Details of the Calculation

We calculated the dipole line strengths as a function of Z using the hydrogen-like Dirac wave functions. In evaluating the matrix elements, we followed the analysis of Babushkin [8], as recently reviewed by Garstang [9]. For a detailed discussion, the reader is referred to Garstang's review; we quote here only the pertinent formulas.

For the case where variation of the electromagnetic field over atomic dimensions is included, the electric dipole line strength for $l \rightarrow l+1$ is given by:

$$S=\frac{9l(l+1)}{2(2l+1)}\frac{1}{k^2}I^2$$

for $j=l-1/2 \rightarrow j'=l+1/2$,

$$S=\frac{9(l+1)}{2(2l+1)(2l+3)}\frac{1}{k^2}I^2$$

for $j=l+1/2 \rightarrow j'=l+1/2$,

$$S=\frac{9(l+1)(l+2)}{2(2l+3)}\frac{1}{k^2}I^2$$

for $j=l+1/2 \rightarrow j'=l+3/2$,

where $I=[R_1+R_2+R_3-R_4+(\kappa_1-\kappa_2)(R_3+R_4)]$,

and

where

$$R_1=\int_0^\infty g_1 g_2 r^2 j_L(kr)dr$$

$$R_2=\int_0^\infty f_1 f_2 r^2 j_L(kr)dr$$

$$R_3=\int_0^\infty f_1 g_2 r^2 j_{L-1}(kr)dr$$

$$R_4=\int_0^\infty f_2 g_1 r^2 j_{L-1}(kr)dr$$

$$k=\frac{2\pi}{\lambda},$$

with $L=1$. f and g are the small and large components, respectively, of the Dirac spinor,

$$\psi=\begin{pmatrix} g(r)\chi_{\kappa\eta} \\ -if(r)\chi_{-\kappa,\eta} \end{pmatrix},$$

and the subscripts differentiate between the initial and final states. A discussion of these wave functions is given by Bethe and Salpeter [10]. The Dirac quantum number κ is defined as:

$$\kappa=\begin{matrix} -(l+1) \text{ if } j=l+1/2 \\ l \text{ if } j=l-1/2. \end{matrix}$$

If one neglects the variation of the field over the dimensions of the atom, which was found to be a reasonable approximation, the expressions for the corresponding $j \rightarrow j'$ transitions are:

$$S=\frac{2l(l+1)}{2l+1}I^2,$$

$$S=\frac{2(l+1)}{(2l+1)(2l+3)}I^2,$$

$$S=\frac{2(l+1)(l+2)}{2l+3}I^2,$$

where

$$I=\int_0^\infty r^3(f_1 f_2+g_1 g_2)dr.$$

The integral transformation to equivalent forms involving products of large and small components in the integrand was not used because of numerical difficulties for low and intermediate values of Z. The above form is also more useful for sorting out specific relativistic effects, since it displays separately the large and small component contributions to the nonretarded integrals. The integrals were evaluated both numerically and analytically—the latter using term by term integration of the radial functions. Doing the integrals both ways provided a mutual check on the calculations as well as providing detailed information on such effects as cancellations in the integrand due to relativistic orbital shifts, etc.

3. Results and Discussion

As mentioned earlier, the $1s$–np series has already been dealt with by Payne and Levinger [6] and Babushkin [8], among others. While calculations were done on a large number of transitions and ions, we present results here only for the $2s$–$2p$, $2s$–$3p$, $2p$–$3d$, $2p$–$3s$, $3s$–$3p$, and $3p$–$3d$ transitions as typical of the relativistic behavior of these hydrogenic line strengths. Furthermore, these are prototypes of the radial integrals needed for resonance transitions in ions isoelectronic with first and second row atoms. The ratios of the relativistic

to nonrelativistic line strengths are shown graphically in figures 1–4 for the *s-p* transitions. Z^2S, rather than the line strength itself, is the natural quantity of interest since the nonrelativistic value is a constant, independent of Z. Deviations from this constant thus display directly the effects of relativity on the line strength.

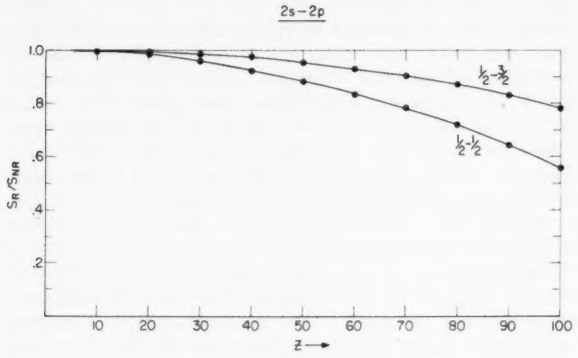

FIGURE 1. *Ratio of relativistic to nonrelativistic line strengths versus nuclear charge for the* 2s–2p *transitions in the hydrogen isoelectronic sequence.*

The nonrelativistic values of Z^2S are 18.0 and 36.0 for the 1/2–1/2 and 1/2–3/2 lines respectively.

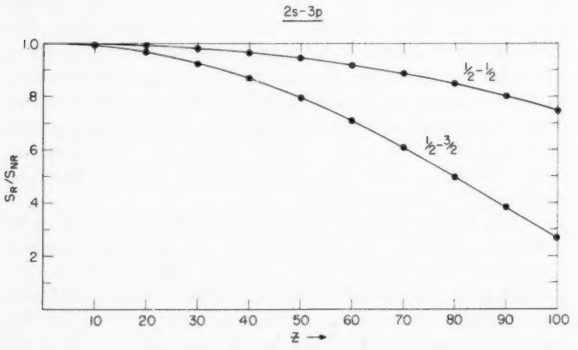

FIGURE 2. *Ratio of relativistic to nonrelativistic line strengths versus nuclear charge for the* 2s–3p *transitions in the hydrogen isoelectronic sequence.*

The nonrelativistic values of Z^2S are 6.26 and 12.52 for the 1/2–1/2 and 1/2–3/2 lines respectively.

Usually one finds the relativistic line strength to decrease with increasing Z, reflecting the well-known contraction of the relativistic wave function toward the origin. As the electron distribution is drawn in toward the nucleus, greater emphasis is placed on smaller radii in the transition integrand. Furthermore, the normal behavior is for the large component contribution to decrease, while that of the small component increases. However, even at large Z the small component term is still only a few percent of the larger, the overall behavior thus being dominated by the large component.

An example of departure from this behavior occurs in the $2p-3s$ transition. While the 1/2–1/2 transition

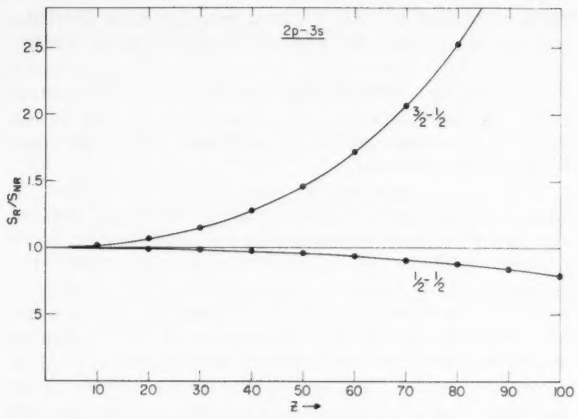

FIGURE 3. *Ratio of relativistic to nonrelativistic line strengths versus nuclear charge for the* 3s–2p *transitions in the hydrogen isoelectronic sequence.*

The nonrelativistic values of Z^2S are 0.587 and 1.174 for the 1/2–1/2 and 1/2–3/2 lines respectively.

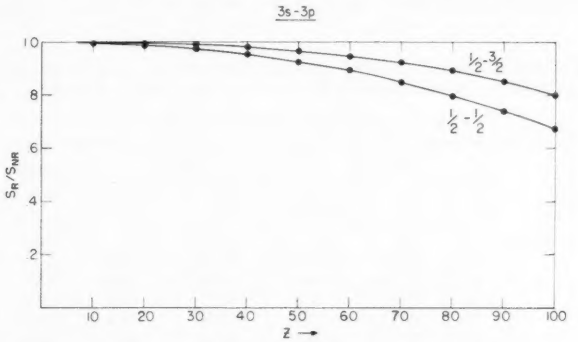

FIGURE 4. *Ratio of relativistic to nonrelativistic line strengths versus nuclear charge for the* 3s–3p *transitions in the hydrogen isoelectronic sequence.*

The nonrelativistic values of Z^2S are 108.0 and 216.0 for the 1/2–1/2 and 1/2–3/2 lines respectively.

follows the usual pattern of decreasing strength with increasing Z, the 3/2–1/2 transition grows larger than the nonrelativistic value as Z increases. The explanation appears to be related to differential interference effects in the transition integral for the two transitions. There is substantial cancellation in the $2p-3s$ integral for the nonrelativistic case—the positive-negative ratios of the integrand being about 2:1. As Z increases, the $2p_{1/2}$ and $3s_{1/2}$ orbitals contract by roughly the same amount maintaining approximately the same integrand ratio. The $2p_{3/2}$, however, does not contract nearly as rapidly, resulting in a significant increase in the integrand ratio, i.e., less cancellation and so a larger transition integral.

The most important observation about these calculations, however, concerns the rate of growth of the relativistic corrections along the isoelectronic sequence. For sufficiently large Z, the relativistic line strength "takes off" and ultimately departs quite drastically from the nonrelativistic one. These cor-

rections, however, don't seem to take hold until the nuclear charge becomes rather large. Thus, for Z=50, which is forty-nine times ionized tin, the relativistic line strengths rarely deviate by more than 10 percent from the nonrelativistic. An exception to this is the $2p_{3/2}-3s_{1/2}$ transition discussed above, which deviates by about 30 percent.

This slow increase in the relativistic effect is further illustrated in tables 1 and 2, where we present the actual numerical results for selected ions for some *p-d*, as well as *s-p* transitions. In these tables the strengths and doublet ratios for Z=1 are the nonrelativistic values so that the remaining numbers display directly the relativistic deviations. At Z=50, for example, one sees corrections ranging from 3 percent to 14 percent for both the doublet ratios as well as the absolute line strengths. Such general conclusions are consistent with the results of Burke and Grant [11], who calculated the Dirac hydrogenic expectation values of r^N and found small and slowly increasing relativistic corrections. Indeed, there is even fairly good semiquantitative agreement between our dipole transition moments and their results for N=1.

TABLE 1. *Relativistic line strengths and doublet ratios for* 2s−2p *and* 3s−3p *transitions in the hydrogen isoelectronic sequence*

The Z=1 results are the nonrelativistic predictions.

		1/2−1/2		1/2−3/2		Doublet ratio
	Z	Z^2S	S_R/S_{NR}	Z^2S	S_R/S_{NR}	
2s−2p	1	18.0	1.0	36.0	1.0	2.00
	10	17.92	0.996	35.94	0.998	2.01
	30	17.28	.960	35.42	.983	2.05
	50	16.01	.890	34.33	.953	2.14
	70	14.11	.784	32.56	.904	2.31
	90	11.57	.643	29.85	.829	2.58
3s−3p	1	108.0	1.0	216.0	1.0	2.00
	10	107.7	0.997	215.7	.999	2.00
	30	104.9	.971	213.2	.987	2.03
	50	99.6	.922	207.8	.962	2.09
	70	91.2	.844	198.7	.920	2.18
	90	79.8	.739	183.9	.851	2.30

While it is tempting to extend these conclusions to the more general case of a multielectron ion, one should do so with some care, and such considerations must remain somewhat conjectural. Probably the safest conclusion is the general qualitative one that the orbital relativistic corrections to a line strength generally tend to remain small, probably not greater than 10 percent up to fairly high Z, say 30 or 40. It would thus appear safe to take the nonrelativistic values for ions where no intermediate coupling effects are expected. For example, the resonance 3*s*−3*p* transitions of sodium-like ions are probably fairly well represented by a nonrelativistic calculation throughout this range of Z. For more accuracy or higher Z, one might even want to apply the correction factors obtained here, namely, the S_R/S_{NR} ratios in tables 1 and 2, although at the present this possibility must remain a conjecture.

There are, however, several reservations which must be kept in mind. In the first place, if one has a transition with a substantial amount of cancellation, small changes in the orbitals can alter the delicate interference pattern in the transition integrand enough to lead to relatively large changes in the transition integral. In such cases a small orbital relativistic effect manifests itself in a much larger line strength correction; see, e.g., our results on the 2*p*−3*s* transitions. Secondly, one should remember that for any realistic one-electron model of the multielectron ion, such as the Hartree-Fock, the orbital nodal structure is not hydrogenic. The effective charge changes from the inner to outer parts of the wave function. For a sodium-like ion, for example, the 1*s* electron sees an effective nuclear charge of essentially Z while the 3*s* electron sees a screened charge more like Z−10, and orthogonalization produces a 3*s* orbital with a nonhydrogenic loop pattern, although this effect should tend to diminish for increasing Z.

While the oscillator strength is often the most convenient quantity to extrapolate in an isoelectronic sequence, one should note that it will deviate much sooner from the nonrelativistic value because of large and rapidly increasing relativistic corrections to the transition energy. The oscillator strength is given by

TABLE 2. *Relativistic line strengths and doublet ratios for the* 2p−3d *and* 3p−3d *transitions in the hydrogen isoelectronic sequence*

The Z=1 results are the nonrelativistic predictions.

		1/2−3/2		3/2−3/2		3/2−5/2		Doublet ratios
	Z	Z^2S	S_R/S_{NR}	Z^2S	S_R/S_{NR}	Z^2S	S_R/S_{NR}	
2p−3d	1	30.00	1.0	6.00	1.0	54.00	1.0	5.00:1:9.00
	10	29.89	0.996	6.00	1.0	53.99	1.0	4.98:1:9.00
	30	28.58	.953	5.93	0.988	53.51	0.991	4.82:1:9.02
	50	25.98	.866	5.79	.965	52.55	.973	4.48:1:9.07
	70	22.11	.737	5.59	.932	51.11	.946	3.96:1:9.15
	90	17.09	.570	5.31	.885	49.18	.911	3.22:1:9.26
3p−3d	1	135.0	1.0	27.0	1.0	243.0	1.0	5.00:1:9.00
	10	134.9	0.999	26.96	0.999	242.7	0.999	5.00:1:9.00
	30	134.0	.993	26.66	.987	241.7	.995	5.03:1:9.07
	50	132.2	.979	26.05	.965	239.6	.986	5.07:1:9.20
	70	128.9	.955	25.13	.931	236.4	.973	5.13:1:9.41
	90	123.2	.913	23.93	.886	232.1	.956	5.15:1:9.70

$$f=\frac{2}{3}\frac{\Delta E}{g}S,$$

where g is the lower state degeneracy, S the line strength, and ΔE the transition energy. Even if S remains essentially nonrelativistic, a large first order relativistic correction to ΔE will have a large effect on f. The line strength itself would thus appear to be the safest and most natural quantity to extrapolate to large Z ions.

In conclusion it appears reasonable to suggest that the first and largest effect of relativity for a light atom isoelectronic sequence will be that due to intermediate coupling. Furthermore, one should be able to calculate these effects reasonably well (providing first order energy shifts are included) with a nonrelativistic basis through something like 30 or 40 stages of ionization. For ionic systems where intermediate coupling does not occur, a nonrelativistic calculation should give the line strengths with adequate accuracy through a similar range of ionization stages. Beyond an effective Z of 50, it appears that relativistic orbital effects will become sufficiently large to necessitate a more fully relativistic treatment.

4. References

[1] Wiese, W. L., and Weiss, A. W., Phys. Rev. **175,** 50 (1968).
[2] Smith, M. W., and Wiese, W. L., Astrophys. J. Suppl. Ser. **23,** #196, 103–192 (1971).
[3] Layzer, D., Ann. Phys. (New York) **8,** 271 (1959).
[4] Condon, E. U., and Shortley, G. H., Theory of Atomic Spectra (Cambridge University Press, New York, 1955).
[5] Massey, H. S. W., and Burhop, E. H. S., Proc. R. Soc. A **153,** 661 (1936).
[6] Payne, W. B., and Levinger, J. S., Phys. Rev. **101,** 1020 (1956).
[7] Scofield, J. H., Phys. Rev. **179,** 9 (1969).
[8] Babushkin, F. A., Opt. Spektrosk. **13,** 141 (1962); Opt. Spektrosk. **19,** 1 (1965); Acta Phys. Pol. **25,** 749 (1964); Sov. Phys.-JETP **21,** 372 (1965).
[9] Garstang, R. H., in Topics in Modern Physics—A Tribute to Edward U. Condon, Edited by W. E. Brittin and H. Odabasi, pp. 153–167 (Colorado Associated University Press, Boulder, Colorado, 1971).
[10] Bethe, H. A., and Salpeter, E. E., Quantum Mechanics of One and Two Electron Atoms (Academic Press, New York, 1957).
[11] Burke, V. M., and Grant, E. I., Proc. Phys. Soc. **90,** 297 (1967).

(Paper 79A5–864)

JOURNAL OF RESEARCH of the National Bureau of Standards—A. Physics and Chemistry
Vol. 79A, No. 5, September–October 1975

The Enthalpies of Combustion and Formation of 2,2′-Dichloroethyl Sulfide

Walter H. Johnson

Institute for Materials Research, National Bureau of Standards, Washington, D.C. 20234

(June 10, 1975)

The enthalpies of combustion and formation of 2,2′-dichloroethyl sulfide (mustard gas) have been determined by combustion in an adiabatic rotating-bomb calorimeter. The bomb process has been corrected to:

$$C_4H_8Cl_2S(liq) + 7O_2(g) + 98H_2O(liq) \rightarrow 4\ CO_2(g) + [2\ HCl + H_2SO_4 + 100\ H_2O](liq)$$

for which the following values were obtained:

$$\Delta Hc°(25\ °C) = -3163.49 \pm 1.26\ kJ/mol \text{ and}$$
$$\Delta Hf°(25\ °C) = -200.57 \pm 1.58\ kJ/mol.$$

Key words: Combustion; dichloroethyl sulfide; enthalpy; formation; heat; mustard gas.

1. Introduction

The enthalpy of formation of 2,2′-dichloroethyl sulfide (more commonly known as mustard gas) has been determined by combustion of the liquid material in an adiabatic rotating-bomb calorimeter. This work was undertaken for Edgewood Arsenal under contract A133051801F4W9 to devise a reliable procedure for the combustion calorimetry of compounds containing both chlorine and sulfur. The problems associated with the combustion of chlorine compounds and those associated with the combustion of sulfur compounds are combined when the compound contains both of these elements. There appears to be no data available on the combustion calorimetry of compounds of this type in the literature. The compound 2,2′-dichloroethyl sulfide was selected because (1) there was need for reliable data on the enthalpies of combustion and formation for this substance and (2) we were able to obtain the results of an unpublished prior investigation [1].[1] The data consisted of the results of two combustion experiments, performed in 1918, in which the nature and quantities of the combustion products were not well-defined. Because of the corrosive nature and the relatively high heats of solution and dilution of the products of combustion, a platinum-lined bomb and a rotating-bomb calorimeter are required.

Because the main purpose of this investigation was to develop calorimetric procedures for compounds containing both chlorine and sulfur, no particular emphasis was placed on the use of a well characterized sample. However, since no previous data on compounds of this type are available, it was decided to publish the results of this investigation.

[1] Figures in brackets indicate the literature references at the end of this paper.

2. Materials

2.1. 2,2′-Dichloroethyl Sulfide

The sample was obtained from K and K Laboratories, Inc., Plainview, N.Y. The sample had a pale amber color which was taken to indicate a significant amount of impurity. The material was distilled in vacuum; about 10 percent of the sample was discarded. The distillate was a clear liquid for which the freezing point was 13.4 ± 0.2 °C.

Analyses of the products of combustion yielded the following results in weight percent:

	Found	*Theor.*
C	30.21	30.20
S	20.11	20.15
Cl	44.29	44.57

The quantity of chloroplatinic acid, usually formed when chlorine compounds are burned in the presence of platinum, was not determined but would be expected to account for approximately 0.3 percent of the chlorine.

2.2. Cotton Fuse

The fuse was taken from a spool of cotton thread which was determined to have the empirical formula $CH_{1.730}O_{0.853}$. The density of the thread was 0.87 g/cm³.

The energy of combustion, determined in a separate experiment, gave $\Delta Uc°$ (28 °C) = −17621 J/g.

2.3. Arsenious Oxide Solution

The arsenious oxide solution was prepared by dissolving arsenic trioxide, SRM 83B, in water. The concentration of the solution was determined by potentiometric titration with standard potassium permanganate. The concentration of the arsenious oxide solution was 23.345 μmol/cm^3.

2.4. Oxygen

High purity oxygen was used for both calibration and combustion experiments. An analysis furnished with the cylinder gave the following impurities in ppm; Kr, 12.0; Xe, 0.7; N_2O, 0.8; N_2, 3.0; and H_2O, 3.0. The presence of these impurities is expected to have no significant effect on the experimental values obtained for the combustion experiments.

2.5. Nitrogen

A cylinder of water-pumped nitrogen was used. This nitrogen was essentially free of combustibles and carbon dioxide but contained some water; for the relatively small quantity of nitrogen that was used this amount of water is negligible.

3. Apparatus and Procedure

The adiabatic rotating-bomb calorimeter, the automatic shield-temperature controls and the temperature-measuring system employed in the investigation have been described [2].

A sample of the liquid material was weighed into a platinum crucible and placed in the crucible support of the platinum-lined silver bomb. A glass cup containing 4.000 cm^3 of arsenious oxide solution was placed on the bottom of the bomb cavity. About 1.5 cm of cotton string was attached to 1 cm of platinum wire, 0.075 mm in diameter, which was connected between the electrodes. The cotton string was positioned such that the lower end was in contact with the sample. The bomb was then sealed and 2.34 atm[2] of nitrogen was introduced; oxygen was then added to bring the total pressure up to 31.62 atm.

The bomb was transferred to the adiabatic calorimeter, the temperature of filling was measured and the bomb was heated electrically to 24.99 °C. The calorimeter jacket was evacuated, the adiabatic temperature controls were placed in operation and the system was left under control overnight to reach temperature equilibrium.

On the following morning temperatures were observed at intervals of a few minutes during an initial rating period and the sample was ignited by discharging an 18 000 μF capacitor previously charged to 24 V, through the platinum wire fuse. The platinum wire ignited the cotton string which in turn ignited the sample. After two minutes the bomb was rotated to mix the contents of the bomb solution. When thermal equilibrium was established, temperatures were observed during a final rating period; the resulting time-temperature curves were extrapolated to the time of firing to obtain the initial and final calorimeter temperatures

The bomb was removed from the calorimeter, connected to a gas train and the gaseous contents were passed successively through a drying tube containing magnesium perchlorate and phosphorus pentoxide, and through a weighed absorption tube containing Ascarite,[3] magnesium perchlorate and phosphorus pentoxide. In each case, the absorption tube was flushed with dry hydrogen before weighing and after the absorption of carbon dioxide to reduce the correction for displacement of gas by the sodium carbonate; a tare was used to reduce the effect of changes in humidity and air density between weighings. The quantity of carbon dioxide was determined by the increase in weight of the absorption tube.

The bomb was opened and the bomb solution transferred to a weighed polyethylene bottle. A weighed aliquot of the bomb solution was titrated potentiometrically with standard potassium permanganate solution using a microburet. This determination is very precise and the end point can be determined within ±0.001 cm^3 of 0.1 *N* soln. A similar titration of the initial solution compared with the bomb solution gives an accurate measure of the remaining As^{+++}. Another aliquot was taken and analyzed for nitric acid by means of a modified Kjeldahl method [3]. The modifications involved heating of the reducing mixture with an infrared lamp instead of an electric heating element in the solution.

When chlorine compounds are burned about 80 percent of the chlorine forms hydrogen chloride and the remainder goes to gaseous chlorine. To insure the complete conversion to hydrochloric acid an excess of a reducing agent such as arsenious oxide is placed in the bomb. Also, in the combustion of sulfur compounds a significant part of the sulfur is found as sulfur dioxide. However, when a small amount of nitrogen is present in the bomb atmosphere the sulfur is all converted to sulfur trioxide which dissolves in the solution forming sulfuric acid. The general procedure for sulfur-containing compounds is to leave one atmosphere of air in the bomb before filling with oxygen. In this investigation, however, the conversion to sulfuric acid was found to be very slow, involving several hours for complete conversion. When at least two atmospheres of nitrogen was used the conversion was rapid and complete.

There was also the possibility that there would be some oxidation of the arsenious acid by the sulfuric acid. Experiments on the combustion of thianthrene in the presence of arsenious acid showed no significant change in the quantity of As^{+++} between the initial and final bomb solutions; therefore, the oxidizing

[2] 1 atmosphere = 101.325 kPa.

[3] Certain commercial materials are identified in this paper in order to specify adequately the experimental procedures. Such identification does not imply recommendation or endorsement by the National Bureau of Standards.

effect on the arsenious acid by the sulfuric acid produced under experimental conditions was considered not significant.

4. Results and Calculations

The results of the analyses of the combustion products is given in table 1. The CO_2-ratio was obtained by subtracting the theoretical quantity calculated from the mass of the cotton fuse from the observed total mass of carbon dioxide and dividing the result by the theoretical quantity calculated from the mass of sample.

TABLE 1. *Results of the analyses of the combustion products*

	551	552	553	554
Mass of sample, g.....	0.311666	0.242445	0.306338	0.433452
Mass of cotton, g.....	.000966	.000636	.000739	.000835
CO_2-ratio.....	.9970	.9953	.9962	1.0126
As_2O_5, μmol.....	57.95	51.69	70.93	92.92
HNO_3 mmol.....	0.1186	0.1494	0.2475	0.3231

The quantities of As_2O_5 and HNO_3 were those determined by the permanganate titrations and the micro-Kjeldahl analyses. The quantities of HCl and H_2SO_4 were assumed to be stoichiometric.

The following values were used in the calculations:

	Density, $g \cdot cm^{-3}$	Cp, $J \cdot g^{-1} \cdot K^{-1}$	$\left(\frac{\partial U}{\partial P}\right)_T$, $J \cdot g^{-1} \cdot atm^{-1}$
Benzoic acid	1.32	1.21	−0.0126
2,2′-Dichloroethyl Sulfide	1.27	1.32	0

The 1971 table of atomic weights [4] were used throughout this paper. The unit of energy is the joule; for conversion from the conventional thermochemical calorie, 1 calorie = 4.184 joules.

The enthalpy of oxidation of $As_2O_{3(aq)}$ to $As_2O_{5(aq)}$ was taken as −319.82 kJ/mol from the data of Sellers, Sunner and Wadso [5]. The heat of decomposition of aqueous nitric acid into nitrogen and water was taken as ΔU_c° (28 °C) = −59.7 kJ/mol.

The effective energy equivalent of the calorimeter was determined by means of a series of combustion experiments using benzoic acid, SRM 39i. The certificate value for the energy of combustion under certificate conditions is −26434 J/g at 25 °C; this corresponds to −26410.36 J/g for the isothermal bomb process under standard conditions at 28 °C. The results of the benzoic acid calibration experiments are given in table 2. *EEE-std* is the effective energy equivalent of the standard calorimeter which includes the empty bomb with all internal platinum parts except the crucible; *Cv-cont(i)* is the heat capacity of the crucible, sample, oxygen and water initially placed in the bomb; *Corr to tm* is a correction for deviation of the actual mean temperature of the system from the standard mean temperature of 26.5 °C; *Corr-parts* is a correction for the effect of changes made to the system during the series of experiments and *EEE-actual* is the effective energy equivalent of the actual calorimeter system obtained as the sum of *EEE-std* and the above corrections.

Temperature rise is the observed increase in temperature of the system following ignition of the sample. *Q-total* is the total energy evolved by the over-all bomb process obtained as the product of *EEE-actual* and the temperature rise; *q-ign* is the electrical energy introduced to ignite the sample; *q-decomp* HNO_3 is the calculated quantity of energy required to decompose the nitric acid, formed in the combustion from traces of nitrogen in the bomb atmosphere, to nitrogen, oxygen and water; *q-WC* is the Washburn correction [6] applied to convert the initial and final contents of the bomb to their respective standard states at the actual final temperature and *q-corr to* 28 °C is a correction to convert the energy evolved by the standard reaction at the actual final temperature to the standard final temperature. *Q-std reaction* is the energy evolved by the isothermal bomb process at the standard final temperature, obtained as $Q\text{-}total + \Sigma q$; division by the mass of sample yields ΔU_c°.

The results of the benzoic acid calibration experiments were calculated by means of a computer program. For these experiments, *EEE-std* was calculated by iteration from the observed temperature rise and mass of sample taking ΔU_c° (28 °C) equal to −26410.36 J/g.

The results of the combustion experiments on 2,2′-dichloroethyl sulfide are given in table 3. The same format has been used but some additional corrections have been listed; *q-comb fuse* is the energy of combustion of the cotton thread used to ignite the sample; *q-oxid* As_2O_3 is the energy evolved by oxidation of As_2O_3 in the reduction of gaseous chlorine to hydrogen chloride; *q-diln* H_2SO_4 and HCl are applied to convert the actual final concentrations to the selected final concentrations of 1:100 H_2O and 1:50 H_2O respectively.

No computer program was available which could accept compounds containing both sulfur and chlorine, it was necessary, therefore, to compute these data manually. Because data on the solubility and heats of solution of oxygen, nitrogen, and carbon dioxide in the resulting solution of sulfuric, hydrochloric, arsenious and arsenic acids were not available it was necessary to make certain assumptions in calculation of the Washburn correction; in each case the heat of solution was taken equal to that in pure water. The error introduced by these assumptions is believed to be less than 10 percent in the correction or ±0.5 J.

The results given in table 2 correspond to the reaction:

$$(1)\quad C_4H_8Cl_2S(liq) + 7\,O_2(g) + 98\,H_2O(liq) \rightarrow 4\,CO_2(g) + [2\,HCl + H_2SO_4 + 100\,H_2O](liq)$$

ΔU_c° (28 °C) = −3156.82 ± 1.26 kJ/mol

TABLE 2. *Results of the benzoic acid calibration experiments*

Expt. No.	495	524	525	526	527	528
EEE-Std ..... J/K...	2519.50	2519.67	2519.44	2519.66	2519.65	2519.42
Cv-cont(i) ..... J/K...	4.82	4.81	4.78	4.79	4.76	4.81
Corr to tm ..... J/K...	.08	.11	.15	.09	.10	.14
Corr-parts ..... J/K...	−.16	.00	.00	.00	.00	.00
EEE-actual ..... J/K...	2524.24	2524.59	2524.37	2524.55	2524.51	2524.37
Temp rise ..... K.....	3.133364	3.108335	3.159280	3.089474	3.100061	3.173467
Q-total ..... J.....	−7909.36	−7847.29	−7975.18	−7799.53	−7826.14	−8011.01
q-ign ..... J.....	1.22	1.06	1.18	.79	1.11	1.16
q-decomp HNO_3 ..... J.....	.70	.21	.30	.47	.17	.84
q-WC ..... J.....	6.39	6.32	6.38	6.26	6.22	6.46
q-*corr* to 28 °C ..... J.....	−.04	−.04	−.06	−.03	−.04	−.06
Q-*std react* ..... J.....	−7901.10	−7839.73	−7967.38	−7792.05	−7818.67	−8002.62
m_s ..... g.....	.299167	.296843	.301676	.295038	.296046	.303011
ΔU°_c(28 °C) ..... J/g ...	−26410.36	−26410.36	−26410.36	−26410.36	−26410.36	−26410.36
Mean, EEE-Std ..... J/K...	2519.56					
sdm ..... J/K...	.048					

TABLE 3. *Results of the combustion experiments on 2,2′dichloroethyl sulfide*

Expt. No.	551	552	553	554
EEE-Std ..... J/K...	2519.56	2519.56	2519.56	2519.56
Cv-cont(i) ..... J/K...	28.01	27.92	28.01	28.22
Corr to *tm* ..... J/K...	−0.48	−0.97	−0.54	0.38
Corr-parts ..... J/K...	.00	.00	.00	.00
EEE-actual ..... J/K...	2547.09	2546.51	2547.03	2548.16
Temp rise ..... K.....	2.446197	1.905797	2.409353	3.394446
Q-total ..... J.....	−6230.68	−4853.13	−6136.69	−8649.59
q-ign, ... J.....	.81	.84	.73	.76
q-decomp HNO_3 ..... J.....	7.08	8.92	14.78	19.29
q-WC ..... J.....	4.01	3.31	4.12	5.65
q-comb fuse ..... J.....	16.67	10.98	12.76	14.41
q-oxid As_2O_3 ..... J.....	18.53	16.53	22.69	29.71
q-diln H_2SO_4 ..... J.....	.37	.80	.42	−.51
q-diln HCl ..... J.....	.50	.04	.55	−1.02
q-corr to 28 °C ..... J.....	−.29	−.46	−.32	.31
Q-std react ..... J.....	−6183.00	−4812.17	−6080.96	−8580.99
m_s ..... g.....	.311666	.242445	.306338	.432452
ΔU°_c(28 °C) ..... J/g ...	−19838.55	19848.50	19850.50	19842.65
Mean ..... J/g ...	−19845.05			
Avg dev ..... J/g ...	±4.46			

ΔH°_c (28 °C) = −3164.33 ± 1.26 kJ/mol

ΔH°_c (25 °C) = −3163.49 ± 1.26 kJ/mol
(−756.09 ± 0.30 kcal/mol)

$\Delta Hf°$ (25 °C) = −200.57 ± 1.58 kJ/mol
(−47.94 ± 0.38 kcal/mol)

The uncertainty assigned to the value for ΔH°_c was obtained by combining (as the square root of the sum of squares) 2 *sdm* for the calibration experiments, the average deviation of the combustion experiments, 0.01 percent for the certified value of benzoic acid, 0.02 percent for purity of the sample, 0.01 percent for calculation of the Washburn correction, 0.01 percent for calculation of the energy of oxidation of As_2O_3 and 0.02 percent for the uncertainty in the energy of mixing of sulfuric acid with the hydrochloric acid-arsenious acid solution. The auxiliary data were obtained by Selected Values of Chemical Thermodynamic Properties, NBS Tech. Note 270–3 [7].

The uncertainty assigned to $\Delta Hf°$ was obtained by combining as the square root of the sum of the squares the uncertainty of ΔH°_c with 0.01 percent in the accepted values for the heats of formation of carbon dioxide, water, aqueous sulfuric acid and aqueous hydrochloric acid [7].

5. Discussion

There are no previous data on the heat of combustion of 2,2′-dichloroethyl sulfide in the available literature. An investigation by R. S. Hall and J. L. Hutchinson of the Chemical Laboratory, Edgewood Arsenal [1], EA–L–87 (1918) and a recalculation of their data by Leo Finkelstein [8], E. A. T. R. 259, dated March 1937 are the only values known.

The recalculation by Finkelstein, gave for the reaction:

(2) $C_4H_8Cl_2S(1) + 7.5\ O_2(g) = 4\ CO_2(g) + 4\ H_2O(1) + SO_3(c) + Cl_2(g)$ $\Delta H = -731.83$ kcal/mol.

Correcting for recent changes in the enthalpies of formation of the products of combustion gives −733.34 kcal/mol (−3068.29 kJ/mol) for the process according to reaction (2). By combination of reaction (2) with the appropriate heats of formation and reaction, the energy of the process corresponding to reaction (1) is found to be −3260.47 kJ/mol. The difference of 3 percent between the results of the present investigation and that obtained by Hall and Hutchinson is not surprising in view of the problems associated with their measurements. The discrepancy is obviously due to a number of factors including the reaction with the bomb surface, and the bomb gasket, the escape of gases during combustion, the nonhomogeneity of the bomb solution, and errors in the determination of the nature and quantities of the combustion products.

6. References

[1] Hall, R. S., and Hutchinson, J. L., Chemical Laboratory, Edgewood Arsenal, EA–L–87 (1918) (unpublished).

[2] Prosen, E. J., and Johnson, W. H., in preparation. For a partial description see Armstrong, G. T., and Johnson, W. H., National Bureau of Standards, informal report, July 1973.

[3] Kieselbach, R., Ind. and Eng. Chem. **16,** 764 (1944).

[4] Commission on Atomic Weights, IUPAC, Pure and Applied Chem. **30,** 637–649 (1972); Atomic Weights of the Elements 1971.

[5] Sellers, P., Sunner, S., and Wadso, I., Acta Chem. Scand. **18,** 202 (1964).

[6] Washburn, E. W., J. Res. Nat. Bur. Stand. (U.S.) **10,** 525 (1933). RP546.

[7] Wagman, D. D., Evans, W. H., Parker, V. B., Halow, I., Bailey, S. M., and Schumm, R. H., Nat. Bur. Stand. (U.S.), Tech. Note 270–3, 264 pages, (Jan. 1967).

[8] Finkelstein, L., Chemical Laboratory, Edgewood Arsenal, E. A. T. R. **259** (1937) (unpublished).

(Paper 79A5–865)

JOURNAL OF RESEARCH of the National Bureau of Standards—A. Physics and Chemistry
Vol. 79A, No. 5, September–October 1975

Barothermal Theory of Two Devices for Measuring Absorption Coefficients

H. S. Bennett

Institute for Materials Research, National Bureau of Standards, Washington, D.C. 20234

(July 2, 1975)

Two devices are proposed for measuring absorption coefficients in weakly absorbing materials. The first device measures cylindrical samples and the second device measures flat plate or disk samples. This paper reports on the derivations for the steady-state and transient solutions to the heat diffusion equations which describe the barothermal behavior of the two proposed devices. In addition, Green's function techniques are used to describe the cyclic heating and cooling of the cylinders and plates.

Key words: Absorption coefficients; barothermal behavior; Green's function; heat diffusion; weakly absorbing materials.

1. Introduction

Optical communications, integrated optics, and high power lasers are developing technologies which depend in part upon highly transparent solids. For example, optical communication systems use optical fibers with absorption coefficients which are less than $10^{-4}\,cm^{-1}$ at operating wavelengths [1].[1] Continuing further advances in these technologies and determining the absorption mechanisms in highly transparent materials require improved methods for measuring very small absorption coefficients.

Four general techniques for measuring absorption coefficients exist. These techniques involve respectively calorimetry, spectrophotometry, emissivity, and gas pressure measurements.

In the calorimetric technique, one measures the temperature rise of the solid which occurs when a fraction of the energy in a beam of radiation is absorbed. When the temperature rise, reflectivity, and laser power are known to within an accuracy of 1 percent, this method is capable of giving absorption coefficients on the order of $10^{-4}\,cm^{-1}$ within an accuracy of a few percent. This method then has reasonably high sensitivity, and requires laser beam powers of the order of tens of mW for absorption coefficients of the order of $10^{-3}\,cm^{-1}$. It also is insensitive to those scattering centers which do not absorb any of the radiation. However, the sample must be contacted with thermocouples to measure its temperature and the absorption coefficient can be determined only at those wavelengths for which sufficiently powerful lasers are available.

The second technique involves measuring the transmission loss of a beam of radiation passing through the solid. Variations of this technique include either a single beam or double beam spectrophotometer and may use samples of two different lengths. Double beam methods using samples of different lengths give products of the absorption coefficients α with the sample thickness d as small as $\alpha d \sim 0.002$ with an accuracy of ± 0.0002. The photometric technique has the advantage of using light sources with continuous values of wavelengths present; but it has the disadvantages that sample preparation is important to avoid surface scratches and dust and that the samples should not have scattering centers such as inclusions.

In the third technique one measures the emission of the sample at a given temperature and compares it directly to a blackbody at the same temperature. When the product αd is very small, the emittance E (the ratio of thermal radiation per unit area emitted by the sample to that emitted by a blackbody at the same temperature) becomes $E \sim \alpha d$. For values of αd less than 0.001, the emittance measurements can be more sensitive for determining α than the photometric measurements. In addition, by this technique, one can obtain values of absorption coefficients over a continuous range of wavelengths. But exceptional temperature control is essential to achieve such sensitivity.

In the fourth technique, the energy absorbed from a beam of radiation passing through the sample produces heat. The heat then diffuses from the solid to a nonabsorbing, confined gas which is adjacent to the sample. The heat transfer process leads to a pressure rise in the gas. Because this technique tends to average over any absorption inhomogeneities in the sample, we also expect that localized absorbing or scattering

[1] Figures in brackets indicate the literature references at the end of this paper.

588-458 O - 75 - 3

centers could be less of a problem for this technique than for the calorimetric techniques in which the placement of thermocouples may be important.

To develop further this last technique, Bennett and Forman recently proposed alternative ways to measure very small absorption coefficients. They considered in a series of papers [2–6] both barothermal and photoacoustic modes of operation for devices to characterize weakly absorbing materials. In these papers, they cited only the results for the solutions to the heat diffusion equations which describe the behavior of the proposed devices. They did not derive the solutions because they wanted to stress in those papers the major conclusions for designing absorption devices with optimum performance.

Figures 1 and 2, respectively, show schematics of their proposed devices for measuring absorption coefficients of long cylindrical samples and of thin disk or plate-shaped samples. Each of these devices has a characteristic frequency which is related to the inverse of the time required for transferring a heat pulse from the solid to the gas. The barothermal mode of operation occurs whenever the modulation frequency of the beam of radiation is less than the characteristic frequency of the device; and the photoacoustic mode of operation occurs whenever the modulation frequency of the beam of radiation is greater than the characteristic frequency of the device [7].

In this paper, the author gives derivations for the steady-state and transient solutions to the heat diffusion equations which describe the barothermal behavior of the two proposed devices. The equations which describe the photoacoustic behavior of the devices are derived in (separate papers [4, 6]).

The steady-state and transient solutions for cylindrical samples are derived here, respectively, in section 2 and section 3; and the steady-state and transient solutions for disk or plate-shaped samples are derived, respectively, in section 4 and section 5. The Green's functions which describe the cyclic heating and cooling of the cylinders and plates are constructed in section 6. And finally, frequently occurring integrals involving the eigenfunctions for the equations are given in appendix A for cylinders and in appendix B for disks or plates.

2. Steady-State Solution—Cylinder

From [3], the steady-state temperature $v(r)$ satisfies the following heat diffusion equations for the proposed device in figure 1: When $0 \leq r \leq r_s$,

$$k_s \frac{d^2 v_s(r)}{dr^2} + \frac{k_s}{r} \frac{dv_s(r)}{dr} + \frac{Q_s(r)}{\rho_s C_s} = 0; \tag{1}$$

and when $r_s \leq r \leq r_i$,

$$k_g \frac{d^2 v_g(r)}{dr^2} + \frac{k_g}{r} \frac{dv_g(r)}{dr} = 0. \tag{2}$$

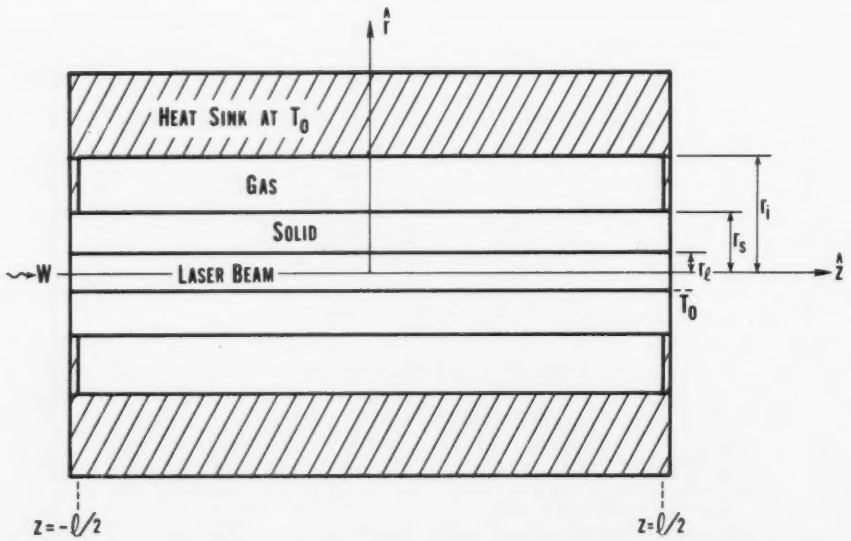

FIGURE 1. *Schematic of an absorption measuring device (barothermal) for long cylindrical samples.*

Insulating annuli support coaxially the long cylindrical transparent sample of radius r_s inside a larger cylinder of radius r_i. A confined nonabsorbing gas at ambient pressure p_0 fills the space between the two cylinders. The walls of the outer cylinder are at a constant temperature T_0. A collimated beam of radiation, such as a laser beam, propagates coaxially through the cylindrical sample. The beam of radiation has a power W_l and an effective radius r_l. A pressure transducer, which is not shown, monitors the pressure at the heat sink–gas interface.

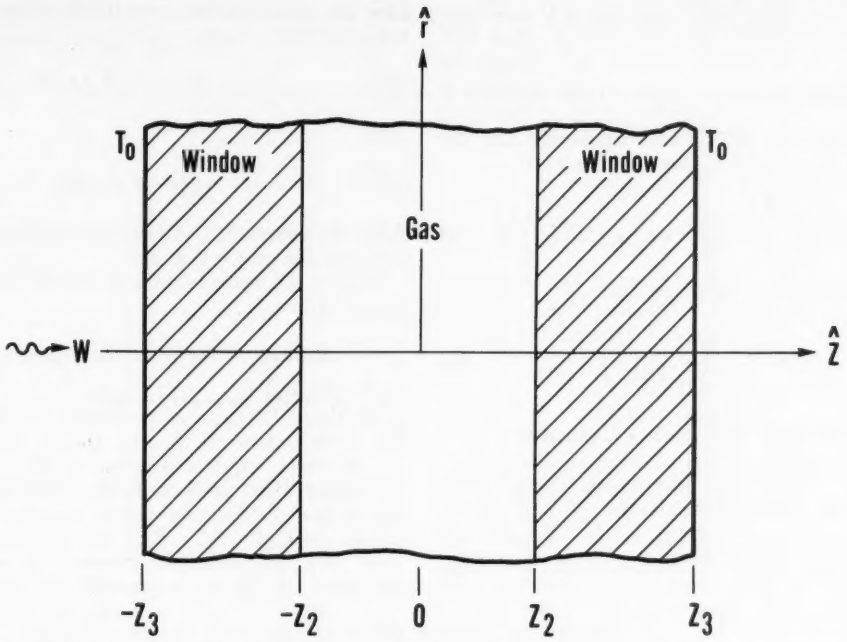

FIGURE 2. *Schematic of an absorption measuring cell (barothermal) for plate-shaped samples.*

A confined, nonabsorbing gas at ambient pressure p_0 fills the space inside the cell between two windows. The walls of the cell may have a polygonal or circular cross section. The windows which enclose the gas at each end of the cell are made from the weakly absorbing material under investigation. The external faces of the two windows are at a constant temperature T_0. A collimated beam of radiation, such as a laser beam, with power W_l and effective radius r_l propagates along the z direction through the pressure cell and its windows. A pressure transducer, which is not shown, measures the pressure in the gas at $|z| \leq z_2$.

The temperature in the solid is $v_s(r)$ and the temperature in the gas is $v_g(r)$. The power absorbed per unit volume in the solid is

$$Q_s(r) = \begin{cases} Q_l \text{ for } 0 \leq r \leq r_l \leq r_s \\ 0 \text{ for } r > r_l, \end{cases} \tag{3}$$

where $Q_l = \alpha_s W_l / \pi r_l^2$, α_s is the absorption coefficient of the solid, W_l is the power of the beam of radiation, and r_l is the effective radius of the collimated beam. The radius of the cylindrical sample is r_s and the radius of the outer cylinder (heat sink) is r_i. The thermal diffusivity $k = K/\rho C$, where K is the thermal conductivity, ρ is the density, and C is the specific heat at constant volume. The subscript s denotes quantities for the solid and the subscript g denotes quantities for the gas.

The boundary conditions are that

$$v_g(r_i) = T_0, \tag{4}$$

where T_0 is the temperature of the heat sink. Continuity of temperature across the solid-gas interface at $r = r_s$ gives,

$$v_s(r_s) = v_g(r_s), \tag{5}$$

and conservation of heat flow across the solid-gas interface at $r = r_s$ gives,

$$K_s \left.\frac{dv_s}{dr}\right|_{r=r_s} = K_g \left.\frac{dv_g}{dr}\right|_{r=r_s}. \tag{6}$$

Rearranging eq (1) and eq (2) yields, respectively,

$$\frac{d}{dr}\left(r \frac{dv_s}{dr}\right) = -\frac{rQ_s(r)}{K_s} \tag{7}$$

and

$$\frac{d}{dr}\left(r \frac{dv_g}{dr}\right) = 0; \tag{8}$$

and integrating these equations twice yields the steady state solutions;

$$v_s(r) = v_s(0) - \frac{Q_l}{4K_s} \begin{cases} r^2 & \text{for } 0 \leq r \leq r_l \\ r_l^2[1 + 2\ln(r/r_l)] & \text{for } r_l \leq r \leq r_s, \end{cases} \tag{9}$$

and

$$v_g(r) = C_{1g} \ln r + C_{2g} \text{ for } r_s \leq r \leq r_i, \tag{10}$$

where C_{1g} and C_{2g} are constants of integration and where the limit that

$$\lim_{r\to 0} r\frac{dv_s}{dr}=0 \tag{11}$$

is invoked to obtain eq (9) (i.e., that v_s remains finite at $r=0$).

Boundary conditions (4), (5), and (6) require that the temperature at the center of the cylinder $r=0$ is

$$v_s(0)=T_0+\frac{Q_l r_l^2}{4K_s}\left\{1-\frac{2K_s}{K_g}\ln\left(\frac{r_s}{r_i}\right)+2\ln\left(\frac{r_s}{r_l}\right)\right\}, \tag{12}$$

and that the temperature in the gas is

$$v_g(r)=T_0-\frac{Q_l r_l^2}{2K_g}\ln\left(\frac{r}{r_i}\right). \tag{13}$$

3. Transient Solution—Cylinder

The transient temperature $u(r, t)$ for times $t\geq 0$ is given in [3] by the diffusion equations

$$k_s\frac{\partial^2}{\partial r^2}u_s(r,t)+\frac{k_s}{r}\frac{\partial u_s(r,t)}{\partial r}=\frac{\partial u_s(r,t)}{\partial t} \tag{14}$$

and

$$k_g\frac{\partial^2}{\partial r^2}u_g(r,t)+\frac{k_g}{r}\frac{\partial u_g(r,t)}{\partial r}=\frac{\partial u_g(r,t)}{\partial t}. \tag{15}$$

At time $t=0$, the sum of the transient and steady-state temperatures is everywhere equal to the ambient temperature T_0,

$$T(r,0)=u(r,0)+v(r)=T_0; \tag{16}$$

and at any time t the temperature at the heat sink $r=r_i$ is T_0, i.e.,

$$u_g(r_i,t)=0, \tag{17}$$

because

$$\lim_{t\to\infty}u(r,t)=0,$$

by the definition of transient solutions and because $v_g(r_i)=T_0$.

A general separable solution to an equation having the form of either eq (14) or (15) is

$$u(r,t)=R(r)\tau(t)=[AJ_0(\xi r)+BY_0(\xi r)]\exp(-\xi^2 kt), \tag{18}$$

where J_n is the nth order Bessel function of the first kind, Y_n is the nth order Bessel function of the second kind [8], ξ is the constant of separation, and A and B are constants. The quantities A, B, ξ, and k have the subscript s for the solid and the subscript g for the gas.

Equation (17) states that

$$R_g(r_i)=0, \tag{19}$$

and the temperature continuity equation at $r=r_s$, requires that

$$R_s(r_s)=R_g(r_s) \tag{20}$$

and

$$\xi_s^2=(k_g/k_s)\xi_g^2. \tag{21}$$

Also, the constant $B_s=0$ because the temperature must be finite for all $r\geq 0$ and t.

Hence, the conservation of heat flow across the solid-gas interface

$$K_s\partial u_r(r,t)/\partial r|_{r=r_s}=K_g\,\partial u_g(r,t)/\partial r|_{r=r_s} \tag{22}$$

and the other boundary conditions eq (19) and eq (20) yield three homogeneous simultaneous equations for the three unknowns A_s, A_g, and B_g. Solutions for this set of three equations exist if and only if the determinant, D, of their coefficients vanishes; the vanishing of the determinant yields the eigenvalues $\xi_g=\xi_j$, where $j=1, 2\ldots$. The jth eigenvalue ξ_j is that value of ξ_g for which the determinant vanishes for the jth time, i.e., $\xi_j<\xi_{j+1}$; namely, $\det D(\xi_j)=0$, where

$$D=\begin{vmatrix} 0 & J_0(\xi_g r_i) & Y_0(\xi_g r_i)\\ J_0(\xi_s r_s) & -J_0(\xi_g r_s) & -Y_0(\xi_g r_s)\\ -K_s\xi_s J_1(\xi_s r_s) & K_g\xi_g J_1(\xi_g r_s) & K_g\xi_g Y_1(\xi_g r_s)\end{vmatrix} \tag{23}$$

The eigenvalues ξ_j also determine the characteristic times t_j for the solid-gas system; namely,

$$t_j=(\xi_j^2 k_g)^{-1}. \tag{24}$$

Expressing A_s and B_g in terms of $A_j=A_g$, we obtain,

$$R_s(r)=\sum_{j=1}^{\infty}A_j F_0(\xi_j, r_i, r_s)\{J_0(\bar{\xi}_j r)/J_0(\bar{\xi}_j r_s)\}, \tag{25}$$

for $0\leq r\leq r_s$ and

$$R_g(r)=\sum_{j=1}^{\infty}A_j F_0(\xi_j, r_i, r)$$

for $r_s\leq, r\leq r_i$, where $\bar{\xi}_j^2=(k_g/k_s)\,\xi_j^2$ and where the function F_n is

$$F_n(\xi_g, r_i, r)=\{Y_0(\xi_g r_i)J_n(\xi_g r)-J_0(\xi_g r_i)Y_n(\xi_g r)\}/Y_0(\xi_g r_i). \tag{27}$$

Relations (25), (26), and (27) are valid only if $J_0(\bar{\xi}_j r_s)\neq 0$ and if $Y_0(\xi_j r_i)\neq 0$.

In terms of the functions $F_n(\xi, r_i, r)$, the eigenvalue equation satisfied by the eigenvalue ξ_j becomes,

$$K_s\xi_j J_1(\bar{\xi}_j r_s)F_0(\bar{\xi}_j, r_i, r_s)-K_g\xi_j J_0(\bar{\xi}_j r_s)F_1(\xi, r_i, r_s)=0.$$

We determine the coefficients A_j by using the $t=0$ relations obtained from eq (16); namely,

$$R_s(r)=T_0-v_s(r) \qquad \text{for } 0\leq r\leq r_s \tag{28}$$

and

$$R_g(r)=T_0-v_g(r) \qquad \text{for } r_s\leq r\leq r_i. \tag{29}$$

First, we consider the eigenfunctions for the solid-gas system

$$E_0(\xi_j, r_i, r) = \begin{cases} F_0(\xi_j, r_i, r_s)\{J_0(\bar{\xi}_j r)/J_0(\bar{\xi}_j r_s)\} & \text{for } 0\leq r\leq r_s \\ F_0(\xi_j, r_i, r) & \text{for } r_s\leq r\leq r_i. \end{cases} \tag{30}$$

Next, we multiply both sides of eq (28) and eq (29) by

$$\frac{K_s}{k_s} rE_0(\xi_i, r_i, r) \quad \text{when } 0\leq r\leq r_s$$

and by

$$\frac{K_g}{k_g} rE_0(\xi_i, r_i, r) \quad \text{when } r_s\leq r\leq r_i$$

and then we integrate the resulting expressions over the interval $0\leq r\leq r_i$. This procedure yields the following expression for the coefficients A_j

$$\begin{aligned} &\sum_{j=1}^{\infty} A_j\Delta(\xi_j, \xi_i) \\ &=\frac{K_s}{k_s}\Big[\{T_0-v_s(0)\}\int_0^{r_s} E_0(\xi_i, r_i, r)rdr \\ &\quad+\frac{Q_l}{4K_s}\Big\{\int_0^{r_l} E_0(\xi_i, r_i, r)rdr \\ &\quad+r_l^2\int_{r_l}^{r_s}\{1+2\ln(r/r_l)\}E_0(\xi_i, r_i, r)r^3dr\Big\}\Big] \\ &\quad+\frac{K_g}{k_g}\Big[\frac{Q_l r_l^2}{2K_g}\int_{r_s}^{r_i}\ln(r/r_i)E_0(\xi_i, r_i, r)rdr\Big]. \end{aligned} \tag{31}$$

where

$$\begin{aligned} \Delta(\xi_j, \xi_i) &= \frac{K_s}{k_s}\int_0^{r_s} E_0(\xi_j, r_i, r)E_0(\xi_i, r_i, r)rdr \\ &\quad+\frac{K_g}{k_g}\int_{r_s}^{r_i} E_0(\xi_j, r_i, r)E_0(\xi_i, r_i, r)rdr. \end{aligned} \tag{32}$$

Appendix A contains the evaluations of the several integrals which occur in eq (31) and eq (32). Using eq (A4) and the fact that $dB_0(\xi r)/dr=-B_1(\xi r)$, we find that $\Delta(\xi_j, \xi_l)$ vanishes unless $\xi_j=\xi_l$; and when $\xi_j=\xi_i$ the factor $\Delta(\xi_j, \xi_j)=\Delta_j$ becomes

$$\begin{aligned} \Delta_j=\frac{K_g r_s^2}{2k_g}\Big[&\Big(\frac{K_s k_g}{K_g k_s}-1\Big)F_0^2(\xi_j, r_i, r_s) \\ &+(r_i^2/r_s^2)F_1^2(\xi_j, r_i, r_i)+\Big(\frac{K_g}{K_s}-1\Big)F_1^2(\xi_j, r_i, r_s)\Big]. \end{aligned} \tag{33}$$

Applying eqs (A1) to (A3) to the right-hand side of eq (31), we obtain, after several steps, an expression for the coefficients A_j, namely,

$$A_j=-\frac{Q_l r_l}{k_s\bar{\xi}_j^3}\frac{J_1(\bar{\xi}r_l)F_0(\xi_j, r_i, r_s)}{\Delta_j J_0(\bar{\xi}_j r_s)}. \tag{34}$$

Because we sum in the computer program used in [3] a finite number of terms in such expressions as eq (25) and eq (26), we normalize the A_j's for $1\leq j\leq N$ by using the relation (29) evaluated at $r=r_s$. To accomplish this normalization, we introduce the normalization factor a_N and replace A_j with $a_N A_j(N)$ in the relation (29). This then gives us an expression for the factor a_N; namely,

$$a_N=-\frac{Q_l r_l^2}{2K_g}\ln\Big(\frac{r_s}{r_i}\Big)\Big/\sum_{j=1}^{N} A_j(N)F_0(\xi_j, r_i, r_s). \tag{35}$$

4. Steady-State Solution—Plate

From [5], the steady-state temperature $v(z)$ satisfies the following heat diffusion equations for the proposed device in figure 2:

When $z_2\leq|z|\leq z_3$,

$$\frac{\partial^2}{\partial z^2}v_s(z)+\frac{Q_l}{K_s}=0\ ; \tag{36}$$

and when $|z|\leq z_2$,

$$\frac{\partial^2}{\partial z^2}v_g(z)=0. \tag{37}$$

The temperature in the cell windows is $v_s(z)$ and the temperature in the gas is $v_g(z)$. The power absorbed per unit volume in the cell windows is $Q_l=\alpha_s W_l/\pi r_l^2$. The absorption coefficient of the windows is α_s.

The boundary conditions are that

$$v_s(\pm z_3)=T_0, \tag{38}$$

where T_0 is the ambient temperature. Continuity of temperature and conservation of heat flow across the solid-gas interface at $z=\pm z_2$ give, respectively,

$$v_s(\pm z_2)=v_g(\pm z_2) \tag{39}$$

and

$$K_s dv_s/dz \mid_{z=\pm z_2} = K_g dv_g/dz \mid_{z=\pm z_2}. \tag{40}$$

We integrate eqs (36) and (37) twice to obtain the general solutions,

$$v_s(z) = -(Q_l z^2/2K_s) + C_s \mid z \mid + D_s, \tag{41}$$

and

$$v_s(z) = C_g \mid z \mid + D_g, \tag{42}$$

where the C's and D's are constants of integration.

The absolute value of z occurs in eqs (41) and (42) because $v(z) = v(-z)$ when $\alpha_s \mid z_3 - z_2 \mid \ll 1$. Also, because $dv_g(z)/dz \mid_{z=0^+} = C_g$ and $dv_g(z)/dz \mid_{z=0^-} = -C_g$, the constant C_g must be zero. (If C_g were not zero, then a heat sink or heat source would exist at $z=0$. This is not the case for the proposed device).

The boundary condition (38) at $z=z_3$ and the boundary conditions (39) and (40) at $z=z_2$ yield three inhomogeneous equations for the three unknown coefficients C_s, D_s, and D_g; namely,

$$\begin{aligned} C_s z_3 + D_s &= T_0 + (Q_l z_3^2/2K_s), \\ -D_g + C_s z_2 + D_s &= (Q_l z_2^2/2K_s), \\ C_s K_s &= Q_l z_2. \end{aligned} \tag{43}$$

A solution for the three equations exists if the determinant of their coefficients does not vanish; i.e.,

$$\det \begin{pmatrix} 0 & z_3 & 1 \\ -1 & z_2 & 1 \\ 0 & K_s & 0 \end{pmatrix} = -K_s \neq 0. \tag{44}$$

Using the matrix method to solve the set of equations (43), we obtain the steady-state temperature:

$$v_s(z) = T_0 + (Q_l/K_s)[z_3\{(z_3/2) - z_2\} - \mid z \mid \{(\mid z \mid/2) - z_2\}], \tag{45}$$

for $z_2 \leq \mid z \mid \leq z_3$, and

$$v_g(z) = T_0 + (Q_l/2K_s)(z_3 - z_2)^2 \tag{46}$$

for $\mid z \mid \leq z_2$.

5. Transient Solution—Plate

The transient solution $u(z, t)$ for times $t \geq 0$ satisfies the following heat diffusion equations: [5]

$$\frac{\partial^2}{\partial z^2} u_s(z, t) = \frac{1}{k_s} \frac{\partial u_s(z, t)}{\partial t} \tag{47}$$

for $z_2 \leq \mid z \mid \leq z_3$, and

$$\frac{\partial^2}{\partial z^2} u_g(z, t) = \frac{1}{k_g} \frac{\partial u_g(z, t)}{\partial t} \tag{48}$$

for $\mid z \mid \leq z_2$.

At time $t=0$, the sum of the transient and steady-state temperature at the exterior sides of the cell windows at $\mid z \mid = z_3$ is T_0, i.e.,

$$u_s(\pm z_3, t) = 0, \tag{49}$$

because

$$\lim_{t \to \infty} u(z, t) = 0 \tag{50}$$

by the definition of transient behavior and because $v_s(\pm z_3) = T_0$.

General separable solutions to eqs (47) and (48) are

$$u(z, t) = R(z)\tau(t)$$

where

$$R(z) = [A \exp(i\xi z) + B \exp(-i\xi z)]$$

and

$$\tau(t) = \exp(-\xi^2 k t).$$

The constant of separation is ξ and the coefficients A and B are constants. The subscripts s and g denote the quantities A, B, ξ, and k respectively for the windows and for the gas.

Equation (49) gives us that

$$R_s(\pm z_3) = 0. \tag{51}$$

The continuity of temperature across the interfaces at $\mid z \mid = z_2$ requires that

$$R_s(\pm z_2) = R_g(\pm z_2)$$

and

$$\xi_s^2 = (k_g/k_s)\xi_g^2. \tag{52}$$

In addition, the conservation of heat flow across the window-glass interface at $\mid z \mid = z_2$ requires that

$$K_s(dR_s/dz)\mid_{z=\pm z_2} = K_g(dR_g/dz)\mid_{z=\pm z_2}. \tag{53}$$

Hence, the boundary conditions (51), (52), and (53) yield six homogeneous simultaneous equations for the six unknown coefficients $A_s^>$, $B_s^>$, A_g, B_g, $A_s^<$, and $B_s^<$, where the superscripts $<$ and $>$ are, respectively, for $z<0$ and $z>0$. Because $A_s^< = B_s^>$, $B_s^< = A_s^>$, and $A_g = B_g$ by symmetry, these six equations reduce to three equations in three unknowns. $A_s = A_s^>$, $B_s = B_s^>$, and $A = 2A_g$. Solutions for this set of equations exist if, and only if, the determinant D of their coefficients vanishes. The vanishing of the determinant yields the eigenvalues $\xi_g = \xi_j$, where $j = 1, 2, 3, \ldots \infty$.

The jth eigenvalue ξ_j is that value of ξ_g for which the determinant vanishes for the jth time, i.e., $\xi_j < \xi_{j+1}$; namely,

$$\det D(\xi_j) = 0, \tag{54}$$

where

$$D = \begin{pmatrix} 0 & \exp(i\xi_s z_3) & \\ -\cos(\xi_g z_2) & \exp(i\xi_s z_2) & \\ \xi_g K_g \sin(\xi_g z_2) & i\xi_s K_s \exp(i\xi_s z_2) & \\ & \exp(-i\xi_s z_3) & \\ & \exp(-i\xi_s z_2) & \\ & -i\xi_s K_s \exp(-i\xi_s z_2) & \end{pmatrix} \tag{55}$$

and $\xi_s^2 = (k_g/k_s)\xi_g^2$. From eqs (54) and (55), the eigenvalue ξ_j satisfies the following equation

$$(K_g/k_g^{1/2}) \sin(\xi_g z_2) \sin(\xi_s d) = (K_s/k_s^{1/2}) \cos(\xi_g z_2) \cos(\xi_s d), \tag{56}$$

where $\xi_g = \xi_j$ and $d = (z_3 - z_2)$.

Expressing A_s and B_s in terms of $A = A_j$, we have

$$R_g(z) = \sum_{j=1}^{\infty} A_j \cos(\xi_j z) \text{ for } |z| \leq z_2 \tag{57}$$

and

$$R_s(z) = \sum_{j=1}^{\infty} \frac{A_j \cos(\xi_j z_2)}{2 \sin^2(\xi_j' d)} \{\cos(\xi_j'(|z| - z_2)) - \cos(\xi_j'(|z| + z_2 - 2z_3))\} \tag{58}$$

for $z_2 \leq |z| \leq z_3$, where $\xi_j' = (k_g/k_s)^{1/2}\xi_j$.

We determine the coefficients A_j by using the $t = 0$ relations obtained from eq (49); namely,

$$R_s(z) = T_0 - v_s(z) \text{ for } z_2 \leq |z| \leq z_3 \tag{59}$$

and

$$R_g(z) = T_0 - v_g(z) \text{ for } |z| \leq z_2. \tag{60}$$

Equations (57) and (58) contain the eigenfunctions for the window-gas system; namely,

$$E(j, z) = \begin{cases} \cos(\xi_j z) & \text{for } |z| \leq z_2 \\ \dfrac{\cos(\xi_j z_2)\{\cos(\xi_j'(|z| - z_2)) - \cos(\xi_j'(|z| + z_2 - 2z_3))\}}{2 \sin^2(\xi_j' d)} & \text{for } z_2 \leq |z| \leq z_3. \end{cases} \tag{61}$$

We multiply both sides of eqs (59) and (60) by

$$K_g(k_s/k_g)^{1/2} E(j, z) \text{ when } -z_2 \leq |z| \leq z_3$$

and by

$$K_s(k_g/k_s)^{1/2} E(j, z) \text{ when } |z| \leq z_3,$$

and we integrate the resulting expressions respectively over the intervals $0 \leq z \leq z_2$ and $z_2 \leq z \leq z_3$. This procedure gives us the following expression for the coefficients A_j:

$$\sum_{j=1}^{\infty} A_j \Delta(\xi_j, \xi_i) = (T_0 - D_g) K_g (k_s/k_g)^{1/2} \int_0^{z_2} E(i, z) dz + (Q_l/K_s) K_s (k_g/k_s)^{1/2} \int_{z_2}^{z_3} [z\{(z/2) - z_2\} - z_3\{(z_3/2) - z_2\}] E(i, z) dz \tag{62}$$

where

$$\Delta(\xi_j, \xi_i) = K_g (k_s/k_g)^{1/2} \int_0^{z_2} E(j, z) E(i, z) dz + K_s (k_g/k_s)^{1/2} \int_{z_2}^{z_3} E(j, z) E(i, z) dz. \tag{63}$$

Appendix B contains the evaluations of the several integrals which occur in eqs (62) and (63). Using eq (B4) gives us that $\Delta(\xi_j, \xi_i)$ vanishes unless $\xi_j = \xi_i$. And when $\xi_j = \xi_i$, the factor $\Delta(\xi_j, \xi_j) = \Delta_j$ becomes from eq (B5)

$$\Delta_j = \frac{K_g (k_s/k_g)^{1/2}}{2} [z_2 + \{K_s k_g d \cos^2(\xi_j z_2)/K_g k_s \sin^2(\xi_j' d)\}]. \tag{64}$$

Applying eq (B1) through eq (B3) repeatedly to the right-hand side of eq (62) gives us an expression for the coefficients A_j; namely,

$$A_j = (K_g k_s Q_l/\xi_j^3 K_s k_g \Delta_j) \{(k_s/k_g)^{1/2} \sin(\xi_j z_2) - (K_s \cos(\xi_j z_2)/K_g \sin(\xi_j' d)\}. \tag{65}$$

Because the computer program in [5] evaluates a finite number of terms in such expressions as eq (57) and eq (58), the coefficients A_j are normalized for $1 \leq j \leq N$ by using the relation (60) evaluated at $z = z_2$. Replacing A_j with $a_N A_j(N)$ in relation (60), one obtains an expression for the normalization factor a_N,

$$a_N = -\frac{(Q_l d^2/2K_s)}{\sum_{j=1}^{N} A_j(N) \cos(\xi_j z_2)} \tag{66}$$

6. Cyclic Heating and Cooling

The Green's function method offers a convenient way for computing the response of the proposed barothermal devices when the beam of radiation is turned on at $t=0$ and is modulated at angular frequency ω for all times $t \geq 0$. We express the power absorbed per unit volume $Q_l(t)$ by the expression,

$$Q_l(t)=\eta(t)\,\eta(r_l-r)Q_l(1+m\cos\omega t), \qquad (67)$$

where $|m| \leq 1$ is the modulation factor for cyclic heating and cooling and where ω is less than the characteristic frequency of the system. The step function $\eta(x)$ is zero for $x \leq 0$ and 1 for $x > 0$.

6.1. Cylinder

The temperature $T(r_0, t_0)=u(r_0, t_0)+v(r_0)-T_0$, satisfies the heat diffusion for the cylinder and the gas; namely, for times $t_0 \geq 0$,

$$\nabla_0^2 T(r_0, t_0)-k^{-1}(\partial T(r_0, t_0)/\partial t_0)=-\rho(r_0, t_0); \qquad (68)$$

where $\rho(r_0, t_0)=\eta(r_l-r_0)(Q_l/K_s)(1+m\cos\omega t)$ for $r_l \leq r_s$; where ∇_0^2 becomes $\{(\partial^2/\partial r^2)+r_0^{-1}(\partial/\partial r_0)$ because the temperature does not depend upon angle θ_0 and coordinate z_0; and where k is subscripted with s when $0 \leq r_0 \leq r_s$ and with g when $r_s \leq r_0 \leq r_i$. We subtract the ambient temperature T_0 from the temperature for later convenience in using the boundary condition $T(r_i, t)=0$.

The Green's function $G(r, t|r_0, t_0)$ for the system satisfies the equation

$$\nabla^2 G(r, t|r_0, t_0)-k^{-1}\partial G(r, t|r_0, t_0)/\partial t = -\frac{\delta(r-r_0)\delta(t-t_0)}{r(K/k)}, \qquad (69)$$

where k and K are subscripted with s when $0 \leq r \leq r_s$ and with g when $r_s \leq r \leq r_i$. We interpret G to be the temperature which occurs at r and t when an impulse source of heat is introduced at r_0 and t_0.

The Green's function satisfies a causality condition:

$$G(r, t|r_0, t_0)=0 \qquad \text{if } t < t_0. \qquad (70)$$

In addition, it satisfies a reciprocity condition under time reversal because the causality condition (70) requires a time sequence

$$G(r, t|r_0, t_0)=G(r_0, -t_0|r, -t), \qquad (71)$$

where the function $G(r_0, -t_0|r, -t)$ gives the temperature at r_0 and $-t_0$ due to a source impulse at r and $-t$. Because $-t_0 > -t$, the time sequence is properly ordered. Hence, from eq (71) we have that

$$\nabla_0^2 G(r, t|r_0, t_0)+k^{-1}\partial G(r, t|r_0, t_0)/\partial t_0 = -\frac{\delta(r-r_0)\delta(t-t_0)}{r_0(K/k)}, \qquad (72)$$

where k and K are subscripted with s when $0 \leq r_0 \leq r_s$ and with g when $r_s \leq r_0 \leq r_i$.

We shall now express the solutions of the inhomogeneous diffusion eq (68) for the solid and gas in terms of the Green's function G. We first multiply eq (68) by $G(r, t|r_0, t_0)$ and eq (72) by $T(r_0, t_0)$ and then subtract the first product-equation from the second product-equation. Keeping in mind that the thermal factor for the solid (K_s/k_s) differs from the thermal factor for the gas (K_g/k_g), we integrate the above result over the time domain $0 \leq t_0 \leq t^-$ and over the volume of the solid-gas system.

$$\int dV(\ldots)=\int_0^{r_s}(\ldots)(K_s/k_s)r_0 dr_0 + \int_{r_s}^{r_i}(\ldots)(K_g/k_g)r_0 dr_0,$$

where $t^+=\lim_{\epsilon \to 0} t+\epsilon$.

The differential form of Green's theorem for our special case,

$$r_0(T\nabla_0^2 G-G\nabla_0^2 T)=\frac{\partial}{\partial r_0}\left(Tr_0\frac{\partial G}{\partial r_0}\right) - \frac{\partial}{\partial r_0}\left(Gr_0\frac{\partial T}{\partial T_0}\right), \qquad (73)$$

enables us to express the temperature in terms of the Green's function. The final result becomes

$$\eta(r)\eta(r_s-r)T_s(r, t)+\eta(r-r_s)\eta(r_i-r)T_g(r, t) = \int_0^{t^+} dt_0\frac{K_s}{k_s}\int_0^{r_s}\rho(r_0, t_0)G(r, t|r_0, t_0)r_0 dr_0 + \int_0^{t^+} dt_0\frac{K_g}{k_g}\int_{r_s}^{r_i}\rho(r_0, t_0)G(r, t|r_0, t_0)r_0 dr_0, \qquad (74)$$

where we have used the following initial conditions and boundary conditions:

$$T_s(r, 0)=0,\ T_g(r, 0)=0,\ G(r, t|r_0, t^+)=0$$

$$T_s(r_s, t)=T_g(r_s, t),\ T_g(r_i, t)=0,$$

$$k_s^{-1}G(r, t|r_s^-, t_0)=k_g^{-1}G(r, t|r_s^+, t_0),$$

$$G(r, t|r_i, t_0)=0,$$

$$K_s\partial T_s/\partial r_0|_{r_0=r_s}=k_g\partial T_g/\partial r_0|_{r_0=r_s}, \text{ and}$$

$$K_s k_s^{-1}\partial G(r, t|r_0, t_0)/\partial r_0|_{r_0=r_s} = K_g k_g^{-1}\partial G(r, t|r_0, t_0)/\partial r_0|_{r_0=r_s^+}.$$

We now proceed to construct the Green's function $G(r, t/r_0, t_0)$. Referring to eqs (30), (32), and (33), we have that the spatial eigenfunctions of the solid-gas system are

$$W_j(r)=\begin{cases}(K_s/k_s\Delta_j)^{1/2}E_0(\xi_j, r_i, r) & \text{for } 0\leq r\leq r_s \quad (75)\\ (K_g/k_g\Delta_j)^{1/2}E_0(\xi_j, r_i, r) & \text{for } r_s\leq r\leq r_i,\end{cases}$$

where

$$\int_0^{r_i} rdrW_{j_1}(r)W_{j_2}(r)=\delta_{j_1, j_2};$$

$$\sum_{j=1}^{\infty} W_j(r)W_j(r_0)=\{\eta(r)\,\eta(r_s-r)\,(K_s/k_s)$$

$$+\eta(r-r_s)\,\eta(r_i-r)\,(K_g/k_g)\}r^{-1}\delta(r-r_0),$$

and $\nabla^2 W_j(r)+\xi_j^2 W_j(r)=0$.

Hence, we may expand the Green's function in terms of the above eigenfunctions $W_j(r)$; namely,

$$G(r, t|r_0, t_0)=\sum_{j=1}^{\infty} C_j(t, t_0)W_j(r)W_j(r_0). \quad (76)$$

Substitution of eq (76) into eq (69) yields the first order differential equation for the coefficients $C_j(t, t_0)$,

$$k_g^{-1}\frac{\partial}{\partial t}C_j(t, t_0)+\xi_j^2 C_j(t, t_0)=\delta(t-t_0). \quad (77)$$

The solution of eq (77) subject to the condition that $C_j(t, t_0)=0$ to $t<t_0$ is

$$C_j(t, t_0)=\eta(t-t_0)\exp\{-\xi_j^2 k_g(t-t_0)\}. \quad (78)$$

The temperature in the gas $(r_s\leq r\leq r_i)$ for the cyclic heating and cooling described by eq (68) becomes according to eq (74)

$$T_g(r, t)=T_0+\sum_{j=1}^{\infty} A_j F_0(\xi_j, r_i, r)f(\omega, \xi_j, k_g, m, t) \quad (79)$$

where we have added the ambient temperature T_0, where

$$f(\omega, \xi_j, k_g, m, t)=[\{\exp(-\xi_j^2 k_g t)-1\} \quad (80)$$

$$+m\{1+(\omega/\xi_j^2 k_g)^2\}^{-1}\{\exp(-\xi_j^2 k_g t)-\cos\omega t$$

$$-(\omega/\xi_j^2 k_g)\sin\omega t\}],$$

where A_j is given by eq (34).

6.2. Plate

The temperature, $T(z_0, t_0)=u(z_0, t)+v(z_0)-T_0$, satisfies the heat diffusion equation for the gas cell; namely, for times $t_0\geq 0$,

$$\frac{\partial^2}{\partial z_0^2}T(z_0, t_0)-k^{-1}\frac{\partial T(z_0, t_0)}{\partial t}=-\rho(z_0, t_0), \quad (81)$$

where $\rho(z_0, t_0)=\eta(|z|-z_2)\,\eta(z_3-|z|)\ (Q_l/K_s)\ (1+m\cos\omega t)$ and where k is subscripted with s when $z_2\leq|z|\leq z_3$ and with g when $z_2\geq|z|\geq 0$.

The Green's function $G(z, t|z_0, t_0)$ for the gas cell satisfies the equation,

$$\partial^2 G/\partial z^2-k^{-1}\partial G/\partial t=-\frac{\delta(z-z_0)\,\delta(t-t_1)}{K(k'/k)^{1/2}}, \quad (82)$$

where, when $0\leq|z|\leq z_2$, $k=k_g$, $k'=k_s$, and $K=K_g$; and where, when $z_2\leq|z|\leq z_3$, $k=k_s$, $k'=k_g$, and $K=K_s$. This Green's function for the gas cell obeys causality and conditions similar respectively to eq (70) and eq (71). It also satisfies the adjoint equation similar to eq (72).

Expressing the temperature in terms of the Green's function involves the same steps as those contained in part A of this section. The thermal factors are $K_s(k_g/k_s)^{1/2}$ for the windows and $K_g(k_s/k_g)^{1/2}$ for the gas. The final result is,

$$T_g(z, t)=T_0+\sum_{j=1}^{\infty} A_j\cos(\xi_j z)f(\omega, \xi_j, k_g, m, t), \quad (83)$$

where A_j is given by eq (65), $f(\omega, \xi_j, k_g, m, t)$ is given by eq (80), and where we have added the ambient temperature T_0.

7. Conclusions

The mathematical expressions contained in eqs (33), (34), (35) and (79) for cylinders and in eqs (64), (65), (67) and (83) for plates form the basis of the computer programs used in references [3] through [6]. The authors of these references predict by computer programs the performance of the proposed devices for measuring absorption coefficients as functions of their operating parameters.

8. Appendix A. Integrals Occurring in Equation (31) and Equation (32)

If $B_n(\xi r)$ is any one of the functions $J_n(\xi r)$, $Y_n(\xi r)$, or $F_n(\xi, r_i, r)$, then from references [9], [10], and [11], we have that

$$\int B_0(\xi r)rdr=(r/\xi)J_1(\xi r)+\text{constant}, \quad (A1)$$

$$\int B_0(r)r^3dr=(r/\xi)[\{r^2-(2/\xi)^2\}B_1(\xi r)$$

$$+(2r/\xi)B_0(\xi r)]+\text{constant}, \quad (A2)$$

$$\int \ln(r)B_0(\xi r)rdr=(r/\xi)\ln(r)B_1(\xi r)$$

$$+(1/\xi^2)B_0(\xi r)+\text{constant}. \quad (A3)$$

If $Z_m(\xi_1 r) = aJ_m(\xi_1 r) + bY_m(\xi_1 r)$ and $X_m(\xi_2 r) = cJ_m(\xi_2 r) + dY_m(\xi_2 r)$ with a, b, c, and d independent of m and r, then

$$(\xi_1^2 - \xi_2^2) \int Z_m(\xi_1 r) X_m(\xi_2 r) r dr$$

$$= \xi_2 r Z_m(\xi_1 r) X_{m-1}(\xi_2 r) - \xi_1 r Z_{m-1}(\xi_1 r) X_m(\xi_2 r). \quad \text{(A4)}$$

9. Appendix B. Integrals Occurring in Equation (62) and Equation (63)

We tabulate in this Appendix the several integrals which appear in eq (62) and eq (63):

$$\int \cos\{\xi(z+b)\} dz = (1/\xi) \sin\{\xi(z+b)\} \quad \text{(B1)}$$

$$\int z \cos\{\xi(z+b)\} dz = (1/\xi)^2 \cos\{\xi(z+b)\} + \xi z \sin\{\xi(z+b)\} \quad \text{(B2)}$$

$$\int z^2 \cos\{\xi(z+b)\} dz = (1/\xi)^3 [2\xi z \cos\{\xi(z+b)\} + (\xi^2 z^2 - 2) \sin\{\xi(z+b)\}]. \quad \text{(B3)}$$

When $\xi_1 \neq \xi_2$, we have that

$$\int \cos\{\xi_1(z+b)\} \cos\{\xi_2(z+c)\}$$

$$= \cos\{\xi_2(b-c)\} \left[\frac{\sin\{(\xi_1 - \xi_2)(z+b)\}}{2(\xi_1 - \xi_2)} + \frac{\sin\{(\xi_1 + \xi_2)(z+b)\}}{2(\xi_1 + \xi_2)} \right]$$

$$+ \sin\{\xi_2(b-c)\} \left[\frac{\cos(\xi_1 - \xi_2)(z+b)}{2(\xi_1 - \xi_2)} - \frac{\cos\{(\xi_1 + \xi_2)(z+b)\}}{2(\xi_1 + \xi_2)} \right]; \quad \text{(B4)}$$

and when $\xi_1 = \xi_2 = \xi$, we have that

$$\int \cos\{\xi(z+b)\} \cos\{\xi(z+c)\} = \frac{\cos\{\xi(b-c)\}}{2\xi} [\xi(z+b) + \sin\{\xi(z+b)\} \cos\{\xi(z+b)\}] + \frac{\sin\{\xi(b-c)\}}{2\xi} \sin^2\{\xi(z+b)\}. \quad \text{(B6)}$$

10. References

[1] White, K. I., and Midwinter, J. E., Opto-Electronics **5**, 323 (1973).
[2] Bennett, H. S., and Forman, R. A., to be published.
[3] Bennett, H. S., and Forman, R. A., to be published.
[4] Bennett, H. S., and Forman, R. A., to be published.
[5] Bennett, H. S., and Forman, R. A., to be published.
[6] Bennett, H. S., and Forman, R. A., to be published.
[7] Bennett, H. S., to be published.
[8] Handbook of Mathematical Functions, edited by M. Abramowitz and I. A. Stegun (Dover Publications, Inc., New York, 1965), p. 355.
[9] Hildebrand, F. B., Advanced Calculus for Engineers (Prentice-Hall, Inc. Englewood Cliffs, 1949), Chap. 4.
[10] Morse, R. M. and Feshbach, H., Methods of Theoretical Physics (McGraw-Hill Book Company, Inc., New York, 1953), p. 1322.
[11] Mathews, J. and Walker, R. L., Mathematical Methods of Physics (W. A. Benjamin, Inc., New York, 1965), p. 174.

(Paper 79A5-866)

JOURNAL OF RESEARCH of the National Bureau of Standards — A. Physics and Chemistry
Vol. 79A, No. 5, September-October 1975

Publications of the National Bureau of Standards*

Citations with Selected Abstracts

J. Res. Nat. Bur. Stand. (U.S.), **79A** *(Phys. and Chem.)*, No. 4 (July-August 1975), SD Catalog No. C13.22/sec.A:79/4.

Radiance temperature (at 653 nm) of iron at its melting point, A. Cezairliyan and J. L. McClure.

Precision measurements of the dimensional stability of four mirror materials, B. Justice.

A correlation for the second interaction virial coefficients and enhancement factors for moist air, R. W. Hyland.

The enthalpies of combustion and formation of thianthrene, W. H. Johnson.

Unbound water content from application of adsorption theory, W. V. Loebenstein.

Monogr. 145, Part I. **Tables of spectral-line intensities. Part I—Arranged by elements,** W. F. Meggers, C. H. Corliss, and B. F. Scribner, Nat. Bur. Stand. (U.S.), Monogr. 145, Part I, 403 pages (May 1975) SD Catalog No. C13.44:145/I, $8.55.

Key words: classification of spectral lines; intensities of spectral lines; spectral-line intensities; tables of spectral-line intensities; wavelengths of spectral lines.

The relative intensities, or radiant powers, of 39 000 spectral lines with wavelengths between 2000 and 9000 Ångstroms have been determined on a uniform energy scale for seventy chemical elements. This was done by mixing 0.1 atomic percent of each element in powdered copper, pressing the powder-mixture to form solid electrodes which were burned in a 10 ampere, 220 volt direct-current arc, and photographing the spectra with a stigmatic concave grating while a step sector was rotating in front ofthe slit. The sectored spectrograms facilitated the estimation of intensities of all element lines relative to copper lines which were then calibrated on an energy scale provided by standardized lamps, and all estimated line intensities were finally adjusted to fit this calibration. Comparisons with other intensity measurements in individual spectra indicate that the National Bureau of Standards spectral-line intensities may have average errors of 20 percent, but first of all they provide uniform quantitative values for the seventy chemical elements commonly determined by spectrochemists. These data are presented by element in part I, and all 39 000 observed lines are given in order of wavelength in part II. Supersedes Monograph 32, Parts I and II and its supplement.

Monogr. 145, Part II. **Tables of spectral-line intensities. Part II—Arranged by wavelengths,** W. F. Meggers, C. H. Corliss, and B. F. Scribner, Nat. Bur. Stand. (U.S.), Monogr. 145, Part II, 228 pages (May 1975) SD Catalog No. C13.44:145/II, $6.80.

**Publications with prices and SD Catalog numbers may be purchased directly from the Superintendent of Documents, U.S. Government Printing Office, Washington, D.C. 20402 (foreign: one-fourth additional). Microfiche copies of the above, plus paper copy and microfiche versions of NBS Interagency Reports (NBSIR's), may be purchased from the National Technical Information Service (NTIS), Springfield, Va. 22161. Prices are subject to change. Reprints from the NBS Journal of Research and non-NBS publications may often be obtained directly from the authors.*

Key words: classification of spectral lines; intensities of spectral lines; spectral-line intensities; tables of spectral-line intensities; wavelengths of spectral lines.

The relative intensities, or radiant powers, of 39 000 spectral lines with wavelengths between 2000 and 9000 Ångstroms have been determined on a uniform energy scale for seventy chemical elements. This was done by mixing 0.1 atomic percent of each element in powdered copper, pressing the powder-mixture to form solid electrodes which were burned in a 10 ampere, 220 volt direct-current arc, and photographing the spectra with a stigmatic concave grating while a step sector was rotating in front of the slit. The sectored spectrograms facilitated the estimation of intensities of all element lines relative to copper lines which were then calibrated on an energy scale provided by standardized lamps, and all estimated line intensities were finally adjusted to fit this calibration. Comparisons with other intensity measurements in individual spectra indicate that the National Bureau of Standards spectral-line intensities may have average errors of 20 percent, but first of all they provide uniform quantitative values for the seventy chemical elements commonly determined by spectrochemists. These data are presented by element in part I, and all 39 000 observed lines are given in order of wavelength in part II. Supersedes NBS Monograph 32, Parts I and II.

Monogr. 147. **Relativistic many-body bound systems,** M. Danos and V. Gillet, Nat. Bur. Stand. (U.S.), Monogr. 147, 149 pages (Apr. 1975) SD Catalog No. C13.44:147, $2.15.

Key words: composite particles; interacting quantum fields; nuclear structure; particle structure; relativistic bound systems; relativistic nuclear physics.

The principles and the mathematical details of a fully relativistic nuclear theory are given. Since the concept of nuclear forces is a strictly non-relativistic construct, it must be abandoned and the forces must be replaced explicitly by their physical origin, i.e., by the interaction between nucleons and mesons. Thus, in this monograph the description of a nucleus has been formulated as a problem of relativistic quantum field theory which is solved by nuclear physics methods. To wit: The physics is described by specifying a Lagrangian which is a functional of the constituent fields (= of the parton fields). The solutions for the physical systems then are obtained in a time-independent treatment as expansions in the parton fields: both particles and nuclei are composite systems, made up of parton configurations, which define a representation of the Hamiltonian (associated with the specified Lagrangian). The Hamiltonian is truncated by omitting all configurations having a diagonal element exceeding that of the lowest configuration by a pre-determined value, E_{max}, and is diagonalized. All formulae needed to carry out this program are derived and given in full detail for spin 0, 1/2, and 1 parton fields for PS, PV, and φ^4 interactions. Particular attention is devoted to the center-of-mass position coordinate which in relativistic kinematics is a non-separable many-body operator. Finally, the configurations up to $E_{max} = 1$ GeV are listed for the nucleon, the deuteron, and the pion.

SP260-50. **Standard reference materials: Thermal conductivity and electrical resistivity standard reference materials:**

Electrolytic iron SRM's 734 and 797 from 4 to 1000 K, J. G. Hust and P. J. Giarratano, Nat. Bur. Stand. (U.S.), Spec. Publ. 260-50, 41 pages (June 1975) SD Catalog No. C13.10:260-50, $1.00.

Key words: electrical resistivity; electrolytic iron; high temperature; iron; Lorenz ratio; low temperature; standard reference material; thermal conductivity; thermopower.

A historical review of the development of Standard Reference Materials, SRM's, is given and selection criteria of SRM's are listed. Thermal conductivity and electrical resistivity data for electrolytic iron and similar irons are compiled, analyzed, and correlated. Recommended values of thermal conductivity and electrical resistivity for electrolytic iron, SRM's 734 and 797, are presented for the range 4 to 1000 K. These values are based on NBS measurements up to 280 K and on measurements by Oak Ridge National Laboratory on a similar iron above 280 K. The average uncertainty of the thermal conductivity values below ambient is 1.5 percent and 3 percent above ambient. The corresponding uncertainties in electrical resistivity are 1 percent and 2 percent.

SP371-1. **Supplementary bibliography of kinetic data on gas phase reactions of nitrogen, oxygen, and nitrogen oxides (1972-1973),** F. Westley, Nat. Bur. Stand. (U.S.), Spec. Publ. 371-1, 88 pages (June 1975) SD Catalog No. C13.10:371-1, $1.45.

Key words: bibliography; chemical kinetics; excited state; gas phase; nitrogen atom; nitrogen molecule; nitrogen oxides; oxygen atom; oxygen molecule; ozone.

A reaction-oriented list of references is provided for papers and reports published in 1972 and 1973, containing rate data for reactions of N, N_2, N_2O, N_2O_2, N_2O_3, N_2O_4, N_2O_5, NO, NO_2, NO_3, NO_4, O, O_2 and O_3 with each other. Some reactions of species in excited states are included. This bibliography, covering about 500 papers, extends the coverage of two previous bibliographies on the same subject, COM-71-00941, NBS-OSRDB-71-2, August 1971 and NBS Special Publication 371, February 1973. Some work published prior to 1972 omitted in the previous publications has been included here.

SP400-11. **Semiconductor measurement technology: A BASIC program for calculating dopant density profiles from capacitance-voltage data,** R. L. Mattis and M. G. Buehler, Nat. Bur. Stand. (U.S.), Spec. Publ. 400-11, 39 pages (June 1975) SD Catalog No. C13.10:400-11, $1.00.

Key words: BASIC; capacitance-voltage measurements; computer programs; dopant profiles; error function; Gaussian diffusion; plotting, computer; semiconductors; silicon.

A computer program is presented which is suitable for calculating dopant density vs. depth profiles from capacitance-voltage data for the case of a Gaussian-diffused *p-n* junction diode. The program includes corrections for peripheral capacitance of round or rectangular diodes and back depletion of the space charge region into the diffused layer. Inputs to the program consist of the surface dopant density, the junction depth, the background dopant density in the diffused layer, the junction diameter, three scaling parameters, and the capacitance-voltage data pairs. Output from the program is in the form of a plot and an optional listing of dopant density as a function of depth. The equations underlying the program are given and are related to the program whose operation is described in detail. A second program, for generating idealized capacitance-voltage data for a Gaussian-diffused diode on material with a constant dopant density is also included.

SP400-12. **Semiconductor measurement technology: Quarterly report, July 1 to September 30, 1974,** W. M. Bullis, Ed., Nat. Bur. Stand. (U.S.), Spec. Publ. 400-12, 59 pages (May 1975) SD Catalog No. C13.10:400-12, $1.15.

Key words: acoustic emission; beam-lead bonds; boron redistribution; Darlington pairs; dopant profiles; electrical properties; electronics; epitaxial layer thickness; flying-spot scanner; gold-doped silicon; hermeticity; incremental sheet resistance; measurement methods; microelectronics; micrometrology; MOS devices; oxide films; resistivity; scanning low energy electron probe; semiconductor devices; semiconductor materials; semiconductor process control; silicon; test patterns; thermally stimulated current; thermal resistance; thermal response; ultrasonic bonding; wire bonds; x-ray photoelectron spectroscopy.

This quarterly progress report describes NBS activities directed toward the development of methods of measurement for semiconductor materials, process control, and devices. The emphasis is on silicon device technologies. Principal accomplishments during this reporting period include (1) completion of Hall effect measurements to determine activation energies of the gold donor and acceptor levels in silicon; (2) successful direct measurement of fast interface state density with the circular CCD test structure; and (3) demonstration of the feasibility of the use of acoustic emission as a non-destructive means for testing individual beam-lead bonds. Results are also reported on a holder for semi-automated sheet resistance measurements, progress on development of mathematical models of dopant profiles, analysis of thermally stimulated current and capacitance measurements on junction diodes, x-ray photoelectron spectroscopy, a comparative study of surface analysis techniques, design and fabrication of a test pattern for resistivity-dopant density evaluation, epitaxial layer thickness measurement, use of the flying-spot scanner, initial work on the scanning low energy electron probe, mathematical modeling of ultrasonic bonding, an improved method for force adjustment and measurement on beam lead bonders, helium mass spectrometery for leak testing, thermal resistance measurements on Darlington pairs, and transistor thermal response measurements. Supplementary data concerning staff, publications, workshops and symposia, standards committee activities, and technical services are also included as appendices.

SP408. **Standard reference materials and meaningful measurements,** R. W. Seward, Ed., Nat. Bur. Stand. (U.S.), Spec. Publ. 408, 820 pages (Mar. 1975) SD Catalog No. C13.10:408, $12.60.

Key words: certification; certified reference materials; materials; meaningful measurements; measurement; reference materials; SRM's; standard materials; standard reference materials; standards.

This book presents the proceedings of the 6th Materials Research Symposium on "Standard Reference Materials and Meaningful Measurement" held at the National Bureau of Standards, Gaithersburg, Maryland, on October 29 through November 2, 1973. The symposium was sponsored by the NBS Institute for Materials Research. The purpose of the symposium was to explore ways that Standard Reference Materials (SRM's) could be used more effectively to bring about meaningful measurements both on a national and international scale, to explore the meaning of meaningful measurements, and to review the major paths now used to reach these measurements.

Starting with the relationship of SRM's to a national measurement system, the symposium reviewed SRM activities at the international level, various national programs, and industrial needs. The use of statistics, selection criteria, and steps for certifying SRM's were reviewed. Fifteen panel sessions reviewed the current status of SRM's and outlined future needs.

SP419. **Selected topics on hydrogen fuel,** W. R. Parrish, R. O. Voth, J. G. Hust, T. M. Flynn, C. F. Sindt, and N. A. Olien, and J. Hord, Ed., Nat. Bur. Stand. (U.S.), Spec. Publ. 419, 212 pages (May 1975) SD Catalog No. C13.10:419, $2.80.

Key words: conservation; conversion; cost; cryogenics; economics; embrittlement; energy; hydrogen; industrial; instrumentation; liquefaction; literature; materials; production; solar; storage; transmission; transportation; utilities.

The National Bureau of Standards played a vital role in developing hydrogen technology for the space age and is now engaged in efforts to adapt and improve this technology for the commercial use of hydrogen fuel. This document is a summary report on selected hydrogen-fuel topics and was prepared to identify cost and technical barriers to the commercial use of hydrogen fuel and to generate reference data for policy-planning, decision-making and design. Cryogenic hydrogen fuel technology is emphasized in the economic and systems analyses reported herein. Using the best available technical and economic data, hydrogen fuel is not currently cost competitive with alternate fuels; however, we must not reject hydrogen on the basis of current economic comparisons. Increased efficiencies of production, liquefaction, and energy conversion may drastically change these comparisons-of-today as will increased fossil fuel prices and more stringent environmental and pollution constraints. Hydrogen appears currently marketable in certain integrated utility systems, in transoceanic transport of energy produced far at sea, and is a necessary element in a wide variety of growing industrial processes and in the liquefaction of coal. This publication identifies research and development needs within selected areas of NBS competence and future research plans are outlined.

SP420. **International Bureau of Weights and Measures 1875-1975,** C. H. Page and P. Vigoureux, Eds., Nat. Bur. Stand. (U.S.), Spec. Publ. 420, 257 pages (May 1975) SD Catalog No. C13.10:420, $3.00.

Key words: base units; centennial volume; history of SI; International Bureau of Weights and Measures; International System of Units; measurements; SI; Treaty of the Metre.

This is the English version of the Centennial volume of the International Bureau of Weights and Measures (BIPM) translated from the French. Metrology—the science of measurement—is traced from man's earlier efforts to the world's most modern, uniform, and coherent measurement system, the International System of Units (SI). Detailed accounts are given of the 1875 Treaty of the Metre—to which 18 nations, including the United States, were signators—and the work of the International Bureau of Weights and Measures which was created by the Treaty and now the international province of 44 nations. Historical reviews are given of the development of the base and derived units of the SI, specifically mass, length, gravimetry, manobarometry, thermometry, electricity, photometry, radioactivity, x and gamma rays, and neutron measurements.

SP421. **A guide to methods and standards for the measurement of water flow,** G. Kulin and P. R. Compton, Nat. Bur. Stand. (U.S.), Spec. Publ. 421, 97 pages (May 1975) SD Catalog No. C13.10:421, $1.65.

Key words: flow measurement, water; instruments, flow measurement; open channel flow measurement; pipe flow measurement; standards, flow measurement.

Selected information sources on methods and standards for making measurements of water and wastewater flow in the field are listed and described. Both closed conduit and free surface flows are treated, but emphasis is on open channel flow measurements needed in water resource engineering and in water pollution control. Instruments and methods covered include weirs, flumes, current meters (and velocity traverse methods), dilution techniques, pipe flow instruments, acoustic meters and others. In addition to summarizing the basic properties of each instrument or method and referring users to the best available sources of detailed information on performance and field application, potential sources of error are described and quantified where possible.

NSRDS-NBS43. Supplement. **Selected specific rates of reactions of transients from water in aqueous solution. Hydrated electron, supplemental data,** A. B. Ross, Nat. Stand. Ref. Data. Ser., Nat. Bur. Stand. (U.S.), 43, Suppl., 43 pages (June 1975) SD Catalog No. C13.48:43, Suppl., $1.10.

Key words: aqueous solution; chemical kinetics; data compilation; hydrated electron; radiation chemistry; rates.

A compilation of rates of reactions of hydrated electrons with other transients and with organic and inorganic solutes in aqueous solution appeared in NSRDS-NBS43, and covered the literature up to early 1971. This supplement includes additional rates which have been published through July 1973.

NSRDS-NBS51. **Selected specific rates of reactions of transients from water in aqueous solution, II. hydrogen atom,** M. Anbar, N. N. Farhataziz, and A. B. Ross, Nat. Stand. Ref. Data Ser., Nat. Bur. Stand. (U.S.), 51, 56 pages (May 1975) SD Catalog No. C13.48:51, $1.20.

Key words: aqueous solution; chemical kinetics; data compilation; hydrogen atom; radiation chemistry; rates.

Rates of reactions of hydrogen atoms (from radiolysis of water and other sources) with organic and inorganic molecules, ions, and transients in aqueous solution have been tabulated. Directly measured rates obtained by kinetic spectroscopy or conductimetric methods, and relative rates determined by competition kinetics are included.

NSRDS-NBS54. **The radiolysis of methanol: product yields, rate constants, and spectroscopic parameters of intermediates,** J. H. Baxendale and P. Wardman, Nat. Stand. Ref. Data Ser., Nat. Bur. Stand. (U.S.), 54, 26 pages (Apr. 1975) SD Catalog No. C13.48:54, 85 cents.

Key words: chemical kinetics; data compilation; methanol; radiation chemistry; rates; review.

Product yields and primary yields in the radiolysis of methanol in the solid, liquid and vapor phase have been compiled and reviewed. Preferred values for G of the major products in the vapor and liquid states are listed. Rates of reactions of solvated and trapped electrons and other transient ions and radicals, and optical absorption and esr parameters for e_s^-, e_t^-, CH_2OH and $CH_3O\cdot$ are also included.

BSS57. **Comparison of measured and computer-predicted thermal performance of a four bedroom wood-frame townhouse,** B. A. Peavy, D. M. Burch, F. J. Powell, and C. M. Hunt, Nat. Bur. Stand. (U.S.), Bldg. Sci. Ser. 57, 62 pages (Apr. 1975) SD Catalog No. C13.29/2:57, $1.20.

Key words: air leakage measurement; building heat transfer; computer programs; dynamic thermal performance; heat flow analysis; heating and cooling loads; temperature predictions; thermal analysis; thermostat setback; transient heat flows.

Measurements of the dynamic heat transfer in a four bedroom townhouse were made under controlled conditions in a large environmental chamber to explore the validity of a computer program developed at NBS, labelled NBSLD, for predicting heating and cooling loads and inside air temperatures. This study was supported jointly by the Department of Housing and Urban Development and the National Bureau of Standards, and is a part of a broader research program supported by both agencies to improve performance test procedures and criteria for housing.

The test house was a factory-produced four bedroom townhouse of modular design and of lightweight (wood) construction. Tests were performed with simulated outside summer, winter and fall diurnal temperature cycles. The inside temperature was maintained at about 75 °F. Also during the tests, the activities of a six-member family were simulated.

The time-varying energy requirements were measured, and these values were compared with computer predicted values. For example, the disparity between predicted and measured daily heating energy requirements averaged 3.1 percent with a maximum departure of 4.9 percent for five tests. The computer program NBSLD was experi-

mentally validated for predicting the peak heating and cooling loads and the energy requirements for the test house.

The air leakage of the house was measured by a tracer gas technique over a range of outdoor conditions, and algorithms were developed to account for its effect on heating loads and energy requirements.

Separate tests were also performed to investigate the energy savings achieved by night temperature setback. An 8-h 9 °F setback from 75 °F produced an 11 percent diurnal savings in energy for an average nighttime temperature of 20 °F and a 9 percent savings in energy was achieved for the same setback when the average nighttime temperature was 2 °F.

BSS63. **Analysis of current technology on electrical connections in residential branch circuit wiring,** W. J. Meese and R. L. Cilimberg, Nat. Bur. Stand. (U.S.), Bldg. Sci. Ser. 63, 23 pages (Mar. 1975) SD Catalog No. C13.29:2/63, 70 cents.

Key words: contact resistance; electrical codes; electrical connections; fire safety; house wiring; materials properties; performance testing.

In the Operation BREAKTHROUGH research and demonstration program the U.S. Department of Housing and Urban Development became concerned with the inability to properly evaluate innovative electrical connections. Long life requirements, fire safety considerations, the lack of adequate technical information, and long established conventional practices and evaluation procedures have led to slow-changing regulations concerning electrical connections used in branch circuit wiring in housing. This report discusses the present methods of evaluating electrical connections, the technical parameters involved, and innovative electrical connection developments. Innovations involving electrical connections may lead to significant advancements in housing construction if it could be demonstrated that functional and safety requirements over the expected life of the electrical connections were adequately satisfied. Research is needed to enable prediction of long term performance of electrical connections based on the results of accelerated performance tests.

BSS66. **Underground heat and chilled water distribution systems,** T. Kusuda, Ed., Nat. Bur. Stand. (U.S.), Bldg. Sci. Ser. 66, 146 pages (May 1975) SD Catalog No. C13.29:2/66, $2.10.

Key words: corrosion of underground pipes; district heating; hot and chilled water systems; insulation of underground pipes; specifications for underground systems.

This publication contains the keynote address and all the technical papers presented during the Symposium on Underground Heat and Chilled Water Distribution Systems, which was held on November 26 and 27, 1973 in Washington, D.C.

The Symposium was sponsored jointly by the National Bureau of Standards, the National Capital Chapter of the American Society of Heating, Refrigerating and Air-Conditioning Engineers, the Building Research Institute and the Association of Physical Plant Administrators.

The subject matter covered in the papers includes energy, economics, design criteria, heat transfer, corrosion protection, specification, operation, and maintenance related to underground pipes.

BSS68. **Review of standards and other information on thermoplastic piping in residential plumbing,** R. S. Wyly, W. J. Parker, D. E. Rorrer, J. R. Shaver, G. C. Sherlin, and M. Tryon, Nat. Bur. Stand. (U.S.), Bldg. Sci. Ser. 68, 65 pages (May 1975) SD Catalog No. C13.29:2/68, $1.25.

Key words: fire performance of piping; functional performance of piping; performance characteristics for piping; thermal/structural performance of piping; thermoplastic piping in plumbing.

The paper is a review of existing information on the physical characteristics of thermoplastic piping that are of particular interest in considering its potential for use in residential, above-ground plumbing. The presentation is oriented to considerations of adequacy of functional performance of plumbing systems from the user's/owner's viewpoint in contrast with the typical product-specifications oriented format reflected in current standards.

Not only are the physical characteristics emphasized that relate most directly to the determination of functional performance of installed systems, but the importance of design and installation detail in the context is discussed.

In conclusion, this review indicates the need for better use of existing knowledge as well as for some research and test development work particularly in the areas of thermal properties, response to building fires, and resistance to water hammer.

BSS70. **Windows and people: A literature survey. Psychological reaction to environments with and without windows,** B. L. Collins, Nat. Bur. Stand. (U.S.), Bldg. Sci. Ser. 70, 93 pages (June 1975) SD Catalog No. C13.29/2:70, $1.55.

Key words: daylight; fenestration; psychological; solar glass; spaciousness; sunshine; view; windowless; windows.

An understanding of human requirements for windows in buildings can be developed through a survey of the literature on the reaction to environments with and without windows. Evaluation of the response to a variety of windowless situations reveals that although the attitudes toward a windowless space are often somewhat unfavorable, the most adverse reaction occurs in a small, restricted and essentially static environment. This suggests that one function performed by a window is the addition of a dynamic, active quality to an interior environment. Consideration of the response to the actual presence of windows indicates that another essential function of a window is the provision of a view of the external world. Although almost any view is acceptable, there is some evidence that views with a high information content are preferable. In addition, windows admit illumination, in the form of daylight and sunshine which furnish a dynamic, changing character to a room. Yet, the functions of windows extend beyond view and illumination to an enhancement of the basic character of a room, such that the mere presence of a window may cause a room to appear more spacious. Finally, the optimum size and shape of a window for fulfilling these various functions is discussed.

FIPS PUB 35. **Code extension techniques in 7 or 8 bits,** J. L. Little, Standards Coordinator, Nat. Bur. Stand. (U.S.), Fed. Info. Process. Stand. Publ. (FIPS PUB) 35, 4 pages (1975) SD Catalog No. C13.52:35, 25 cents.

Key words: American Standard Code for Information Interchange; ASCII, coded character subsets; codes; data communication, data interchange, data processing; Federal Information Processing Standards; graphic character subsets; graphic subsets; information interchange; information processing; standards; subsets.

This FIPS PUB announces the adoption of the American National Standard X3.41-1974, Code Extension Techniques for Use with the 7-Bit Coded Character Set of ASCII. This standard specifies methods of extending the 7-bit code of ASCII (FIPS 1), remaining in a 7-bit environment or increasing to an 8-bit environment, building upon the structure of ASCII to describe various means of extending the control and graphic sets of the code. It also describes techniques for constructing codes related to ASCII so as to allow application dependent usage without preventing the interchangeability of their data and describes 8-bit codes for general information interchange in which ASCII is a subset.

FIPS PUB 36. **Graphic representation of the control characters of ASCII (FIPS 1),** J. L. Little, Standards Coordinator, Nat.

Bur. Stand. (U.S.), Fed. Info. Process. Stand. Publ. (FIPS PUB) 36, 4 pages (1975) SD Catalog No. C13.52:36, 25 cents.

Key words: American Standard Code for Information Interchange; ASCII, coded character subsets; codes; data communication, data interchange, data processing; Federal Information Processing Standards; graphic character subsets; graphic subsets; information interchange; information processing; standards; subsets.

This FIPS PUB announces the adoption of the American National Standard X3.32-1973, Graphic Representation of the Control Characters of American National Standard Code for Information Interchange. This standard specifies graphical representations for the 34 characters of ASCII (FIPS 1) for which a graphic representation is not indicated in FIPS 1. Graphical representations are given for the 32 control functions of columns 0 and 1 as well as the characters "Space" and "Delete." Two forms of graphical representations for each of the 34 characters are provided: a pictorial symbol, and a 2-letter alphanumeric code.

PS61-74. **Plastic containers (jerry-cans) for petroleum products,** *(ANS MH 17.1-1974),* K. G. Newell, Jr., Technical Standards Coordinator, Nat. Bur. Stand. (U.S.), Prod. Stand. 61-74, 6 pages (May 1975) SD Catalog No. C13.20/2:61-74, 45 cents.

Key words: containers for petroleum products; jerry-cans; petroleum products, containers for; plastic containers for petroleum products.

This Voluntary Product Standard covers requirements and methods of test for the material, design, and properties of plastic containers (jerry-cans) intended for use with petroleum products. Methods of identifying containers that conform to the requirements of the standard are included.

PS63-75. **Latex foam mattresses for hospitals,** *(ANS Z 255.1-1975),* G. S. Chaconas, Technical Standards Coordinator, Nat. Bur. Stand. (U.S.), Prod. Stand. 63-75, 8 pages (Apr. 1975) SD Catalog No. C13.20/2:63-75, 50 cents.

Key words: foam mattresses; hospital mattresses; latex; latex foam mattresses; latex foam for hospitals; mattresses.

The purpose of this Voluntary Product Standard is to establish nationally recognized dimensional and quality requirements for latex foam mattresses intended for use in hospitals, and to provide producers, distributors, and users with a basis for common understanding of the characteristics of this product.

TN659. **An earth-based coordinate clock network,** N. Ashby, Nat. Bur. Stand. (U.S.), Tech. Note 659, 34 pages (Apr. 1975) SD Catalog No. C13.46:659, 85 cents.

Key words: clocks; coordinate time; general relativity; time.

This paper investigates some of the possible operational procedures for synchronizing clocks at fixed sites spread around on the earth's surface, to within a 1 nanosecond level of accuracy. Since a common synchronization procedure is by transport of standard clocks in commercial jet airline flights, and most of the effects we shall discuss are fractional corrections to the elapsed time, as a criterion of whether an effect is significant at the 1 nanosecond level we take for comparison purposes an elapsed time $T_e = 10$ hours. This is a typical time for an intercontinental airplane flight. Analysis of a number of effects which might affect clock synchronization is carried out within the framework of general relativity. These effects include the gravitational fields of the earth, sun, and moon, and orbital motion, rotation, and flattening of the earth. It is shown that the only significant effects are due to the gravitational field and rotation of the earth, and motion of the transported clocks. Operational procedures for construction of a synchronized coordinate clock network using light signals and transported standard clocks are discussed and compared.

TN789-1. **Emergency workshop on energy conservation in buildings,** S. A. Berry, Nat. Bur. Stand. (U.S.), Tech. Note 789-1, 31 pages (July 1975) SD Catalog No. C13.46:789-1, 80 cents.

Key words: building codes; buildings; energy conservation; standards.

This report contains the non-technical presentations given at the National Conference of States on Building Codes and Standards/National Bureau of Standards Joint Emergency Workshop on Energy Conservation in Buildings.

Presentations included in this document are those of other Federal Agencies, States, technical societies and industry organizations.

This document is a companion document to NBS Technical Note 789, "Technical Options for Energy Conservation in Buildings."

TN857. **Real-time acquisition and processing of fluorimetry data,** P. S. Shoenfeld, Nat. Bur. Stand. (U.S.), Tech. Note 857, 45 pages (June 1975) SD Catalog No. C13.46:857, $1.05.

Key words: analytical chemistry; computers; data acquisition; data processing; fluorimetry; laboratory automation; real-time.

The National Bureau of Standards Analytical Chemistry Division uses a centralized computer system to automate a number of experiments. Computer software for a fluorimetry application is described in this report. The file and program structure used is quite general and can be applied to other experiments as well.

TN862. **Application of ion beam milling to the characterization of cracks in metals,** L. K. Ives, A. Harper, and A. W. Ruff, Nat. Bur. Stand. (U.S.), Tech. Note 862, 29 pages (Apr. 1975) SD Catalog No. C13.46:862, 80 cents.

Key words: cracks; flaws; ion beam milling; metals; microscopy; surfaces.

The technique of ion beam milling coupled with subsequent optical and scanning electron microscopy has been applied as a means of detecting and characterizing small surface intersecting cracks. Two types of cracked specimens involving different metals were studied. Various orientations of the crack plane, crack direction, and ion beam were explored. The technique is capable of increasing the sensitivity for detection of small cracks and also removing distorted surface layers and revealing the crack more accurately.

TN863. **Fatigue tests of bituminous membrane roofing specimens,** G. F. Sushinsky and R. G. Mathey, Nat. Bur. Stand. (U.S.), Tech. Note 863, 32 pages (Apr. 1975) SD Catalog No. C13.46:863, $1.15.

Key words: bituminous roof membranes; fatigue testing; flexural fatigue; performance criteria; roofing; temperature effects; tensile fatigue; test methods.

Tensile and flexural fatigue tests were performed on built-up roof membrane specimens (ASTM Designation: D2523-70) fabricated from four different material systems. The tensile fatigue tests were run under cyclic load control conditions while specimens tested in flexural fatigue were run under cyclic midspan displacement control. Tests were run at ambient laboratory conditions, generally 70 ± 2 °F (21 ± 1 °C), and at 0 ± 2 °F (-18 ± 1 °C). Curves based on the experimental results are plotted relating the peak load or displacement to the median fatigue lifetimes for specimens fabricated from each material. Performance criteria for roof membranes subject to fatigue loading are recommended.

TN864. **Cost recovery in pricing and capacity decisions for automated information systems,** J. A. Dei Rossi, Nat. Bur. Stand. (U.S.), Tech. Note 864, 60 pages (Apr. 1975) SD Catalog No. C13.46:864, $1.20.

Key words: automated information retrieval; cost benefit; public good; scientific and technical information; semi-public good; subsidization; total cost recovery; user charges.

This paper examines the cost-benefit implications of alternative pricing and capacity investment decisions for automated scientific and technical information retrieval systems. Two typical systems are examined and numerical examples presented. In the first system, search requests are entered on-site. The numerical examples show how setting price to maximize net social benefit precludes total cost recovery and implies subsidization. In the second hypothetical system, search requests are entered from remote access terminals. Allowance is made for random arrival rates, and distinction is made between system charges to users and other user incurred costs. With these refinements, the numerical examples show how, for certain ranges of output, total cost recovery is consistent with the maximization of net social benefit. The paper then examines the "public good" attributes of scientific and technical information retrieval systems and concludes that such systems can be viewed as "semi-public goods," since the information stored has the characteristics of a public good while access to this information has the characteristic of a private good. Based on the public good considerations and the numerical examples, the paper concludes that subsidization for the fixed costs is warranted to the extent that all reasonable alternatives which maximize net social benefit preclude total cost recovery.

TN865. **Critical electrical measurement needs and standards for modern electronic instrumentation,** P. Richman, Ed., Nat. Bur. Stand. (U.S.), Tech. Note 865, 74 pages (May 1975) SD Catalog No. C13.46:865, $1.35.

Key words: data conversion; dynamic measurements; electrical measurements; electronic instrumentation; signal conditioning; systems; time domain.

Recognizing the proliferation of sophisticated modern electronic instrumentation in the field of electrical measurements, the Electricity Division of the National Bureau of Standards recently initiated a new program in the general area of dynamic measurements and standards in support of such instrumentation. Recognizing further that the vastness and complexity of the field would require, at the earliest stages of the program, identification of the most critical problem areas, the Electricity Division held a workshop on 23 and 24 September, 1974, at the Bureau's Gaithersburg site, to assist it in ascertaining just what these areas in fact were. The basic idea of the Workshop was to bring together a broadly representative group of some twenty-five leading manufacturers and prime users, working in a free and open atmosphere, in order to have them delineate the present and future critical support needs in the field of dynamic electrical measurements for modern electronic instrumentation, with emphasis on physical standards, standardized measurement methods, new calibration and measurement assurance services, relevant data, and most important, new measurement methodologies. The overall objectives of the Workshop were generally met, and a number of significant specific programs and projects consistent with the mission of the Electricity Division were identified.

TN869. **Temperature section activity summary, 1974,** J. F. Schooley, Ed., Nat. Bur. Stand. (U.S.), Tech. Note 869, 28 pages (June 1975) SD Catalog No. C13.46:869, 80 cents.

Key words: annual report; calibrations; progress report; standards; temperature scale; thermometry.

This report summarizes the progress in calendar 1974 of the technical program of the temperature section of the Heat Division, Institute for Basic Standards. Separate sections of the report are devoted to the various projects, to highlights of the year's activities, and to other agency interactions.

TN874. **Software testing for network services,** R. B. Stillman and B. Leong-Hong, Nat. Bur. Stand. (U.S.), Tech. Note 874, 40 pages (July 1975) SD Catalog No. C13.46:874, $1.00.

Key words: dynamic analysis; NBS analyzer; NBS FORTRAN test routines; networking; systematic testing; testing tools.

This report is a first step toward indentifying effective software test and measurement tools, and developing a guide for their usage network-wide. The utility of two tools, the NBS FORTRAN Test Routines and the NBS Analyzer, is studied experimentally, and indications of their role in systematic testing in a networking environment are given.

NBSIR 73-145. **Study of relationships between activity, reaction, garment parameter patterns and injury severity for fire incidents involving apparel,** L. B. Buchbinder, 33 pages (Apr. 1973). Order from NTIS as COM 75-10541, $3.75.

Key words: accident patterns; apparel; apparel fires; burn injury; FFACTS; fire; flammable fabrics; garment fires; garmen parameters; injury severity; victim's activity; victim's reactions

Fire accidents result from the interaction of a number of environmental, human, and physical factors, all of which may effect the severity of the burn injury. Using information gathered from case histories in the Flammable Fabrics Accident Case and Testing System, this study seeks to identify patterns in the apparel fire accident variables: (1) activity preceding the accident, (2) parameters of fabrics and garments involved, (3) reaction of victim, and (4) severity of the burn injury. It will also attempt to define the extent and nature of the relationships between these accident variables.

This interim report gives a detailed description of the methodology employed in the development and completion of the study, with emphasis on accident pattern identification and classification for apparel fire incidents. Preliminary results of the study are included which identify certain recurring patterns of activity leading to burn injuries.

NBSIR 74-355. **Carbon thin film thermometry,** R. S. Collier, L. L. Sparks, and T. R. Strobridge, 65 pages (Oct. 1973). Order from NTIS as N74-30195, $4.25.

Key words: calibration; carbon films; low temperature; thermometry; vacuum deposition.

This is a summary of work done on NASA(Marshall Space Flight Center) purchase order H-92167A concerning Carbon Thin Film Thermometry. Optimum film deposition parameters were sought on an empirical basis for maximum stability of the films. One hundred films were fabricated for use at the Marshall Space Flight Center; 10 of these films were given a precise quasi-continuous calibration of temperature vs. resistance with 22 intervals between 5 and 80 K using primary platinum and germanium thermometers. Sensitivity curves were established and the remaining 90 films were given a three point calibration and fitted to the established sensitivity curves. Hydrogen gas-liquid discrimination set points are given for each film.

NBSIR 74-541. **An evaluation of potentially useful separator materials for nickel-cadmium (Ni-Cd) satellite batteries,** H. A. Baker, S. D. Toner, and W. F. Cuthrell, 37 pages (Oct. 1974). Order from NTIS as COM 75-10618, $3.75.

Key words: battery separators; nickel-cadmium batteries; satellite batteries; separator materials.

An evaluation intended to determine the potential suitability and probable efficacy of a group of separator materials for use in nickel-cadmium (Ni-Cd) satellite batteries was carried out. These results were obtained using test procedures established in an earlier evaluation of other separator materials, some of which had also been used in experimental battery cells subjected to simulated use conditions.

The properties that appear to be most important are: high electrolyte absorptivity, good electrolyte retention, low specific resistivity, rapid wettability and low resistance to air permeation. Wicking characteristics and wet-out time seem to be more important with respect to the initial filling of the battery with the electrolyte.

While the properties of some of these materials indicate that they

would be satisfactory, no specific conclusions can be drawn as to their actual effectiveness without further testing after they have been subjected to simulated use conditions in experimental cells.

NBSIR 74-586. **Calibration of platinum resistance thermometers using an intercomparison scheme,** R. M. Schoonover and H. H. Ku, 19 pages (Dec. 1974). Order from NTIS as COM 75-10525, $3.25.

Key words: adjustment for trend; calibration; capsule type thermometers; intercomparison; IPTS-68; platium resistance thermometers; wire-to-wire calibration.

In this report we describe a procedure for the calibration of capsule pe platinum resistance thermometers, PRT(s), using one or more tandard platinum resistance thermometers, SPRT(s), in the temperature range of 0-35 °C. These PRT(s) were designed to be used in density work through hydrostatic weighing where SPRT(s) cannot be used because of space and other limitations, but the procedure is thought to be generally useful in other applications as well.

The schedule of intercomparisons was designed to eliminate possible trends in temperature variations of the constant temperature bath setup. Results of calibration can be expressed either in terms of the two constants alpha (α) and delta (δ), or in a table relating $R(t)/R(0)$ to t_{68} within the range of calibrations.

The uncertainty of the values of t_{68} calibrated by this procedure is believed to be within 2 millidegrees Celsius, not including the uncertainty of the SPRT that is used as standard.

NBSIR 74-600. **Thermodynamics of chemical species important to rocket technology,** C. W. Beckett, 200 pages (Oct. 1, 1974). Order from NTIS as AD-A008935, $7.00.

Key words: bibliography on spectroscopy of fluorides and oxides of the lanthanide series; calculation of dissociation energies; electrical resistivity; enthalpy of transition; graphite; infrared matrix isolation spectroscopy; melting point; radiance temperature; reaction of Ba(g) and excited ozone; reaction of Fe(g) and oxygen; review of literature on rate of effusion and mass-spectrometric data; scandium group and rare-earth gaseous monoxides; specific heat; total emittance; vanadium; zirconium.

Using a subsecond-duration transient technique the specific heat, electrical resistivity, and hemispherical total emittance were simultaneously measured over the temperature range 1500-3000 K for some grades of graphite. Similar measurements were made on vanadium, and zirconium in the temperature range of 1500-2100 K. Melting points and radiance temperature (at 650 nm) are reported for zirconium and molybdenum. The temperature of the transition from the α-β phase of zirconium and the energy difference of these phases has also been measured using the subsecond duration transient technique.

The products of the reaction of Fe(g) and 0_2 have been investigated and identified using the methods of infrared matrix isolation spectroscopy. A preliminary report on the study of the reaction of Ba(g) with vibrationally excited ozone is also presented.

The dissociation energies of the scandium group and rare-earth gaseous monoxides are evaluated by reviewing the literature available on Knudsen effusion rates and mass-spectrometric data. Criteria are discussed for choosing data for evaluation of dissociation energies. A bibliography of the available literature on the spectroscopy of fluorides, oxides, and oxyfluorides belonging to the lanthanide series is given.

NBSIR 74-633. **The NBS computerized carpool matching system: User's guide,** J. F. Gilsinn and S. Landau, 64 pages (Dec. 1974). Order from NTIS as COM 75-10691, $4.25.

Key words: carpool matching; carpools; computer programs; transportation; urban transportation.

This report documents the NBS computerized carpool matching programs and the procedures used in maintaining the coordinate data base required by the matching system. The report includes flowcharts, input/output formats, and program listings for the programs, plus details of the manual process for coordinate coding. The matching program produces, for each person desiring it, a list of others residing within a pre-specified distance of him, and is thus applicable to a single work destination having primarily one work schedule. The system is currently operational on the National Bureau of Standards' UNIVAC 1108 computer and was run in March of 1974, producing lists for about 950 employees in less than four minutes computer time. Subsequent maintenance of the system will be carried out by the NBS Management and Organization Division.

NBSIR 74-634. **Method of testing for rating thermal storage devices based on thermal performance,** G. E. Kelly and J. E. Hill, 45 pages (May 1975). Order from NTIS as COM 74-10685, $3.75.

Key words: solar energy; standard; standard test; thermal performance; thermal storage; thermal test.

A study has been made at the National Bureau of Standards of the different techniques that could be used for testing thermal storage devices and rating them on the basis of thermal performance. This document outlines a proposed standard test procedure based on that study. It is written in the format of a standard of the American Society of Heating, Refrigerating, and Air Conditioning Engineers and specifies the recommended apparatus, instrumentation, and test procedure.

NBSIR 75-660. **Voluntary labeling program for household appliances and equipment to effect energy conservation: Annual report for calendar year 1974,** B. J. McGuire and E. A. Vadelund, 46 pages (Feb. 1975). Order from NTIS as COM 75-10609, $3.75.

Key words: consumer information; consumer products; energy conservation; energy efficiency; energy use; household appliances; household equipment; labeling; residential.

The Voluntary Labeling Program for Household Appliances and Equipment to Effect Energy Conservation was established in response to an April 18, 1973 Presidential directive. Final procedures for the program became effective October 26, 1973. Only major energy consuming household appliances and equipment are covered. Purposes of the program are to encourage manufacturers to place energy efficiency labels on their appliances and to encourage consumers to utilize this information in making purchase decisions.

Specifications containing labeling requirements for each type of product are developed by NBS with assistance from consumers, retailers, manufacturers and interested Federal agencies. During the first full year of program operation, final specifications for labeling room air conditioners and proposed specifications for labeling refrigerators, combination refrigerator-freezers, and freezers were issued. Two consumer information pamphlets were published and other consumer information and education activities were undertaken. Labeling specifications for water heaters, clothes washers and dryers, and ranges and ovens were under development. This was accomplished, with assistance from manufacturers, retailers, consumers and other agencies, by a staff of six funded at a level of $375,000 per year.

At year's end, twenty-four room air conditioner manufacturers and private brand labelers, representing an estimated 95 percent of U.S. sales of this appliance, were participating in the program.

NBSIR 75-675. **Evaluation of x-ray fluorescence analysis for the determination of mercury in coal,** R. L. Myklebust, M. M. Darr, K. F. J. Heinrich, 20 pages (Dec. 1974). Order from NTIS as COM 75-10685, $3.25.

588-458 O - 75 - 4

Key words: background; mercury in coal; trace analysis; x-ray fluorescence; x-ray spectrography.

Limits of detection for mercury in coal have been determined on both a wavelength-dispersive and an energy-dispersive x-ray spectrometer. They are between 2 and 3 ppm under best conditions for both spectrometers. Techniques for reducing the background intensity measured by the energy-dispersive system are discussed along with methods of preparing coal specimens for analysis in both instruments.

NBSIR 75-682. **Basic considerations of densitometer adjustment and calibration,** R. E. Swing, 18 pages (Feb. 3, 1975). Order from NTIS as COM 75-10524, $3.25.

Key words: calibration; calibration table; densitometer; densitometry; optical density; optical density standard.

The adjustment and calibration of a densitometer are considered. This is accomplished through the use of physical measurement standards with a procedure appropriate for the instrument, and brings the instrument response in line with measurements traceable to NBS. The difference between primary and secondary physical measurement standards for diffuse (visual) density is discussed. A calibration table is suggested for best use of the instrument and a computer program (BASIC language) is provided that will calculate and print a table relating instrument reading to diffuse (visual) density.

NBSIR 75-685. **Improved ultrasonic standard reference blocks,** D. G. Eitzen, G. F. Sushinsky, D. J. Chwirut, C. J. Bechtoldt, and A. W. Ruff, 83 pages (Apr. 1975). Order from NTIS as COM 75-10690, $4.75.

Key words: aluminum ultrasonic standards; ASTM-type reference blocks; fabrication of reference blocks; immersion testing; longitudinal waves; metallurgical variables; nondestructive testing; pulse-echo; steel ultrasonic standards; titanium ultrasonic standards; ultrasonics.

A program to improve the quality, reproducibility and reliability of nondestructive testing through the development of improved ASTM-type ultrasonic reference standards is described. Reference blocks of aluminum, steel, and titanium alloys are to be considered. Equipment representing the state-of-the-art in laboratory and field ultrasonic equipment was obtained and evaluated. RF and spectral data on ten sets of ultrasonic reference blocks have been taken as part of a task to quantify the variability in response from nominally identical blocks. Techniques for residual stress, preferred orientation, and micro-structural measurements were refined and are applied to a reference block rejected by the manufacturer during fabrication in order to evaluate the effect of metallurgical condition on block response. New fabrication techniques for reference blocks are discussed and ASTM activities are summarized.

NBSIR 75-696. **Proceedings of GSA/ETIP Symposium on Procurement Practices, May 29-31, 1974,** 96 pages (Jan. 1975). Order from NTIS as COM 75-10527, $4.75.

Key words: ETIP; incentives; innovation; procurement; product improvement; specifications.

The topic of the symposium was "Government and Industry—A Joint Effort Toward Technological Innovation in Product Development for Government and Public Procurement." The general objectives of the symposium were to open government-industry dialogue on ways to encourage technological innovation in the development of products purchased by the Federal Government; to explore methods of developing a "spin-off" effort so that the consumer marketplace might benefit from such innovations; to set up a procedure for analyzing the effect on the consumer marketplace and to establish procedures for continuing a government-industry dialogue. The plenary session provided participants with information designed to generate dialogue and to develop source material. Workshops were organized to consider specific product grouping in: Office Machines (typewriters, calculators, copiers, and microfiche); Furniture (wood and metal office types); Containerization/Packaging; ADP-Peripheral/Supplies; Instrumentation (optical and electrical measuring devices); Electrical Equipment (appliances and powered hand tools); Automotive Products (after market replacement parts and tires); Photographic and Audio Visual; Chemical (coatings, cleaning agents and detergents).

NBSIR 75-711. **Site analysis and field instrumentation for an apartment application of a total energy plant,** J. B. Coble and P. R. Achenbach, 65 pages (May 1975). Order from NTIS as COM 75-10689, $4.25.

Key words: air conditioning; air pollution; central utility systems; data acquisition system; efficiencies; electrical power; energy conservation; energy costs; fuel utilization; heat recovery; total energy systems; utilities for housing; utility system performance.

Under sponsorship of the Department of Housing and Urban Development, the National Bureau of Standards developed criteria in a feasibility study to select a site for, and to evaluate the requirements of a total energy system on one or more OPERATION BREAKTHROUGH housing sites. The total energy system produces its own electrical, heating and cooling energy services independent of the local utility system. Six OPERATION BREAKTHROUGH sites were selected for the feasibility study: Jersey City, N.J.; Macon, Ga.; Memphis, Tenn.; Indianapolis, Ind.; St. Louis, Mo.; and Sacramento, Calif. Ranking parameters for final selection were: number of dwelling units, density of dwelling units, climatic factors, energy utilization, owning and operating costs, and developer's attitude.

The Jersey City site was chosen as the location for the installation, evaluation, and field study of the total energy system. The site covers six acres, has four apartment buildings containing 488 dwelling units, a 50,000-sq.ft commercial building, an elementary school, a swimming pool, and the total energy plant.

The buildings and the total energy plant are being extensively instrumented to provide data on fuel utilization, system efficiencies, electrical and thermal energy generation, energy utilized and rejected. The environmental impact of the total energy plant with respect to noise, vibration, air pollution, and esthetics is under evaluation. The installed system will be compared with several types of conventional energy systems.

NBSIR 75-718. **Report of fire test on an AM General Metro Bus,** E. Braun, 21 pages (June 1975). Order from NTIS as COM 75-10750, $3.25.

Key words: AM General Bus; arson; critical radiant flux; fire retardant; flammability; flooring radiant panel test; Metro; motor vehicle safety standard 302; urethane.

The Center for Fire Research at the National Bureau of Standards has conducted a study of the fire safety of a bus supplied by the Washington, D.C., Metropolitan Transit Authority. The objectives of the work were: (1) to determine the minimum ignition from source necessary to initiate a fire in the bus, and (2) to determine the means by which a fire, once started, is most likely to grow and spread.

A series of small-scale laboratory tests were run in addition to the three full-scale tests. Tests showed that accidental ignition by a cigarette or dropped match is unlikely. However, the seat can be ignited with one or two matches, if applied at the proper location, as by an arsonist. In full-scale tests, ignition of the seat occurs readily with the following ignition sources: (1) a small bag of paper trash on the seat, (2) a newspaper under the seat, (3) if the contents of a can of lighter fluid is poured on the seat.

Fire growth and spread in the bus is primarily through involvement of the seat cushioning. Fire spreads from seat to seat with little direct involvement of other interior materials. In all three tests, between

one and two minutes after the urethane ignited, dense smoke filled the bus space seriously reducing visibility. Spread of fire beyond the seat of origin is not necessary for the level of smoke to be formed.

This column lists all outside publications by the NBS staff, as soon after issuance as practical. For completeness, earlier references not previously reported may be included from time to time.

Angel, W. T., Bean, V. E., **Tracking, pulsed ultrasonic interferometer,** *Rev. Sci. Instrum.* **46,** No. 5, 533-535 (May 1975).

Key words: interferometer; phase locked loop; tracking; ultrasonic.

A pulsed ultrasonic interferometer was designed and constructed that has the ability to track changes in transit time as the ambient pressure and temperature of the sample are changed. The stability over 17 h approached one part in 10^7. This instrumentation will be incorporated into an automated high pressure transfer standard calibration system.

Arp, V., **Thermodynamics of single-phase one-dimensional fluid flow,** *Cryogenics* **15,** No. 5, 285-289 (May 1975).

Key words: helium; hydrodynamics; one dimensional flow; single phase fluid; thermodynamics; transposed critical line.

Fluid flow processes in helium within the range 4-10 K and 10-100 N cm^{-2} pressure are similar to those of ordinary fluids near their critical points. Three thermodynamic parameters, the Gruneisen parameter, isentropic compressibility, and velocity of sound, which are weakly non-catalytic near the critical point, are used to describe fluid flow processes in fluids in the near critical range. It is found that if temperature is not used as a variable in a fluid state equation, flow profiles can be easily evaluated in a single-phase fluid region, including close to or transecting the transposed critical line.

Artru, M. C., Kaufman, V., **Extension of the analysis of triply ionized aluminum (Al IV),** *J. Opt. Soc. Amer.* **65,** No. 5, 594-599 (May 1975).

Key words: aluminum; spectra; wavelengths.

A total of 225 new lines of Al IV have been observed in the wavelength range 400-4700 Å, leading to the determination of all of the levels of the $2p^5 4p$, $4d$, $4f$, $5s$, $5f$, and $5g$ configurations. Results of parametric calculations for the configurations are presented. An ionization energy of 967 804 ± 15 cm^{-1} has been derived.

Barton, J. A., Jr., Brauer, G. M., Antonucci, J. M., Raney, M. J., **Reinforced polycarboxylate cements,** *J. Dent. Res.* **54,** No. 2, 310-323 (1975).

Key words: base, dental; cement, dental; cement, polycarboxylate; cement, reinforced; fiber reinforcement; poly(acrylic-itaconic acid); polycarboxylate; potassium titanate.

Mechanical properties of polycarboxylate cements are greatly improved by incorporation of high modulus fibers such as potassium titanate into acrylic-itaconic acid and acrylic-itaconic-aconitic acid copolymers. Other desirable properties of the cements are not changed by the addition of fibers.

Bennett, L. H., Cuthill, J. R., McAlister, A. J., Erickson, N. E., Watson, R. E., **Electronic and catalytic properties of tungsten carbide,** *Science* **187,** 858-859 (Mar. 7, 1975).

Key words: catalysis; electronic structure; platinum; soft x-ray appearance potential; tungsten; tungsten carbide; x-ray photoemission.

The purpose of this comment is to note that two sets of experimental data, namely x-ray photoemission and soft x-ray appearance potential, are only apparently inconsistent in their measurement of the electron distribution in tungsten carbide.

Biedenharn, L. C., Trivedi, M., Danos, M., **Giant multipole resonances and the three-fluid hydrodynamical model of nuclei,** *Phys. Rev. C* **11,** No. 4, 1482-1484 (Apr. 1975).

Key words: collective model; giant resonances; isospin purity; nuclear charged density; nuclear models; nuclear structure.

The recently observed resonance at ~ 11 MeV in ^{208}Pb is interpreted as the miniature quadrupole resonance (associated with the giant quadrupole resonance at 22 MeV) implied by the three-fluid hydrodynamical model. A difficulty arises with the miniature dipole resonance; this may signify that the simple hydrodynamic model has reached the limits of its validity. A numerical error in a previous publication is corrected.

Blackburn, D. L., Oettinger, F. F., **Transient thermal response measurements of power transistors,** *IEEE Trans. Ind. Electron. Control Instrum.* **IECI-22,** No. 2, 134-141 (May 1975).

Key words: computer simulation (transient thermal); current crowding (transistors); power transistors; thermal impedance measurements; thermal response measurements; transistors (thermal measurements).

Differences between the measured thermal impedance of power transistors when determined by the pulsed heating curve and cooling curve techniques are discussed. These differences are shown to result primarily because the power density distributions of these devices change as the devices heat; as a result of these changes the heating curve and the cooling curve are not conjugate. It is shown that the cooling curve technique, when the cooling curve is initiated from the most non-uniform steady-state thermal distribution, (maximum voltage, maximum power) will indicate a larger value for the thermal impedance than will the pulsed heating curve technique, even for pulses in excess of the dc power level. A one-dimensional model for power transistor cooling is described. The theoretical predictions of the model are shown to be in good agreement for practical applications with three-dimensional computer simulations and experimental results. Using this model, it is possible to estimate an average junction temperature and the area of power generation at steady-state. Both TO-66 and TO-3 encased devices of mesa and planar structures were included in this study.

Brennan, J. A., Stokes, R. W., Kneebone, C. H., Mann, D. B., **NBS-CGA cryogenic flow measurement program,** (Proc. ISA International Instrumentation-Automation Conf. and Exhibit, New York, N.Y., Oct. 28-31, 1974), Paper in *Advances in Instrumentation* **29,** 612-1/612-13 (Instrument Society of America, Pittsburgh, Pa., 1974).

Key words: angular momentum; cryogenic; flowmeter; liquid nitrogen; measurement; positive displacement; turbine; vortex shedding.

This paper reviews the joint National Bureau of Standards-Compressed Gas Association program in which (1) all the types of flowmeters used in the U.S. for custody transfer of liquid nitrogen were tested, (2) a tentative national code on cryogenic liquid-measuring devices was adopted, (3) use of transfer standards for testing cryogenic flowmeters was started and (4) tests on some temperature and density compensation devices were completed.

Data from the test program are presented in summary form for flowmeters operating on several principles. Highlights of the code requirements and transfer standard test results are described. Densitometer and temperature compensation test data are presented.

Brown, W. E., **Physicochemistry of apatite dissolution,** (Transactions of Colloquium on Physico-Chimie et Cristallographie des Apatites D'Intérêt Biologique, Paris, France, 1973), *Colloq. Int. Cent. Nat. Rech. Sci.*, No. 230, 355-368 (1975).

Key words: bone mineral; dental caries; electric currents; mechanism; solubility.

The dissolution of apatites, during formation of caries lesions in enamel or remodeling of bone, has two aspects, thermodynamic and kinetic, which are intimately related. One can approach a full understanding of these processes by taking into account how each aspect affects the other.

The rate of transport of calcium relative to that of phosphate ions is a dominant consideration. These rates are likely to be controlled to a considerable degree by the permselective properties of the plaque and the outer layer of enamel acting as a very complex and variable membrane. Alteration of the properties of this membrane, therefore, becomes a potentially valuable means for preventing caries.

The thermodynamic properties of the apatite enter into the caries dissolution process in another way: the subsurface nature of the typical incipient lesion very probably relates to the variable solubility of the apatite in enamel mineral. Solubility measurements with enamel show that much of it is more soluble than synthetic preparations of pure hydroxyapatite and that its solubility changes with its composition and location.

Bussey, H. E., **Rapport sur la comparaison internationale des mesures de permittivité complexe á 9 GHz,** (Proc. Comité Consultatif. D'Electricité Comité International des Poids et Mesures, Sèvres, France, Oct. 12-13, 1972). Paper in *Comité International Des Poids et Mesures*, pp. 124-137 (Bureau International des Poids et Mesures, Sèvres, France, 1972).

Key words: cavity method for dielectrics; dielectric constant; dielectric loss; international comparison; laboratory intercomparison; permittivity; standard dielectric.

Dielectric constant and loss measurements made by three national laboratories (of the USSR, Canada, and USA) are compared. The two materials measured were glasses. The measurements utilized cavity resonators in the H_{01n} mode. The errors in dielectric constant reported by the laboratories were usually ± 0.3 percent; actual differences between laboratories of the average corrected results were only ± 0.05 percent. The loss tangent results disagreed when multimoding occurred; however, the errors may be as low as $\pm 0.000\,02$ or ± 3 percent, whichever is the larger, if multimoding is avoided.

Ciarlo, D. R., Schultz, P. A., Novotny, D. B., **Automated inspection of IC photomasks,** *Proc. Society of Photo-Optical Instrumentation Engineers, Seminar 8, Technological Advances in Micro and Submicro Photofabrication Imagery, San Diego, Ca., Aug. 1974*, **55,** 84-89 (May 1975).

Key words: automated inspection of photomasks; critical dimension determination; defects; detection of visual defects; integrated circuit photomasks; photomask inspection; photomasks; photoplate quality.

The results of a nationwide review of automated IC photomask inspection methods are presented. Major photomask inspection problems of detection of visual defects and registration errors, and the determination of critical dimensions and photoplate quality are discussed. This review indicates that for high-volume, large-scale integrated circuits, the greatest concern is for the detection of visual defects. Next in order of importance are the detection of registration errors, and then the accurate determination of critical dimensions. Automated inspection systems and technologies currently available for this are discussed including: microdensitometer-digital computer systems, laser beam scanning systems, spatial filtering systems and microscope-television-digital computer systems. Suggested criteria for an ideal photomask inspection system are the simultaneous inspection for 2-μm visual defects, the determination of registration tolerances to within ± 0.5 μm and the determination of the accuracy of the critical dimensions to tolerances of ± 0.5 μm on a single photomask in ten minutes.

Clifton, J., Frohnsdorff, G., **Fiber-reinforced cementitious materials,** Special Review in *Cements Research Progress 1974*, F. Young, Ed., pp. 201-234 (American Ceramic Society, Columbus, Ohio, 1975).

Key words: cement; concrete; fiber-reinforced cements fiber-reinforced concretes; glass fibers; mechanical properties; organic fibers; review; steel fibers.

This review is concerned with developments, through 1974, in the research and technology, but not applications, of fiber reinforced cementitious materials including hardened cement pastes of gypsum, portland and high alumina cement and their concretes. Essentially, only materials reinforced with short, discontinuous and discrete fibers are covered, because long rods, continuous meshes and woven fabrics are not classified as discrete fibers in this review.

Clough, R. B., Simmons, J. A., **Thermodynamics of dislocation motion in multiaxial stress fields,** (Proc. from the John E. Dorn Symp., Cleveland, Ohio, Oct. 1972). Paper in *Rate Processes in Plastic Deformation of Materials*, J. C. M. Li and A. K. Mukherjee, Eds., pp. 266-283 (American Society for Metals, Metals Park, Ohio, 1975).

Key words: dislocation; multiaxial; plasticity; thermodynamics.

This paper presents a first-order consideration of dislocation motion through a multiaxial stress field. The concept of plastic power dissipation is developed as a measure of plastic flow due to multiaxial stresses. A result which emerges is the concept of the second-order activation volume tensor for plastic power dissipation. Usually, this is a deviatoric tensor with the same principal axes as the stress, which then only interacts with the deviatoric stress. Results are given for a biaxial yield surface calculated as a surface of constant plastic power dissipation. The yield surface varies from a Tresca to a von Mises shape, depending on the scalar activation volume, the uniaxial yield stress, and the temperature. Generally for low temperature conditions the yield surface resembles the Tresca yield surface, and its shape approaches the von Mises shape as a high temperature limit. The activation volume tensor is explicitly demonstrated for all materials in a state of uniaxial tension and for materials with a von Mises-like yield surface in any multiaxial stress state. Extension of this treatment to include the internal stress and prestrain and stress history effects on the yield surface is discussed.

Collin, G. J., Ausloos, P., **Réactions des ions moléculaires cyclohexane en phase gazeuse,** *Can. J. Chem.* **53,** No. 5, 680-687 (1975).

Key words: cyclohexane; cyclopropanes; ion-molecule reactions; olefins; photoionization.

The *cy*-$C_6H_{12}^+$ ions formed in the photoionization of cyclohexane (resonance lines of argon: 11.6-11.8 eV) react with cyclic (C_3 and C_4) and unsaturated hydrocarbons by H_2 transfer. This reaction is quantitative with propene, 1-butene, 1-pentene, 1,3-butadiene, and isobutene. This transfer is efficient only if there is a terminal double bond. There is ring opening with the C_3 and C_4 hydrocarbons. H atom transfer reactions are also observed between *cy*-$C_6H_{12}^+$ ions and several compounds and the structure of the radical formed in such a reaction is determined by chemical analysis. With *cis*-2-butene, there is only charge transfer reaction.

Costrell, L., **Standardized instrumentation system for computer automated measurement and control,** *IEEE Trans. Ind. Appl.* **IA-11,** No. 3, 319-323 (May-June 1975).

Key words: CAMAC; computer interfacing; control systems; instrumentation; instrumentation standards; standards.

A standardized instrumentation system for computer automated measurement and control (CAMAC) is gaining wide international acceptance for industrial and laboratory applications. The system features a fully specified dataway together with modular functional units that are completely compatible with each other and that are available

from diverse sources. The system is nonproprietary and can be freely used without license or restriction of any kind.

Crandall, D. H., Phaneuf, R. A., Dunn, G. H., **Electron impact excitation of Hg^+,** *Phys. Rev. A* **11,** No. 4, 1223-1232 (Apr. 1975).

Key words: crossed beams; cross section; electron impact; excitation; Hg^+.

Crossed beams of electrons and Hg^+ ions have been employed to measure absolute cross sections for 165.0-nm emission, corresponding to the transition $Hg^+(6p\ ^2P_{3/2}{}^0) \rightarrow Hg^+(6s\ ^2S_{1/2})$. The emission cross section, which is nearly identical to the excitation cross section for $Hg^+(6p\ ^2P_{3/2}{}^0)$ near threshold, has a value of about 1.2×10^{-16} cm^2 at the 7.51-eV threshold, rises to a maximum of 2.26×10^{-16} cm^2 at 13 eV, and falls to 0.64×10^{-16} cm^2 at 274 eV. The cross section exhibits considerable structure in the energy region from threshold to the onset of the first cascade ($7s\ ^2S_{1/2}$) at 11.9 eV; this structure is likely due to interference from autoionizing states of neutral Hg. The total uncertainty at a "good" confidence level is about 18 percent, taken as the quadrature sum of random uncertainty (5% at 90% confidence level) with systematic uncertainties (17% at a level equivalent to 90% confidence level). At threshold, the Gaunt-factor formula of Seaton predicts a value of about 3 times that measured, but the two converge to within about 15 percent for electron energies ranging from 13 to 274 eV. The results are also in reasonable agreement with a semiclassical Gryzinski-type calculation for energies above several times threshold. The data give an emission cross section of $(2.8 \pm 0.5) \times 10^{-16}$ cm^2 at 6.8 eV for 194.2 nm ($6p\ ^2P_{1/2}{}^0 \rightarrow 6s\ ^2S_{1/2}$). Analysis of data taken with some metastable $6s^2\ ^2D$ ions in the target beam indicates that the mean cross section for excitation of the $6s\ ^2P_{3/2}{}^0$ level from the $6s^2\ ^2D$ metastable states is larger than that for excitation from the $6s\ ^2S_{1/2}$ ground state. Additional measurements of 398.4-nm emission ($6p\ ^2P_{3/2}{}^0 \rightarrow 6s^2\ ^2D_{5/2}$) yield a cross section of about 6×10^{-19} cm^2 near threshold, and a branching ratio $(^2P_{3/2} \rightarrow {}^2S_{1/2})/(^2P_{3/2} \rightarrow {}^2D_{5/2})$ of 350/1.

DiChio, D., Natali, S. V., Kuyatt, C. E., **A new form for the third-order asymptotic aberration coefficients of electrostatic lenses; application to the two-tube electrostatic lens,** *Rev. Sci. Instrum.* **46,** No. 1, 71-76 (Jan. 1975).

Key words: aberration integrals; asymptotic aberration coefficients; electron optics; electrostatic lens; third-order aberration coefficients; two-tube lens.

The third-order asymptotic aberration coefficients of round electrostatic lenses are reformulated in terms of the coordinates formed by the projections of the asymptotic incident and final rays onto the reference plane of the lens. In this formulation, all aberration coefficients are finite for all lenses, in contrast to the formulation in terms of coordinates projected onto the focal planes of the lenses, where all of the coefficients become infinite in the limit of very weak lenses and for certain strong lenses. Equations for the six third-order aberration coefficients are derived in the form of integrals involving derivatives of the axial potential no higher than the second. Using these equations and previously calculated potentials and first-order trajectories, we have computed the six aberration coefficients for the accelerating and decelerating two-tube electrostatic lens for voltage ratios from 1.1 to 10 000. The results are believed accurate to better than 0.2 percent.

Ederer, D. L., Lucatorto, T. B., Saloman, E. B., **Photoabsorption from the 4d and 5p shells of barium,** (Proc. IV Int. Conf. on VUV Radiation Physics, Hamburg, Germany, July 17-26, 1974), Chapter 3.5 in *Proceedings of the IV International Conference on VUV Radiation Physics*, E. Koch, R. Haensel, and C. Kunz, Eds., pp. 245-246 (Friedr. Vieweg Sohn Verlagsgesellschaft, mbH, Braunschweig, West Germany, 1974).

Key words: absorption spectrum; barium; heat pipe; inner shell excitation; shape resonance; two-electron excitations.

A plastic windowed heat pipe was used in conjunction with the NBS-170 MeV synchrotron and a 3-m grazing incidence spectrograph to observe transition $4d^{10}5s^25p^66s^2 \rightarrow 4d^94s^25p^66s^2$ nf,np in the spectral region 110Å-150Å. By replacing the plastic windows with tin, excitations involving transitions $5p^66s^2 \rightarrow 5p^56s^2$ nd,ns were observed in the spectral region 520Å-650Å.

Eisenhart, C., **A supplementary list of publications of S. S. Wilks,** *Amer. Statist.* **29,** No. 1, 25-27 (Feb. 1975).

Key words: bibliographic citations; publications; Samuel Stanley Wilks; S. S. Wilks.

Full bibliographic citations for thirty-one "other writings" of Samuel Stanley Wilks not included in "The Publications of S. S. Wilks," in February 1965 issue of the *Annals of Mathematical Statistics* (Vol. 36, No. 1, pp. 24-27), together with the observation that his writings and those of his younger brother, Syrrel Singleton Wilks, are lumped together under "S. S. Wilks" in the volumes of the *Science Citation Index*.

Ekberg, J. O., **Term analysis of Fe VI,** *Phys. Scr.* **11,** No. 1, 23-30 (1975).

Key words: iron; spectra; ultraviolet; wavelengths.

The spectrum of Fe VI has been observed by using a vacuum sliding-spark discharge and the 10.7-m grazing-incidence spectrograph and the 10.7-m normal-incidence spectrograph at the National Bureau of Standards, Washington, D.C. More than 400 lines have been classified in the region 250-1 580 Å. All terms of the configurations $3d^3$, $3d^24s$ and $3d^24p$, except $3d^2(^1S)4s\ ^2S$ have been established. The estimated uncertainty of the level values is ± 0.4 cm^{-1}. The $3d^3$, $3d^24s$ and $3d^24p$ level structure has been theoretically interpreted. The energy parameters determined from a least-squares fit of the observed level values are compared with Hartree-Fock calculations. From the complete set of $3d^3$ levels all forbidden lines of Fe VI from 1 387 to 10 000 Å have been predicted. All but two lines in the spectrum of the star RR Telescopii previously identified as forbidden Fe VI lines have been confirmed and 6 of the otherwise unexplained lines have been identified as [Fe VI].

Ekin, J. W., Deason, V. A., **Technique for preparing homogeneous bulk samples of concentrated alloys,** *Rev. Sci. Instrum. Notes* **46,** No. 3, 327-328 (Mar. 1975).

Key words: aluminum alloys; bulk alloy samples; casting; directional solidification; rapid quenching.

A technique has been developed for casting relatively large samples (~ 100 g) of concentrated alloys. It was used to prepare Al-Mg castings having Mg concentrations near the maximum limit of solid solubility. Concentration gradients and nonequilibrium eutectic solidification were minimized by the rapid cooling and directional solidification that are characteristic of the technique.

Ensslin, N., Bertozzi, W., Kowalski, S., Sargent, C. P., Turchinetz, W., Williamson, C. F., Fivozinsky, S. P., Lightbody, J. W., Jr., Penner, S., **Electron scattering from excited states in ^{14}N and ^{9}Be,** *Phys. Rev. C* **9,** No. 5, 1705-1717 (May 1974).

Key words: deduced wave functions; electron scattering; measured form factors; nuclear reactions; ^{14}N; ^{9}Be(e,e′).

Electron scattering form factors have been measured for the first six excited states in ^{14}N and for the 2.429-MeV (5/2$^-$) level in ^{9}Be. The form factors for the lowest $T=1$ level in ^{14}N along with the previously measured ground-state magnetic moment are used to specify the $T=0$ and $T=1$ wave functions for the mass-14 system assuming two p-shell valence particles in an LS-coupling basis. The amplitudes of the various configurations so derived are generally in poor agreement with previous determinations, although the present wave functions yield values of the lifetime of the first $T=0$ state in ^{14}N and of the ^{14}N ground-state quadrupole moment that are in excellent agreement

with previous measurements. The present data are not sufficiently precise to allow a direct separation of the $T=0$ and $T=1$ components for the first four negative-parity excited states. However, for two of these states which are excited primarily by $C1$ transitions, a comparison of the radiative strengths determined in this experiment with previous lifetime measurements sets a lower limit of 2 percent for the $T=1$ admixture.

Epstein, M. S., Rains, T. C., Menis, O., **Determination of cadmium and zinc in standard reference materials by atomic fluorescence spectrometry with automatic scatter correction,** *Can. J. Spectrosc.* **20,** No. 1, 22-26 (Jan.-Feb. 1975).

Key words: accuracy; atomic fluorescence; automatic scatter correction; cadmium; chemical interferences; data evaluation; precision; production of atomic vapor; zinc.

The scattering of exciting radiation by matrix components is a major physical interference for trace analysis in atomic fluorescence spectrometry (AFS), which must be eliminated before practical "real sample" analysis can be performed. Using an instrumental arrangement for automatic scatter correction, trace cadmium and zinc are analyzed in Standard Reference Materials, Coal, Bovine Liver, Orchard Leaves, and Fly Ash, without prior separation or preconcentration. The effects of scatter and chemical interferences are evaluated for premixed argon (entrained air)—hydrogen and air—acetylene flames. Precision and accuracy of the results of AFS analysis are compared with data from analysis by atomic absorption.

Fivozinsky, S. P., Penner, S., Lightbody, J. W., Jr., Blum, D., **Electron scattering from ^{88}Sr and ^{89}Y,** *Phys. Rev. C* **9,** No. 4, 1533-1542 (Apr. 1974).

Key words: elastic and inelastic electron scattering; low lying levels; weak coupling; ^{88}Sr; ^{89}Y.

Inelastic scattering cross sections of low-lying levels and elastic scattering cross sections have been measured in ^{88}Sr and ^{89}Y using the National Bureau of Standards Linac and electron scattering facility. Incident-electron energies were varied between 45 and 121 MeV corresponding to a momentum transfer range of 0.4 to 1.0 fm^{-1}. Data were accumulated at two scattering angles, 110.5 and 128.2°. We present elastic scattering form factors and inelastic scattering form factors and $B(EL)\uparrow$'s for the 1.84- and 2.74-MeV states in ^{88}Sr, and the 1.51-, 1.74-, 2.21-, 2.52-, 2.86-, and 3.1-MeV states in ^{89}Y. A simple configuration mixing model based on the weak-coupling model has been applied to the octupole states in ^{89}Y. The measured elastic form factors for both nuclei have been fitted with a Fermi charge distribution.

Fong, J. T., **Construction of a strain-energy function for an isotropic elastic material,** *Trans. Soc. Rheol.* **19,** Issue 1, 99-113 (1975).

Key words: compressibility; elasticity; finite deformation; hyperelasticity; rubbery materials; strain-energy function; volume-extension.

Experimental data on the volume changes accompanying simple tension of peroxide vulcanizates of natural gum rubber, as first reported by Penn in *Trans. Soc. Rheol.* **14,** 509 (1970), are further interpreted within the framework of the theory of a hyperelastic material. Motivated by the formal connection between a hyperelastic material and a nonlinear viscoelastic fluid (*Trans. Soc. Rheol.* **9,** 27 (1965)), and a mathematical result on the decomposition of the scalar potential of that fluid (*Z. Angew. Math. Phys.* **23,** 780 (1972)), the interpretation of Penn's data leads to an explicit construction of a strain-energy function for rubbery materials:

$$W(I_1, I_2, I_3) = C_1(I_1 - 3) + C_2(I_2 - 3)$$

$$+ \tilde{H}(I_1, I_2)(I_3 - 1) + \frac{1}{8K}(I_3 - 1)^2.$$

Franzen, D. L., **Precision beam splitters for CO_2 lasers,** *Appl. Opt.* **14,** No. 3, 647-652 (Mar. 1975).

Key words: beam splitter; CO_2 laser; high power laser material.

Beam splitters for 10-μm lasers are discussed and then applied to the precision measurement of high average powers. In particular, beam splitter stability has been investigated in various materials over the 20—600-W power range with power densities up to 1 kW/cm^2. The absolute beam splitter ratios are given along with the achieved measurement precisions. The semiconductors investigated were GaAs, CdTe, and ZnSe in addition to one alkali-halide KCl. Standard deviations for the beam splitter ratios of 1 percent over the power range were typical. Absolute ratios agree with the predictions from Fresnel's equations to 1 percent or better. The best measurement was made on ZnSe when a standard deviation of 0.4 percent was obtained for the measurement of a ratio that agreed with a calculation from Fresnel's equations to better than 0.5 percent.

Freund, S. M., Sweger, D. M., **Vinyl chloride detection using carbon monoxide and carbon dioxide infrared lasers,** *Anal. Chem.* **47,** No. 6, 930-932 (May 1975).

Key words: detector; laser; pollution; vinyl chloride.

Stark modulated absorption of CO and CO_2 infrared laser radiation by vinyl chloride is the basis for sensitive and selective detection of this gas. Using the P(13) line of the 20-19 band of the CO laser (1609 cm^{-1}, 6.22 μm), a 2 ppm C_2H_3Cl in air sample is observed in an extracavity absorption cell with a 5/1 signal-to-noise ratio after 50 seconds of integration. The response of the signal to concentration of C_2H_3Cl is linear over at least 3 orders of magnitude to within experimental uncertainty which is a few percent. Similar results are obtained using a CO_2 laser operating on the P(42) line of the 001-100 band (922.9 cm^{-1}, 10.84 μm).

Fuggle, J. C., Madey, T. E., Steinkilberg, M., Menzel, D., **X-ray photoelectron spectroscopy (XPS) of adsorbate valence bands,** *Phys. Lett.* **51A,** No. 3, 163-164 (Feb. 24, 1975).

Key words: chemisorption; CO; ESCA; ruthenium; x-ray photoelectron spectroscopy.

The CO valence levels for a monolayer of CO adsorbed on the basal (001) face of ruthenium have been observed by XPS. The assignment of the observed peaks is discussed.

Gadzuk, J. W., **Electron spectroscopy of chemisorbed atoms and surface molecules,** (Proc. 2nd Int. Conf. on Solid Surfaces, Kyoto, Japan, March 25-29, 1 74), *Jap. J. Appl. Phys. Suppl.* **2,** Part 2, 851-858 (1974).

Key words: chemisorption; field emission; ion neutralization; photoemission; surface spectroscopy.

Chemical bonds formed between substrate and adsorbed atoms are characterized by new electronic energy levels which are derived from the atomic orbitals of each constituent. These energy levels are being observed experimentally through the techniques of field emission energy distributions, uv photoemission spectroscopy, and ion neutralization spectroscopy. These spectroscopies will be considered in the light of present day theoretical understanding of both the measurement and the chemisorption process.

Gadzuk, J. W., **Relaxation energies in chemisorption spectroscopy,** *J. Vac. Sci. Technol.* **12,** No. 1, 289-292 (Jan.-Feb. 1975).

Key words: chemisorption; image potential shifts; polarization energy shift; relaxation energies.

The upward shift in atomic energy levels (or decrease in electron binding energies) which occurs upon sorption of an atom on a metal surface due to polarization of the valence band electrons, is considered. The polarization shift or extra-atomic relaxation energy is

treated within the framework established by Hedin, Johansson, and Lundqvist and the results are related to image potential shifts which have been previously discussed in chemisorption theories.

Gadzuk, J. W., **Surface molecules and chemisorption, II. Photoemission angular distributions,** *Phys. Rev. B* **10,** No. 12, 5030-5044 (Dec. 15, 1974).

Key words: angular distributions; chemisorption; photoemission; photoionization; surfaces.

A theory of the angular distributions of electrons photoemitted from submonolayer films of chemisorbed atoms is presented. Chemisorption is treated within the surface-molecule limit of the Anderson model. It is shown that the key features which differentiate between solid-state photoemission and atomic photoionization are the localization of the hole left behind in the photoexcitation process and the preferential orientation of atomic or molecular orbitals (in photoemission from solids or chemisorbed atoms). The differential photoionization cross sections or angular distributions for spatially oriented atoms and surface molecules are obtained and contours of constant emission intensity, as projected on a flat fluorescent screen which is parallel to the surface, are presented. It is shown that the chemisorption bonding geometry can be ascertained from such measurements.

Giarratano, P. J., Jones, M. C., **Deterioration of heat transfer to supercritical helium at 2.5 atmospheres,** *Int. J. Heat Mass Transfer* **18,** No. 5-E, 649-653 (1975).

Key words: correlation; forced convection; heat transfer; helium; supercritical.

Heat transfer has been investigated for supercritical helium at 2.5 atm flowing inside a vertical tube with inlet bulk fluid temperatures less than the transposed critical temperature. Results indicate that for high heat flux conditions, the heat-transfer coefficient passes through a maximum and then deteriorates as the fluid temperature approaches the transposed critical temperature. This is contrary to the predictions of a correlation developed in an earlier study of supercritical helium heat transfer under low heat flux conditions, which only predicts enhancement in heat transfer as the transposed critical temperature is approached.

The experimental data are presented and conditions under which heat-transfer deterioration was observed are discussed. The probable limitations to the validity of the above mentioned heat-transfer coefficient correlation, developed for a different range of experimental data, are also discussed.

Gilsinn, J. F., **Validation of maximum airport throughput levels estimated by the DELCAP simulation model,** *FAA Report No. FAA-RD-75-66,* 72 pages (National Technical Information Service, Springfield, Va. 22151, Jan. 1975).

Key words: airport; airport capacity; airport simulation; models; model validation; runway capacity; simulation.

This report documents exercises of the DELCAP airport terminal area simulation model performed to validate the maximum throughput calculations of that model. DELCAP was run for five different runway configurations, with three or four appropriate operating policies chosen for each, and for three different mixes of aircraft types. Throughput estimates from DELCAP are found to be in general agreement with current values provided by the FAA. One specific instance of greater discrepancy is identified, and a remedy for it is proposed. Changes made in DELCAP since its original documentation in 1971 are described in an appendix.

Grundl, J. A., Gilliam, D. M., Dudey, N. D., Popek, R. J., **Measurement of absolute fission rates,** *Nucl. Technol.* **25,** 237-257 (Feb. 1975).

Key words: cross sections; fission; neptunium-237; neutron reactions; pile neutrons; plutonium-239; uranium-234; uranium-235; uranium-238.

The capability to measure absolute fission rates per nucleus at a remote laboratory site [the Coupled Fast Reactivity Measurement Facility (CFRMF) at Aerojet Nuclear Company] has been established to a precision level of better than ± 1 percent and was sustained at that level for a period of two years. Double fission ionization chambers and solid-state track recorders were used in a series of irradiations designed to calibrate fission activation detectors used for reactor fuels and materials dosimetry. The array of reference and working fissionable deposits involved in the measurements included five isotopes: ^{239}Pu, ^{235}U, ^{238}U, ^{237}Np, and ^{234}U. Isotopic masses for the fissionable deposits were determined from interrelated components of mass assay: (a) relative and absolute alpha counting, (b) fission comparison counting in thermal-neutron beams, (c) mass spectrometry, and (d) quantitative deposition employing solutions of known fissionable element concentration. Absolute accuracies for the fission rates per nucleus measured in CFRMF are in the range of ± 1.5 to ± 2.5 percent and are dominated by uncertainties in the fissionable deposit masses. Fission cross-section ratios for the CFRMF central spectrum are ($1.000 : 1.145 \pm 0.017 : 0.0485 \pm 0.0007 : 0.354 \pm 0.008$) for ($^{235}U$:$^{239}Pu$:$^{238}U$:$^{237}Np$), respectively.

Heydemann, P., **Pulse shaper,** *Rev. Sci. Instrum. Notes* **46,** No. 3, 329-330 (Mar. 1975).

Key words: NMR; switching; ultrasonics.

The rounding of pulses is a convenient way to suppress transients when rf signals are switched with balanced mixers or semiconductor switches. The use of a serial-in, parallel-out shift register for shaping the leading and trailing edges of pulses is described. The original pulse is clocked through a shift register and the outputs of the register are weighted and added to form a new pulse. The maximum rise time is equal to the clock period times the bit-capacity of the register.

Hughes, C. E., **The general decision problem for Markov algorithms with axiom,** *Notre Dame J. Formal Logic* **XVI,** No. 2, 208-216 (Apr. 1975).

Key words: combinatorial systems with axiom; degrees of unsolvability; general decision problems; Markov algorithms; many-one reducibility; recursive functions; r.e. many-one degrees; r.e. one-one degrees; semi-Thue systems; splinters.

A constructive proof is presented which shows the existence of a Markov algorithm with axiom whose decision problem is of any prescribed r.e. many-one degree of unsolvability. This result is then shown to be best possible in that it does not hold for r.e. one-one degrees. And, finally, a theorem concerning the degree representation of splinters of recursive functions is proven as a direct corollary to the forementioned results.

Hust, J. G., **Low temperature thermal conductivity measurements on longitudinal and transverse sections of a superconducting coil,** *Cryogenics* **15,** No. 1, 8-11 (Jan. 1975).

Key words: composite; cryogenics; superconducting coil; thermal conductivity.

Thermal conductivity measurements have been performed on longitudinal and transverse sections of a superconducting coil at 5, 79, 196, and 276 K. The composite coil sections are composed of copper-stabilized niobium-titanium wire embedded in epoxy. Tabular and graphical data are presented. These data are compared to values calculated on the bases of components of the coil sections. Reasonably good agreement is obtained.

Hust, J. G., **Low-temperature thermal conductivity of two fibre-epoxy composites,** *Cryogenics* **15,** No. 3, 126-128 (Mar. 1975).

Key words: aramid fiber; composites; cryogenic; epoxy; glass fiber; thermal conductivity.

Thermal conductivity data are presented for two fibre-epoxy composites. The fibre in one composite is glass and an aramid-class polymer in the other. Measurements were conducted on a glass-epoxy specimen in the direction perpendicular to the fibres at temperatures from 14 to 100 K. The aramid-epoxy specimen was measured parallel to the fibres at 5, 76, 196, and 276 K. Data are presented both in graphical and tabular form.

Jacox, M. E., **Matrix isolation study of the vibrational spectrum and structure of HC_2,** *Chem. Phys.* **7,** 424-432 (1975).

Key words: acetylene; discharge; ethynyl (HC_2); infrared spectrum; interstellar molecule; matrix isolation; structure; vacuum ultraviolet photolysis.

Detailed isotopic studies of the infrared absorptions characteristic of the products of the decomposition of C_2H_2 in a mild discharge through argon trapped at 14 K indicate that HC_2 is an important product and that an absorption at 3612 cm^{-1} can be assigned to the carbon-hydrogen stretching fundamental of this species. The data suffice for determination of the stretching and stretching-interaction force constants of HC_2, which, in turn, have permitted estimates of the bond lengths. The carbon-hydrogen bond is found to be exceptionally strong, and the carbon-carbon bond is intermediate between that characteristic of ground-state C_2 and that of C_2H_2. The estimated rotational spacing is in excellent agreement with that found for HC_2 in recent observations of the interstellar medium.

Jennings, D. A., Petersen, F. R., Evenson, K. M., **Extension of absolute frequency measurements to 148 THz: Frequencies of the 2.0- and 3.5-μm Xe laser,** *Appl. Phys. Lett.* **26,** No. 9, 510-511 (May 1, 1975).

Key words: absolute frequency measurements; laser frequency synthesis; xenon laser.

Absolute infrared frequency measurement has been extended to 148 THz (the highest frequency ever directly measured) with measurement of the two strong cw laser lines of Xe. The frequencies were synthesized with stabilized CO_2 and 3.39-μm He-Ne lasers and mixed on a W-Ni point-contact diode. The measured frequencies are $\nu_{Xe(2.0\mu m)} = 147.915\,850(15)$ THz and $\nu_{Xe(3.5\mu m)} = 85.459\,997(3)$ THz.

Jennings, D. A., **Simple, adjustable lens holder,** *Rev. Sci. Instrum.* **46,** No. 4, 487-488 (Apr. 1975).

Key words: adjustable; lens holder.

The construction of a simple, adjustable lens holder is described. This lens holder is unique in that it will firmly hold small lenses without taking up space at the edge of the lens or stopping them down.

Jickling, R. M., Shafer, J. F., **Repeaters for law enforcement communication systems,** *LESP-RPT-0206.00*, 18 pages (U.S. Department of Justice, Law Enforcement Assistance Administration, National Institute of Law Enforcement and Criminal Justice, Washington, D.C., Oct. 1974).

Key words: duplexer; fm transceiver; land-mobile communications; law enforcement; repeater; vertical antenna.

This report is concerned with FM repeaters used in land mobile communications systems. Repeater systems are described with emphasis on appropriate antenna site selection, signal-rejection techniques, and specialized transmission-line components for the transmission and reception of signals. Repeaters using the vehicle transceiver are mentioned. Repeaters at microwave frequencies are described to the extent that their use for control and as audio links is pertinent. Measurement techniques that are unique to land-mobile repeaters are discussed.

Johnson, D. R., Clark, F. O., **Observations of circular polarization of the $J=2-1$, $v=1$ transition of the SiO maser,** *Astrophys. J.* **197,** L69-L72 (Apr. 15, 1975).

Key words: circular polarization; maser; orion; pumping processes; radio astronomy; silicon monoxide.

Circular polarization has been observed in the $J=2-1$, $v=1$ SiO emission from the Orion A molecular source (OMC 1). The net polarization was observed at two different times separated by three days.

Jordan, T. H., Dickens, B., Schroeder, L. W., Brown, W. E., **The crystal structure of $Ca(BF_4)_2$,** *Acta Crystallogr.* **B31,** Part 3, 669-672 (Mar. 1975).

Key words: calcium fluoroborate; calcium salts; crystal structure; single crystal; tetrahedral anion; x-ray diffraction.

$Ca(BF_4)_2$ crystallizes in the orthorhombic space group *Pbca* with $Z=8$. The unit-cell parameters are $a=9.2792$ (6), $b=8.9103$ (10) and $c=13.3719$ (10) Å. The structure was refined by full-matrix least-squares calculations to $R_w(F)=0.025$, $R=0.024$, using 2896 measurable x-ray data collected by a counter method and corrected for absorption. The refinement allowed for anisotropic thermal motion, isotropic secondary extinction and anomalous dispersion. The structure consists of columns of BF_4^- ions and columns of alternating Ca^{2+} and BF_4^- ions, all parallel to [010]. There are twice as many [Ca^{2+}, BF_4^-] columns as [BF_4^-, BF_4^-] columns. All columns are linked together through Ca...F bonds. The Ca^{2+} ion is coordinated by a square antiprism of fluorine atoms, each from a different BF_4^- ion. Each fluorine atom is bonded to one Ca^{2+} ion, and the four Ca^{2+} ions bonded to a BF_4^- ion are arranged approximately tetrahedrally about the BF_4^- ion. Although neither of the two crystallographically discrete BF_4^- ions occupies a site of special symmetry, each is essentially tetrahedral in configuration.

Kamper, R. A., **Review of superconducting electronics,** *IEEE Trans. Magn.* **MAG-11,** No. 2, 141-146 (Mar. 1975).

Key words: electronics; Josephson effect; precise measurements; superconductivity.

This review will sketch the present state of affairs in applications of Josephson junctions and SQUIDs to: magnetometry, DC and RF metrology, detection and amplification of electromagnetic signals, frequency metrology, noise thermometry and computers. It will also mention recent progress in super-stable oscillators using superconducting resonant circuits, pulse transmission lines, and thin-film devices to detect radiation or charged particles. Many of these topics are maturing nicely.

Kanda, M., **Accuracy considerations in the measurement of the power gain of a large microwave antenna,** (Proc. 1974 Int. IEEE/AP-S Symp., Atlanta, Ga., June 10-12, 1974), Paper in *1974 International IEEE/AP-S Symposium Digest*, 43-45 (IEEE Inc., New York, N.Y., June 1974).

Key words: calibration accuracy; effective area; effective radiated power; extrapolation method; gain comparison method; microwave antenna; power gain; satellite.

Accuracy considerations in the measurement of the power gain of a large microwave antenna are discussed. Using the gain comparison method with a standard antenna of approximately 40-dB gain, a large antenna with a power gain of approximately 60-dB can be calibrated to within an error of 0.17 dB (3σ).

Kan, P. T., Peterson, G. A., Webb, D. V., Fivozinsky, S. P., Lightbody, J. W., Jr., Penner, S., **Electroexcitation of ^{11}B,** *Phys. Rev. C* **11,** No. 2, 323-331 (Feb. 1975).

Key words: boron; electron scattering; giant resonance; longitudinal; reduced widths; transverse.

Electrons with incident energies between 52.3 and 90.0 MeV have been scattered from the nucleus of ^{11}B. Spectra of scattered electrons corresponding to excitation energies up to 32 MeV were observed at angles of 75° and 145°. Form factors of the states at 2.12, 4.44, 5.02, 8.57, and 8.93 MeV, and of the continuum region up to 30 MeV, have been separated into longitudinal and transverse components. The ^{11}B dipole giant resonance is smooth relative to those of ^{12}C and ^{13}C. A mixed $M1$-$E2$ transition was observed at 13.0 MeV and a broad transverse resonance, possibly magnetic, was seen at 15.5 MeV.

Kapsch, R. J., **Life cycle costing techniques applicable to law enforcement facilities,** *LESP-RPT-0801.00*, 23 pages (U.S. Department of Justice, Law Enforcement Assistance Administration, National Institute of Law Enforcement and Criminal Justice, Washington, D.C., Oct. 1974).

Key words: analysis; construction; cost; design; economics; flexibility; law enforcement facilities; performance; planning; present value analysis.

This report is concerned with the application of techniques from building economics to the problems involved in the planning, design and construction of law enforcement facilities. The formulas involved in the present value method of analysis are derived, and their use in analyzing the costs of alternative courses of action are explained and illustrated. Tabular equivalents of the formulas are given to facilitate the costing analysis.

Komarek, E. L., **An application of the power equation concept and automation techniques to precision bolometer unit calibration,** (Proc. 1974 IEEE S-MTT Int. Microwave Symp., Atlanta, Ga., June 12-14, 1974), Paper in *Microwave Symposium Digest*, pp. 263-265 (IEEE Inc., New York, N.Y., June 1974).

Key words: automation techniques; bolometer units; calibration; power equation concept.

The power equation concept has been implemented into a multioctave precision bolometer unit calibration system employing automation techniques in conjunction with an automatic network analyzer system. The system was qualified as a calibration transfer system operating in the 2-12.4 GHz frequency range at 1 to 10 mW with a single measurement standard deviation of 0.2 percent to 1 percent from 2-10 GHz.

Kurylo, M. J., Braun, W., Xuan, C. N., Kaldor, A., **Infrared laser enhanced reactions: Temperature resolution of the chemical dynamics of the $O_3^\ddagger + NO$ reaction system,** *J. Chem. Phys.* **62,** No. 6, 2065-2071 (Mar. 15, 1975).

Key words: apparatus and methods; chemiluminescence; emission spectra; free radicals; kinetics of reactions; lasers, infrared; photochemistry.

The rate constant for the decay of vibrationally excited ozone, $O_3^\ddagger$, in the $O_3^\ddagger + NO$ reaction system has been measured from 153 to 373 K. Vibrationally excited O_3 was produced in the asymmetric stretch normal mode by absorption of square wave modulated emission from a CO_2 laser tuned to the $P(30)$ 9.6 μm transition. Under appropriate experimental conditions, a rapid $V \rightarrow V$ coupling process involving all three normal modes of O_3 is believed to set up a Boltzmann population distribution among them. Reaction or relaxation of $O_3^\ddagger$ out of this subset of normal modes is observed to proceed through a weighted average of rate constants. From the effects of temperature and buffer gas pressures an assessment can be made as to the predominant loss mechanism for the various modes. While there are three separate convolution schemes which appear to fit our data, we are persuaded to emphasize one whereby all three modes contribute via a reaction channel described by $k_D = (2.0 \times 10^{-11}) \exp(-1525/T)$ cm^3 molecule^{-1} · sec^{-1} while ν_2 alone is active in a $V \rightarrow T$ relaxation process given by $k_A = (1.0 \times 10^{-13}) \exp(-39.2/T)$ cm^3 molecule^{-1} · sec^{-1}. A comparison of the Arrhenius parameters for the reaction channels of $O_3^\ddagger$ with parameters for the corresponding processes involving thermal O_3 yields specific information about the effect of vibrational energy on the reaction dynamics.

LaVilla, R. E., **The sulfur Kβ emission and K-absorption spectra from gaseous H_2S, III,** *J. Chem. Phys.* **62,** No. 6, 2209-2212 (Mar. 15, 1975).

Key words: H_2S; sulfur $K\beta$ emission and K-absorption spectra; sulfur K shell binding energy; x-ray spectra.

The sulfur $K\beta$ emission in fluorescence and K absorption from gaseous H_2S were measured on a double crystal spectrometer. The sulfur $K\beta$ spectrum consists of four peaks. The three strongest peaks are shown to be single vacancy transitions of electrons from the three outer MO's to fill the single K shell vacancy. The weak fourth peak on the high energy side of the three line structure is identified as a double vacancy transition. The sulfur K-absorption spectrum consists of three peaks of decreasing intensity with increasing photon energy. The unusual breadth (FWHM of 1.50 eV) and asymmetry on the high energy side of the first peak is ascribed to the Frank-Condon factors of the transitions to the unoccupied antibonding MO's $3b_2$ and $6a_1$. The other two peaks, which are narrow, are identified as transitions to Rydberg levels. In addition, the binding energy of the sulfur K shell electron was estimated to be 2478.3 eV. The sulfur $L_{2,3}$ absorption of H_2S is also discussed briefly.

Lawless, W. N., **Dielectric and thermal properties of a machinable glass-ceramic at low temperatures,** *Cryogenics* **15,** No. 5, 273-277 (May 1975).

Key words: cryogenics; dielectric constant; loss tangent; machinable glass-ceramic; specific heat; thermal conductivity.

Measurements of the dielectric properties (2-300 K), specific heat (2-20 K), and thermal conductivity (2-22 K) are reported for a mica-containing glass-ceramic which has a machinability in the range from brass to low-carbon steel. The dielectric constant increases with increasing temperature and is field independent for field strengths up to at least 70 kV cm^{-1} at low temperatures. Power-supply-limited attempts to measure the dielectric breakdown strength at low temperatures are consistent with the reported strength at room temperature (1.4 MV cm^{-1}). The thermal properties are similar to fused SiO_2 with two exceptions: the thermal conductivity does not show the "knee" at ~ 10 K typical of amorphous materials, and the specific heat deviates strongly from a T^3 law below 3.5 K.

Leasure, W. A., Jr., Corley, D. M., **Truck noise-1B: Spectral and directional characteristics of noise generated by truck tires,** *Report No. DOT-TST-75-71*, 180 pages (Available from the National Technical Information Service, Springfield, Va., 22161, Sept. 1974).

Key words: acoustics; noise measurement; noise pollution; noise (sound); sound transmission; tire noise; transportation noise; truck; urban planning.

This report is the third in a series of reports published as a result of Department of Transportation sponsored truck tire noise research conducted by the National Bureau of Standards. The previous reports (OST-ONA-71-9 and OST/TST-72-1) contained details of the test design, test procedures, and an inventory of maximum A-weighted sound level data for typical rib, crossbar, and retread type truck tires. A test sample of nine tread designs, estimated to represent 70-80 percent (based on discussions with fleet owners) of the truck tire population on the road today, was investigated considering noise levels as a function of the following variables: wear, loading, speed, pavement surface, and tire location. Test vehicles included both single-chassis vehicles and tractor trailers. The existing data base is expanded in this report to include one-third octave band spectral data, directionality data in the form of equal A-weighted sound level contours and other refined analysis of the data. Such data can serve as

the groundwork for understanding the generation mechanisms by which tires produce noise—the first step in developing the necessary data to design quiet tires scientifically.

Livingston, R. C., Rowe, J. M., Rush, J. J., **Neutron quasielastic scattering study of the ammonium ion reorientations in a single crystal of NH_4Br at 373 K,** *J. Chem. Phys.* **60,** No. 11, 4541-4546 (June 1, 1974).

Key words: ammonium bromide; ammonium ion; neutron scattering; orientational disorder; reorientation; residence time; single crystal.

The ammonium ion reorientations in a single crystal of NH_4Br in its disordered CsCl phase have been investigated by quasielastic neutron scattering at 373 K. Neutron spectra were measured at four different crystal orientations (with the [110] planes of the crystal in the scattering plane) and data were recorded simultaneously at a variety of scattering angles providing a range of momentum transfers for elastic scattering, $0.5\ \text{Å}^{-1} \leq Q \leq 2.5\ \text{Å}^{-1}$. The experimental results were fit to models allowing instantaneous random jumps around the C_2 and C_3 axes of the $(NH_4)^+$ ions using a variety of analytical procedures that are described in some detail. The results of these fits establish conclusively that the ammonium ion reorientations are dominated by 90° jumps around the C_2 axes with an average time τ between jumps of 3.2 ± 0.4 psec at 373 K. The inelastic part of the measured neutron spectra shows a torsional vibration peak at 305 cm^{-1}, in good agreement with previous values. The results and analysis demonstrate the value of single crystal measurements in neutron studies of dynamic orientational disorder in solids.

Loebenstein, W. V., **The surface area of aggregates applied to dental materials,** *J. Biomed. Mater. Res.* **9,** 35-53 (1975).

Key words: adsorption theory; aggregate, adsorption by; collagen; dental materials; dentin; enamel; surface area; teeth; water vapor adsorption.

There is a continuing need for the complete characterization of the physical and chemical properties of dental materials. Among these properties is surface area. The problem is further complicated by the fact that most dental materials are, themselves, mixtures of two or more identifiable components. If the vapor adsorptive properties of these components are different in the mixture from that which would be expected of them collectively, then interaction is present. Interaction must not be confused with the lack of additivity which results from the limitations of the BET theory applied to mixtures. Equations are derived herein to estimate the extent of this latter source of variability and to correct for it giving a "true" surface area for the aggregate. Conversely, the adsorptive properties of either component can be calculated from the properties of the mixture and the remaining component together with the percentage composition. An immediate application can be made in determining the water-vapor adsorptive properties of human dental collagen without necessitating its removal from dentin. Any attempt to extract it chemically may produce denaturation or chain rupture thus precluding the possibility of direct determination. In the case of nitrogen adsorption, however, interaction definitely is indicated.

Mabie, C. P., **Evaluation of the physical properties of crown dental porcelain and the effect of newly developed anti-balling additive,** *J. Biomed. Mater. Res.* **9,** 1-25 (1975).

Key words: additive; deformation; dental; porcelain; properties.

A colloidal silica-based substitute for the water added to dental porcelain has been developed which restricts rounding on firing and gives greater and indefinitely prolonged unfired biscuit strength. In conjunction with product evaluation, it has been found that both the modulus of rupture and the diametrical tensile strength of dental porcelains can be measured with a high degree of precision.

Madden, R. P., Ederer, D. L., **SURF-II, a new synchrotron ultraviolet radiation facility at the NBS,** (Extended Abstract), *Proc. IV Int. Conf. on VUV Radiation Physics, Hamburg, Germany, July 17-26, 1974,* No. 10.3, 774-776 (1974).

Key words: electron accelerator; new facility; radiation; storage ring; synchrotron radiation; vacuum ultraviolet.

At NBS the accelerator providing synchrotron radiation in the vacuum ultraviolet is being converted from a synchrotron to a storage ring which we anticipate will accelerate a 50 mA electron beam to a maximum energy of 240 MeV. These changes will extend the useful spectral range of the continuum vacuum ultraviolet radiation down to wavelengths somewhat below 40 Å. Increased intensity, greater spacial and temporal stability are other advantages that this conversion will provide. Even at wavelengths greater than 200 Å the intensity is expected to increase by a factor of at least 100 to a value of 4×10^{11} photons per sec per milliradian of orbit for an instrument resolution of $\Delta\lambda/\lambda = 0.001$. It should be of general interest that SURF-II is being constructed so as to be compatible with a large user group.

Madey, T. E., Engelhardt, H. A., Menzel, D., **Adsorption of oxygen and oxidation of CO on the ruthenium (001) surface,** *Surface Sci.* **48,** 304-328 (1975).

Key words: adsorption; carbon monoxide; catalysis; LEED; oxygen; ruthenium.

The adsorption of oxygen on the ruthenium (001) surface has been studied using a combination of techniques: LEED/Auger, Kelvin probe contact potential changes, and flash desorption mass spectrometry. Oxygen is rapidly adsorbed at 300 K, forming an ordered LEED structure having apparent (2×2) symmetry. Two binding states of oxygen are inferred from the abrupt change in surface work function as a function of oxygen coverage. LEED intensity measurements indicate that the oxygen layer undergoes an order–disorder transition at temperatures several hundred degrees below the onset of desorption. The order–disorder transition temperature is a function of the oxygen coverage, consistent with two binding states. A model involving the adsorption of atomic oxygen at $\theta < 0.5$ and the formation of complexes with higher oxygen content at $\theta > 0.5$ is proposed. The oxidation of CO to form CO_2 was found to have the maximum rate of production at a ruthenium temperature of 950 K.

Miller, T. R., Weikel, M. K., **Blood donor eligibility, recruitment, and retention,** *Transfusion* **14,** No. 6, 616-622 (Nov.-Dec. 1974).

Key words: blood banking; donor attitudes; donor eligibility; donor participation rates; donor recruitment; donor retention; foreign donor programs; non-donor attitudes.

To study the motivation and actions of potential and active blood donors, a literature search, a limited survey, and associated analytic efforts were undertaken. It is estimated that 61 million of the 114 million age-eligible donors meet Red Cross criteria of health-eligibility. The 1971 donor participation rate, calculated as the percentage ratio of active donors to eligible donors, was estimated to be between 8 and 9 percent. Total collections appear to be increasing at a stable rate of 1 percent per year and 15 percent of each year's collections apparently come from first-time donors. Thus, 14 percent of those who donate blood in any given year must replace other donors who have stopped donating. Roughly 25 percent of those who are health-eligible to donate blood have done so in the last ten years. Literature and survey analyses indicate that donor reaction rates are considerably underestimated by most collectors. A limited survey showed that the main reason for nonparticipation is fear, while common reasons for discontinuing participation are adverse reaction and medical disqualification.

Mills, R., Yee, K., **Hand-held metal detectors for use in weapons detection,** *NILECJ-STD-0602.00,* 13 pages (U.S. De-

partment of Justice, Law Enforcement Assistance Administration, National Institute of Law Enforcement and Criminal Justice, Washington, D.C., Oct. 1974).

Key words: metal detector; weapons detection.

Performance requirements and methods of test have been established for hand-held metal detectors used for determining the location of metal weapons carried on a person. Requirements are specified which indicate a detector's suitability for use in each of specified applications.

Misra, D. N., Bowen, R. L., Wallace, B. M., **Adhesive bonding of various materials to hard tooth tissues. VIII nickel and copper ions on hydroxyapatite; role of ion exchange and surface nucleation,** *J. Colloid Interface Sci.* **51,** No. 1, 36-43 (Apr. 1975).

Key words: adsorption; hydroxyapatite; ion exchange; nucleation; reaction rate; surface.

The interaction of synthetic hydroxyapatite with nickelous [Ni(II)] or cupric [Cu(II)] ions from aqueous nitrate solutions was investigated. Nickelous ions exchange with the calcium ions of the adsorbent and follow the Langmuir adsorption isotherm; the saturation amounts of the adsorbate for two apatite samples have approximately the same ratio as their surface areas. With Cu(II), the initial uptake seems to be independent of concentration and almost equal to the saturation amount of nickelous ions for the same apatite sample. Subsequently, the apatite dissolves in concert with the growth of some form of copper phosphate as a separate phase on the apatite surface if an excess of cupric ions is present. This reaction follows a zero order rate law for dilute solutions. A phenomenological theory is developed which explains the various kinetic facets.

Mohan, K., Schaefer, A. R., Zalewski, E. F., **Measurement of geometrically total spectral radiant power,** *Appl. Opt.* **14,** No. 4, 1035-1038 (Apr. 1975).

Key words: geometrically total spectral radiant power; gonioradiometer.

In this paper, the measurement of geometrically total spectral radiant power, i.e., the spectral radiant power emanating in all directions from a light source, is discussed. A gonioradiometer employing a silicon photodiode and a set of narrow band interference filters was used for these measurements. The experiment is described, some exploratory measurements are presented, and the uncertainties which this method introd ces are estimated.

Mount, G. H., Linsky, J. L., **One- and multi-component models of the upper photosphere based on molecular spectra. IV. Non-LTE treatment of the CN violet system,** *Solar Phys.* **41,** No. 1, 17-33 (Mar. 1975).

Key words: carbon abundance; molecular spectra; non-LTE; solar model; upper photosphere.

Non-LTE synthetic spectra derived from a detailed analysis of the formation of the CN(0,0) λ3883 Å spectrum are compared with center-limb photoelectric spectra taken at Kitt Peak National Observatory. Significant non-LTE effects are found and the Kurucz, Altrock-Cannon, Mount-Linsky II, and HSRA models are compared. We derive a solar carbon abundance of log $A_c = 8.30 \pm 0.10$ for the Mount-Linsky model and log $A_c = 8.40 \pm 0.10$ for the Altrock-Cannon model, compared to the HSRA value of log $A_c = 8.55 \pm 0.10$, assuming a nitrogen abundance of log $A_N = 7.93$. In addition we specify the regions of formation for the CN(0,0) 3883.35 Å bandhead at disc center and limb.

Newell, A. C., Crawford, M. L., **Planar near-field measurements on phased array antennas,** Abstract only, (Proc. Int. IEEE AP-S Symp., Atlanta, Ga., June 10-12, 1974), Paper 6-7 in *1974 International IEEE/AP-S Symposium Digest*, p. 423 (IEEE Inc., New York, N.Y., June 1974).

Key words: antennas; near-field measurements; phased arrays.

The results of applying the planar near-field measurement technique to two experimental phased array antennas are described. Fast and efficient tests are used to determine the required scan area and data point spacings. The use of these tests enable one to reduce the amount of data required for some antennas without seriously increasing the errors in computed far-field parameters.

Measurements were made at different distances from the antennas, with the probe transmitting and receiving, and for both sum and monopulse difference patterns of the test antenna. Comparisons between the far-field patterns computed from the near-field data and those measured on far-field ranges are presented.

Newman, M., **Congruence subgroups of the modular group,** *Math. Comput.* **29,** No. 129, 207-213 (Jan. 1975).

Key words: automorphs; elliptic classes; finite fields; genus; modular group; natural homomorphism; parabolic classes.

The congruence subgroups of the classical modular group which can be defined as the automorphs modulo q of some fixed matrix are studied, and their genera determined.

Newman, M., **Formulas and multiplicative relationships for the parameters of subgroups of the modular group,** *Math. Ann.* **212,** 173-182 (1974).

Key words: classical modular group; congruence groups; elliptic class numbers; genus; index; level; parabolic class number.

Explicit formulas in terms of coset decompositions are derived for the parabolic class number and elliptic class numbers of any subgroup of finite index of the classical modular group Γ. It is shown that these are multiplicative arithmetic functions of the level for congruence subgroups of Γ.

Okabe, H., **Photodissociation of acetylene and bromoacetylene in the vacuum ultraviolet: Production of electronically excited C_2H and C_2,** *J. Chem. Phys.* **62,** No. 7, 2782-2787 (Apr. 1, 1975).

Key words: acetylene; bond dissociation energy; bromoacetylene; C_2; C_2H; fluorescence; photodissociation; vacuum ultraviolet.

The photodissociation of C_2H_2 and BrC_2H in the vacuum ultraviolet produces nearly identical quasicontinuous emissions in the region 4000 to above 5500 Å. It is concluded that the continua are most likely associated with the electronically excited C_2H (C_2H^*) in both cases. Based on this conclusion the following spectroscopic and thermochemical data are derived from the thresholds of incident wavelength to produce the continua (1305 ± 3 Å and 1540 ± 3 Å, respectively, for C_2H_2 and BrC_2H): The electronic energy of C_2H, $E_0(C_2H) \leq 4.11 \pm 0.05$ eV, $D_0(Br - C_2H) = 91 \pm 1$ kcal mol^{-1} (381 ± 4 kJ mol^{-1}), and $\Delta H_{f0}^{\circ}(BrC_2H) = 64.2 \pm 1.5$ kcal mol^{-1} (269 ± 6 kJ mol^{-1}). The photolysis of BrC_2H yields the C_2 Swan bands in addition to the C_2H^* by the spin forbidden process. The fluorescence yield has been measured as a function of incident wavelength for C_2H_2 and BrC_2H. The fluorescence yield curves follow the absorption spectra of C_2H_2 and BrC_2H, indicating that the C_2H^* is predissociated from the initially formed electronic states. The C_2H^* yield from C_2H_2 increases rapidly below the incident wavelength, 1200 Å. Bond dissociation energies and the heats of formation of haloacetylenes are estimated in comparison with the corresponding cyanogen halides. Primary photochemical processes in C_2H_2 are discussed.

Orloski, M. J., **The numbers game in stacks and drains,** (Proc. Sixty-Eighth Annual Meeting of the American Society of Sanitary Engineering, New Orleans, La., Oct. 13-16, 1974), Paper in *ASSE Yearbook* **52,** 122-136 (ASSE, Cleveland, Ohio, 1975).

Key words: National Bureau of Standards; performance of plumbing systems; plumbing code; principles of hydraulics.

This paper discusses some of the historical aspects of plumbing research and plumbing code committee work (Part I). Fundamentals of hydraulics are reviewed as they relate to the intent of plumbing codes (Part II), and current NBS programs on the evaluation of plumbing systems in the laboratory and in the field are discussed (Part III). Considerations involved in implementing the performance approach are covered briefly.

Plummer, E. W., Waclawski, B. J., Vorburger, T., **Experimental observations of electronic energy levels at a solid-vacuum interface,** (Proc. Symp. on Electrocatalysis, San Francisco, Calif., May 13-15, 1974), Paper in *Electrocatalysis*, M. W. Breiter, Ed., pp. 43-57 (Electrochemical Society Inc., Princeton, N.J., 1974).

Key words: chemisorption; field emission; photoemission; single crystals; surface electron spectroscopy; surface state; tungsten.

A knowledge of the distribution of electrons both in energy and space at a surface is essential to the understanding of surface properties. Several techniques have been developed recently which have the potential capability of measuring the energy level spectrum of a surface. Two of these techniques, field emission and photoemission, will be discussed including a description of what can be measured, how it can be interpreted and the degree of consistency of the data. Experimental data will be presented to illustrate: (1) the surface density of states on clean single crystals and its relationship to bulk density of states; (2) the nature of the chemisorption bond and density dependent transitions; (3) dissociative or non-dissociative adsorption and (4) catalytic reactions involving adsorption of hydrocarbons.

Rebbert, R. E., Lias, S. G., Ausloos, P., **The photolysis of neopentane and isobutane with 7.6, 8.4, and 10.0 eV photons,** *J. Photochem.* **4,** 121-137 (1975).

Key words: free radical scavenging; hydrocarbons; isobutane; neopentane; primary photochemical processes; quantum yields; vacuum ultraviolet photolysis.

The photolysis of neopentane has been studied using photons of energies 7.6, 8.4, and 10.0 eV, at pressures in the range 1-760 torr and in the liquid phase. Quantum yields of all molecular and radical products smaller than C_5 have been determined in the gas phase experiments, and have been estimated in the liquid phase. In contrast to results obtained with other alkanes studied to date, hydrogen elimination is found to be an unimportant process in the photolysis of neopentane. The two predominant primary processes are elimination of methane (neo-$C_5H_{12} \rightarrow CH_4 + $iso-$C_4H_8$) and direct C-C bond cleavage (neo-$C_5H_{12} \rightarrow CH_3 + $t-$C_4H_9$). A fraction of the t-$C_4H_9$ radicals dissociate further unless collisionally stabilized, either by loss of a H atom or by loss of a methyl radical (presumably preceded by an initial rearrangement to the isobutyl structure). With an increase in photon energy, the importance of direct bond cleavage increases at the expense of the methane elimination process. In the liquid phase, secondary decomposition processes are quenched, and the estimated quantum yields of primary processes are similar, at all energies, to those found in the 7.6 eV gas phase photolysis at high pressures.

Quantum yields of molecular and radical products formed in the 7.6 and 8.4 eV photolysis of isobutane are also reported and are discussed briefly, with particular emphasis on the effect of energy on the mechanisms of the molecular elimination processes: (iso-$C_4H_{10} \rightarrow CH_4 + C_3H_6$) and (iso-$C_4H_{10} \rightarrow$ iso-$C_4H_8 + H_2$). For both of these primary processes, the lower energy pathway, in which the olefin is formed directly, predominates at 7.6 eV, but diminishes in importance relative to the higher energy channel (presumably involving carbene formation) when the photon energy is increased.

Roberts, J. R., Voigt, P. A., Czernichowski, A., **Experimentally determined absolute oscillator strengths of Ti I, Ti II, and Ti III,** *Astrophys. J.* **197,** 791-798 (May 1, 1975).

Key words: arc; experimental; oscillator strengths; Ti I; Ti II; Ti III.

Absolute oscillator strengths of Ti I, Ti II, and Ti III transitions in the wavelength region from 2440 Å to 3500 Å have been experimentally determined using a wall-stabilized arc. Titanium in the form of heated $TiCl_4$ was admixed with argon plus 5 percent H_2 and introduced into the arc, which was operated at a current of 40-60 amperes. Axis temperatures and electron densities ranged from 11,000 K to 12,500 K and 3.5×10^{16} cm^{-3} to 8.7×10^{16} cm^{-3}, respectively.

Roszman, L. J., **Effects of time ordering on plasma-broadened hydrogen profiles,** *Phys. Rev. Lett.* **34,** No. 13, 785-788 (Mar. 31, 1975).

Key words: Balmer lines; four dimensional rotation group; hydrogen; plasma; plasma broadening; pressure broadening; scattering matrix; spectral line broadening; Stark broadening; symmetry group; time ordering.

The plasma-broadened H_α and H_β spectral-line profiles of hydrogen were calculated retaining the time ordering in the S matrices of the width-shift operator by diagonalizing with the O(4) group. Significant changes occur: The H_α peak is decreased 15 percent, the half-width is increased 25 percent, and the H_β relative dip is decreased 23 percent without significant alteration of the maximum intensity of half-width. Agreement with experiment is improved appreciably.

Rowe, J. M., Rush, J. J., Smith, H. G., Mostoller, M., Flotow, H. E., **Lattice dynamics of a single crystal of $PdD_{0.63}$,** *Phys. Rev. Lett.* **33,** No. 21, 1297-1300 (Nov. 18, 1974).

Key words: coherent neutron scattering; dispersion relation; lattice dynamics; palladium deuteride; phonon frequency distribution; single cyrstal.

The frequency-wave-vector dispersion relations of a single crystal of $PdD_{0.63}$ have been measured by coherent neutron inelastic scattering at 78, 150, 220, and 295 K. The acoustic modes are considerably lower in frequency than the corresponding modes for pure Pd, in accord with the observed lattice expansion. The optic modes, in which D motions predominate, show considerable dispersion. In particular, the shape of the motions predominate, show considerable dispersion. In particular, the shape of the [100] LO branch shows conclusively that second-like-neighbor D-D interactions are comparable to the first-like-neighbor D-D interactions.

Saloman, E. B., Ederer, D. L., **Absolute radiometric calibration of detectors between 200-600 Å,** *Appl. Opt.* **14,** No. 4, 1029-1034 (Apr. 1975).

Key words: calibration of detectors; corrections for second order radiation; far ultraviolet; noble gas double ionization chamber; synchrotron radiation; transfer standard detectors.

Radiometric transfer standards consisting of windowless diodes with cathodes made of anodized aluminum oxide on aluminum are now available from the National Bureau of Standards with calibrations in the 200–600-Å wavelength range. This extends the previously existing range of calibration for these diodes (600–1200 Å). For wavelengths shorter than 600 Å, synchrotron radiation at NBS-SURF is used as the source of radiant energy. A noble gas double ionization chamber is used to calibrate a secondary standard diode that is then intercompared with the transfer standards. Monitors take into account variations in the intensity of synchrotron radiation and in beam position. Methods of accounting for the effects of second-order radiation in the incident flux and secondary ionization in the double ionization chamber are discussed. Calibration uncertainties are about 10 percent.

Saloman, E. B., Ederer, D. L., Madden, R. P., **Radiometry in the EUV spectral region: Standard source and detectors,**

(Proc. IV Int. Conf. on VUV Radiation Physics, Hamburg, Germany, July 17-26, 1974), Chapter 10.12 in *Proceedings of the IV International Conference on VUV Radiation Physics*, E. Koch, R. Haensel, and C. Kunz, Eds., pp. 798-800 (Friedr. Vieweg Sohn Verlagsgesellschaft, mbH, Braunschweig, West Germany, 1974).

Key words: continuum radiation; diodes; irradiance standard; synchrotron radiation; transfer standard detectors; vacuum ultraviolet radiation standards.

Conceptually it is straight-forward to apply the calculable continuum distribution of synchrotron radiation to problems requiring a source of known irradiance. However, in practice many factors affect the accuracy of such a calibration. These factors will be discussed with reference to the NBS 170 MeV synchrotron. The calibration facility at NBS-SURF has been utilized in the 200Å-1200Å spectral range by Air Force Cambridge Research Laboratories and the Naval Research Laboratory to calibrate rocket monochromators. Transfer radiometric standards consisting of windowless diodes with cathodes made of anodized aluminum oxide on aluminum have been developed and calibrated for wavelengths between 200Å-600Å. Diodes have been calibrated with a double ionization chamber using synchrotron radiation from NBS-SURF as a source. Methods accounting for beam motion, second order radiation in the beam, as well as multiple ionization in the double ionization chamber will be discussed.

Sams, R. L., Maki, A. G., **High-resolution infrared measurements of ν_1 and force-field calculations for thioborine (HBS),** *J. Mol. Struct.* **26,** 107-115 (1975).

Key words: absorption spectra; force constants; HBS; infrared; molecular spectra; spectra; thioborine.

The gas-phase high-resolution spectrum is reported for ν_1 of the linear molecule thioborine (HBS) from 2775 cm^{-1} to 2720 cm^{-1}. Band centers and rotational constants are given for the 10^00-00^00 transitions of $H^{11}B^{32}S$, $H^{10}B^{32}S$, $H^{11}B^{34}S$ and $H^{10}B^{34}S$ and for the 11^10-01^10 transitions of $H^{11}B^{32}S$ and $H^{10}B^{32}S$. A valence force field is determined from measured values of ν_1, D_0 (the centrifugal distortion) and q (the l-doubling constant). The remaining unobserved vibrational fundamentals are calculated from the force constants.

Schwarz, F. P., Okabe, H., **Fluorescence detection of nitric oxide in nitrogen,** *Anal. Chem.* **47,** No. 4, 703-707 (Apr. 1975).

Key words: air; automotive exhaust emission; detection; fluorescence; nitric oxide; nitrogen; quencher.

An accurate, rapid, and simple technique is described for the measurement of nitric oxide in standard reference mixtures of NO in N_2. The technique investigated is based on the measurement of the fluorescence intensity emitted by NO when it absorbs 213.8-nm radiation from a Zn discharge lamp (the $A^2\Sigma$ $(v=1) \leftarrow X^2\pi_{1/2}$ $(v=0)$ transition). The fluorescence is in the 220- to 300-nm region and its intensity is proportional to the 213.8-nm light intensity and the NO concentration. The fluorescence intensity at a constant light intensity level increases linearly with NO concentration in the 0.015- to 7-ppm range to within 1 percent error. In the 7- to 932-ppm range, the intensity increases sublinearly with NO concentration because of efficient self-quenching of the fluorescence. The signal-to-noise ratio is 1.0 at 10 ppb for a 1-minute counting time. The quenching half pressures of NO, H_2O, CO_2O_2, O_2, C_2H_4, C_3H_8, and H_2 are, respectively, 0.34 ± 0.03, 0.65 ± 0.06, 8.3 ± 0.6, 0.65 ± 0.05,05, 1.1 ± 0.1, 5.6 ± 0.4, 56 ± 4, and 115 ± 8 torr. The application of this method to detect NO and SO_2 in automotive exhaust is discussed.

Sunjić, M., Sokčević, D., Gadzuk, J. W., **Determination of electron attenuation lengths in metals: Transmission through thin adsorbed films,** (Proc. 2nd Int. Conf. on Solid Surfaces, Kyoto, Japan, March 25-29, 1974), *Jap. J. Appl. Phys. Suppl.* **2,** Part 2, 753-756 (1974).

Key words: attenuation length; inelastic electron scattering; surface plasmons.

A quantitative theory of surface and bulk plasmon excitation in several electron spectroscopies (transmission, XPS, and Auger from thin film sandwiches) is presented. It is shown under what circumstances, the usual exponential attenuation law is valid.

Swartzendruber, L. J., Evans, B. J., **Electronic structure and ^{121}Sb hyperfine fields in the Heusler alloys $Ni_{1-x}Cu_xMnSb$,** *J. Phys.* **35,** No. 12, C6-265/C6-268 (Dec. 1974).

Key words: alloys; Cu; hyperfine fields; magnetism; Mn; Mössbauer effect; Ni; Sb; Pd.

At 4.2 K the magnetic hyperfine field, H_n, at Sb in the Cl_b structure alloys $Ni_{1-x}Cu_xMnSb$, $0<x<1$, increases from 296 kG at $x=0$ to 504 kG at $x=0.6$. For $x<0.7$, H_n decreases rapidly and is characterized by a broad Gaussian distribution. For example, at $x=0.8$ the average H_n is 327 kG and the width of the distribution, σ_{Hn}, is 130 kG. Using the recent model of Blandin and Campbell based on the RKKY interaction, the increase of H_n with x for $x<0.7$ can be shown to arise primarily from the increase in electron concentration. A similar explanation might also apply to the 600 kG H_n at Sb in Pd_2MnSb if it is assumed that Pd contributes 0.25 electron to the conduction band. The large hyperfine fields at Sb in the above alloy systems appear to be consistent with the predictions of extant theoretical models.

Weber, L. A., **Thermodynamic and related properties of parahydrogen from the triple point to 300 K at pressures to 1000 bar,** *NASA Spec. Publ. 3088*, 100 pages (National Aeronautics and Space Administration, Washington, D.C., Mar. 1975). (Available from the National Technical Information Service, Springfield, Va. 22161).

Key words: density; enthalpy; entropy; hydrogen; properties of fluids; specific heat; velocity of sound.

NBS compressibility measurements and thermodynamic properties data for parahydrogen have been extended to higher temperatures and pressures. Results of an experimental program are presented in the form of new PVT data in the temperature range 23-300 K at pressures up to 800 bar. Also given are tables of thermodynamic properties on isobars to 1000 bar including density, internal energy, enthalpy, entropy, specific heats at constant volume and constant pressure, velocity of sound, and the surface derivatives $(\partial P/\partial T)_\rho$ and $(\partial P/\partial \rho)_T$. The accuracy of the data is discussed and comparisons are made with previous data.

West, E. D., Schmidt, L. B., **Spectral-absorptance measurements for laser calorimetry,** *J. Opt. Soc. Amer.* **65,** No. 5, 573-578 (May 1975).

Key words: absorptance; calorimeter; cavity; laser energy measurements; laser power measurements; radiometry.

Methods used at the National Bureau of Standards for determining the power or energy in laser beams depend on calorimetric comparison of laser power or energy and the calibrating electrical power or energy. For this comparison, it is essential to know the fraction of the incident radiant energy that is converted to heat and measured by the calorimeter. This fraction, the effective spectral absorptance, is measured by adding an auxiliary calorimeter, which covers practically all of the opening in the main calorimeter. A laser beam enters the main calorimeter through a small hole in the auxiliary calorimeter. The reflected laser energy and the excess thermal radiation are measured by the auxiliary calorimeter. The data analysis is based on the theory of calorimetery derived from a linear heat-flow problem. Time-dependent functions relating the transient temperature responses of the calorimeters to various constant power inputs are determined experimentally from known electrical inputs. The effective absorptance is found by comparing transient responses for electrical and laser inputs.

Yakowitz, H., **Future growth of SEM—toward super efficient microscopy,** *Proc. 8th Annual Scanning Electron Microscope*

Symposium, St. Louis, Mo., Apr. 7-11, 1975, Part 1, 1-10 (IIT Research Institute, Chicago, Ill., Apr. 1975).

Key words: Auger electron spectrometry; electron probe x-ray microanalysis; energy loss spectrometry; scanning electron microscopy; scanning transmission electron microscopy.

Some predictions concerning future trends in the SEM field have been made. Economic and personnel considerations have been taken into account in arriving at these predictions. Micrographic and analytical requirements and capabilities were also considered. For electron transparent specimens, scanning transmission electron microscopy (STEM) will become a major research method. Auger and energy loss spectrometry will join x-ray emission as analytical methods used for the analysis of such samples. Greater advantages will probably arise from improvements in electron source brightness and from advantages afforded by low energy loss electron detectors. Finally, the SEM field can only profit as the quality and quantity of educational opportunities in the field expand.

Yakowitz, H., Newbury, D. E., **Magnetic domain structures in Fe-3.2Si revealed by scanning electron microscopy—A photo essay,** *J. Test. Eval.* **3,** No. 1, 75-78 (Jan. 1975).

Key words: iron-silicon alloys; Lorentz force; magnetic domains; photomicrography; scanning electron microscope; strain effects.

The mechanism and experimental arrangement by which magnetic contrast can be observed from materials of cubic anisotropy are indicated. Transformer alloy Fe-3.2Si is used as an example to illustrate the effects of tensile strain, magnetic field switching, residual stress, and inclusions on magnetic structure.

Yakowitz, H., Newbury, D. E., Myklebust, R. L., **Approaches to particulate analysis in the SEM with the aid of a Monte Carlo program,** (Proc. 8th Annual Scanning Electron Microscope Symp., St. Louis, Mo., Apr. 7-11, 1975), Paper in *Scanning Electron Microscopy/1975*, Part 1, 93-102 (ITT Research Institute, Chicago, Ill., Apr. 1975).

Key words: backscattered electrons; electron specimen interaction; Monte Carlo simulation; particulate analysis; scanning electron microanalysis; x-ray microanalysis; x-ray source size.

Conventional quantitative electron microanalysis methods have been shown to be satisfactory when semi-infinite, planar specimens normal to the electron beam are analyzed. However, in the case of particulate analysis, the surface may be irregular, the specimen dimensions may be less than the electron beam interaction volume and the x-ray absorption path will be irregular. Currently the only tractable approach to the analysis of particulates is to use a Monte Carlo simulation of electron and x-ray interactions to predict x-ray intensity as a function of particle geometry. A program to carry out this task was devised and tested in several ways for both electron and x-ray parameters. A detailed document of results of these tests, and results on a variety of specimens including aluminum spheres, nickel cylinders, alloy steel wear particles and others show good agreement between theory and experiment.

Some practical considerations have to be taken into account when such methods are used in real analytical situations, e.g., (1) the cost of preparing a calibration curve by the Monte Carlo method, (2) analytical strategy, e.g., what specimen tilt to use in the SEM, what operating voltage and what is the effect of using either energy dispersive or wavelength dispersive detection systems, and (3) applicability to multicomponent particles. From a discussion of these we conclude that the Monte Carlo method can be employed profitably by laboratories having a need for quantitative information concerning particulate matter.

Zecca, A., Lazzizzera, I., Krauss, M., Kuyatt, C. E., **Electron scattering from NO and N_2O below 10 eV,** *J. Chem. Phys.* **61,** No. 11, 4560-4566 (Dec. 1, 1974).

Key words: electron impact; electron scattering resonances; exponential attenuation; low energy; negative ions; nitric oxide; nitrous oxide; total scattering cross section.

Total electron scattering cross sections for NO and N_2O in the energy range 0-10 eV were obtained from exponential attenuation in a straight-line collision chamber without a confining magnetic field. Good agreement is obtained with previous measurements where available. For NO, cross sections have been obtained for the first time for resonance structure in the energy range 0-2.5 eV. There appear to be small, sharp resonances between the large resonances. For both NO and N_2O the cross section is observed to increase rapidly at very low energies. Structure in the cross sections is interpreted in terms of electronic states of NO^- and N_2O^-.

Zimmerman, J. E., Campbell, W. H., **Tests of cryogenic SQUID for geomagnetic field measurements,** *Geophysics* **40,** No. 2, 269-284 (Apr. 1975).

Key words: geomagnetism; magnetometer; SQUID; superconducting device.

A type of cryogenic SQUID (superconducting quantum interference device) magnetometer was designed for geomagnetic measurements. Field tests of the instrument including comparisons to observatory variometers, a rubidium magnetometer, an induction loop, and a flux-gate magnetometer showed the new cryogenic systems to be reliable, accurate, portable, and simple to operate. Directional measurements of natural magnetic field fluctuations as small as 0.0001 gamma with periods from 0.5 sec to several hours were demonstrated.

Zuckerman, B., Turner, B. E., Johnson, D. R., Clark, F. O., Lovas, F. J., Fourikis, N., Palmer, P., Morris, M., Lilley, A. E., Ball, J. A., Gottlieb, C. A., Litvak, M. M., Penfield, H., **Detection of interstellar trans-ethyl alcohol,** *Astrophys. J.* **196,** L99-L102 (Mar. 15, 1975).

Key words: ethyl alcohol; interstellar chemistry; molecular cloud; molecular spectroscopy; radio astronomy; Sagittarius B2.

Three transitions of *trans*-ethyl alcohol (CH_3CH_2OH) were detected in emission toward the Sagittarius B2 molecular cloud. The $6_{06} - 5_{15}$ transition at 85,265.46 MHz, the $4_{14} - 3_{03}$ transition at 90,117. 1 MHz, and the $5_{15} - 4_{04}$ transition at 104,808.58 MHz were observed at $V_{lsr} \sim 60$ km s^{-1}. The abundance of ethyl alcohol in the Sgr B2 cloud is comparable to that of many molecules previously detected there. Careful comparison of the abundance of ethyl alcohol with chemically related molecules such as its isomer dimethyl ether, acetaldehyde, and methyl alcohol may provide important information about mechanisms for molecular formation in the interstellar medium.

U.S. GOVERNMENT PRINTING OFFICE : 1975 OL—588—458

NBS TECHNICAL PUBLICATIONS

PERIODICALS

JOURNAL OF RESEARCH reports National Bureau of Standards research and development in physics, mathematics, and chemistry. It is published in two sections, available separately:

• **Physics and Chemistry (Section A)**

Papers of interest primarily to scientists working in these fields. This section covers a broad range of physical and chemical research, with major emphasis on standards of physical measurement, fundamental constants, and properties of matter. Issued six times a year. Annual subscription: Domestic, $17.00; Foreign, $21.25.

• **Mathematical Sciences (Section B)**

Studies and compilations designed mainly for the mathematician and theoretical physicist. Topics in mathematical statistics, theory of experiment design, numerical analysis, theoretical physics and chemistry, logical design and programming of computers and computer systems. Short numerical tables. Issued quarterly. Annual subscription: Domestic, $9.00; Foreign, $11.25.

DIMENSIONS/NBS (formerly Technical News Bulletin)—This monthly magazine is published to inform scientists, engineers, businessmen, industry, teachers, students, and consumers of the latest advances in science and technology, with primary emphasis on the work at NBS. The magazine highlights and reviews such issues as energy research, fire protection, building technology, metric conversion, pollution abatement, health and safety, and consumer product performance. In addition, it reports the results of Bureau programs in measurement standards and techniques, properties of matter and materials, engineering standards and services, instrumentation, and automatic data processing.

Annual subscription: Domestic, $9.45; Foreign, $11.85.

NONPERIODICALS

Monographs—Major contributions to the technical literature on various subjects related to the Bureau's scientific and technical activities.

Handbooks—Recommended codes of engineering and industrial practice (including safety codes) developed in cooperation with interested industries, professional organizations, and regulatory bodies.

Special Publications—Include proceedings of conferences sponsored by NBS, NBS annual reports, and other special publications appropriate to this grouping such as wall charts, pocket cards, and bibliographies.

Applied Mathematics Series—Mathematical tables, manuals, and studies of special interest to physicists, engineers, chemists, biologists, mathematicians, computer programmers, and others engaged in scientific and technical work.

National Standard Reference Data Series—Provides quantitative data on the physical and chemical properties of materials, compiled from the world's literature and critically evaluated. Developed under a world-wide program coordinated by NBS. Program under authority of National Standard Data Act (Public Law 90-396).

NOTE: At present the principal publication outlet for these data is the Journal of Physical and Chemical Reference Data (JPCRD) published quarterly for NBS by the American Chemical Society (ACS) and the American Institute of Physics (AIP). Subscriptions, reprints, and supplements available from ACS, 1155 Sixteenth St. N. W., Wash. D. C. 20056.

Building Science Series—Disseminates technical information developed at the Bureau on building materials, components, systems, and whole structures. The series presents research results, test methods, and performance criteria related to the structural and environmental functions and the durability and safety characteristics of building elements and systems.

Technical Notes—Studies or reports which are complete in themselves but restrictive in their treatment of a subject. Analogous to monographs but not so comprehensive in scope or definitive in treatment of the subject area. Often serve as a vehicle for final reports of work performed at NBS under the sponsorship of other government agencies.

Voluntary Product Standards—Developed under procedures published by the Department of Commerce in Part 10, Title 15, of the Code of Federal Regulations. The purpose of the standards is to establish nationally recognized requirements for products, and to provide all concerned interests with a basis for common understanding of the characteristics of the products. NBS administers this program as a supplement to the activities of the private sector standardizing organizations.

Federal Information Processing Standards Publications (FIPS PUBS)—Publications in this series collectively constitute the Federal Information Processing Standards Register. Register serves as the official source of information in the Federal Government regarding standards issued by NBS pursuant to the Federal Property and Administrative Services Act of 1949 as amended, Public Law 89-306 (79 Stat. 1127), and as implemented by Executive Order 11717 (38 FR 12315, dated May 11, 1973) and Part 6 of Title 15 CFR (Code of Federal Regulations).

Consumer Information Series—Practical information, based on NBS research and experience, covering areas of interest to the consumer. Easily understandable language and illustrations provide useful background knowledge for shopping in today's technological marketplace.

NBS Interagency Reports (NBSIR)—A special series of interim or final reports on work performed by NBS for outside sponsors (both government and non-government). In general, initial distribution is handled by the sponsor; public distribution is by the National Technical Information Service (Springfield, Va. 22161) in paper copy or microfiche form.

Order NBS publications (except NBSIR's and Bibliographic Subscription Services) from: Superintendent of Documents, Government Printing Office, Washington, D.C. 20402.

BIBLIOGRAPHIC SUBSCRIPTION SERVICES

The following current-awareness and literature-survey bibliographies are issued periodically by the Bureau:

Cryogenic Data Center Current Awareness Service

A literature survey issued biweekly. Annual subscription: Domestic, $20.00; foreign, $25.00.

Liquefied Natural Gas. A literature survey issued quarterly. Annual subscription: $20.00.

Superconducting Devices and Materials. A literature survey issued quarterly. Annual subscription: $20.00. Send subscription orders and remittances for the preceding bibliographic services to National Technical Information Service, Springfield, Va. 22161.

Electromagnetic Metrology Current Awareness Service Issued monthly. Annual subscription: $24.00. Send subscription order and remittance to Electromagnetics Division, National Bureau of Standards, Boulder, Colo. 80302.

U.S. DEPARTMENT OF COMMERCE
National Bureau of Standards
Washington, D.C. 20234

OFFICIAL BUSINESS
Penalty for Private Use, $300

POSTAGE AND FEES PAID
U.S. DEPARTMENT OF COMMERCE
COM-215

SPECIAL FOURTH-CLASS RATE
BOOK

SJRA UNIVE300UA R 1
UNIVERSITY MICROFILMS INC
ATTN SERIALS SECTION
300 NORTH ZEEB RD
ANN ARBOR MI 48106

JOURNAL OF RESEAI ol. 79A, No. 5 Sept.–Oct. 1975
A. Physics and Chem

Page

Surface films on polyoxymethylene single crystals, J. B. Jones and P. H. Geil. 609

On the origin of the amorphous component in polymer single crystals and the nature of the fold surface, John D. Hoffman and G. Thomas Davis. 613

Some thermodynamic properties of bromobenzene from 0 to 1500 K, Joseph F. Masi and Russell B. Scott. 619

Relativistic effects on line strengths for transitions in the hydrogenic isoelectronic sequence, S. M. Younger and A. W. Weiss. 629

The enthalpies of combustion and formation of 2,2′-dichlorethyl sulfide, W. H. Johnson. 635

Barothermal theory of two devices for measuring absorption coefficients, H. S. Bennett. 641

Publications of the National Bureau of Standards. 651

Library of Congress Catalog Card Number: 62–37059

For sale by the Superintendent of Documents, U.S. Government Printing Office, Washington, D.C. 20402. (Order by SD Catalog No. C 13.22/sec.A:79/5). Single copy price varies. Subscription price: $17.00 a year; $4.25 additional for foreign mailing.

UNITED STATES GOVERNMENT PRINTING OFFICE, WASHINGTON : 1975